Lakehead University

Diamondiferous Mass-Flow and Traction Current Deposits in a Neoarchean Fan Delta, Wawa Area, Superior Province

Corey Wendland

A thesis submitted to the Department of Geology in partial fulfillment of the requirements for the Degree Masters of Science

May 2010

Acknowledgements

I would like to thank Drs. P. Hollings and P. Fralick for their guidance, patience, and supervision of this thesis. Gratitude is expressed to Dianor Resources for access to their property and analytical work. Anne Hammond provided assistance in sample preparation. The research was supported by NSERC Discovery Grants to Drs. Hollings and Fralick. The faculty of the Geology Department supplied helpful suggestions and recommendations during preparation of the thesis. Thanks to my family and friends for their encouragement and unwavering support.

Abstract

Diamond bearing Neoarchean metaconglomerates are present in the Michipicoten greenstone belt, Wawa-Abitibi Subprovince, near Wawa, Ontario. They form a portion of the Dore Metasedimentary rocks in the Arliss Lake subbasin, and unconformably overlie a succession of mafic metabasalts. The conglomerates are transitional into argillite and are also overlain by argillite, which in turn is conformably overlain by metabasalts. The conglomeratic succession has a maximum thickness of 454 meters and is confined to what appears to be a deformed paleovalley at the base of the sedimentary succession.

Three lithofacies associations were recognized, and interpreted to indicate that the Leadbetter Conglomerate represents a high-energy, alluvial fan-delta succession. Lithofacies Association One is dominated by weakly sheared and highly viscous debris-flows and represents the upper reaches of the alluvial fan. Lithofacies Association Two is dominated by superimposed longitudinal bars that represent the transformation of the depositional environment to a mid-fan and lower-fan proximal braided system. Lithofacies Association Three is dominated by distributary channel mouth-bars, graded turbiditic density deposits and argillite facies, which represent a transgression and transition to a delta-front and subsequently pro-delta environment.

Whole rock geochemical studies of the Leadbetter Conglomerate indicated that the elements Co, Ni, Sc, TiO_2, V, Al_2O_3, Y, Nb, Zr, Hf, Ta, Th and U are chemically immobile. The immobile elements were used to investigate possible source rock compositions. A mixture of source rocks (mafic, intermediate and felsic igneous rocks, lamprophyre, and possibly kimberlitic occurrences) contributed sediment to the depositional system of the Leadbetter Conglomerate. Of these mafic volcanic rocks and lamprophyres provided the majority of the sediment. Ratio plots used to investigate whether placer accumulation of the

heavy minerals chromite and zircon were present indicated that significant placer accumulation had not occurred.

Possible source rocks for the diamonds include either diamond-bearing, ultramafic, lamprophyre dikes and breccias, which have been observed and described near the Leadbetter Conglomerate, or a more commonly diamond-associated rock type, such as kimberlite, which have yet to be observed in the area. The presence of kimberlites could be investigated by a study of mineral chemistry, but that was beyond the scope of this thesis.

Table of Contents

List of Appendices

List of Figures

Chapter 1

Introduction

1.1. Background

The research described in this thesis was conducted on the Leadbetter Conglomerate, which lies within the Michipicoten greenstone belt. The Michipicoten greenstone belt is located in the eastern portion of the Wawa Subprovince, an Archean volcanic-sedimentary sequence of rocks. Volcanism within the belt occurred and was metamorphosed, between 2744-2699 Ma (Sage, 1994). The main rock types that make up the Michipicoten greenstone belt are mafic volcanic rocks, felsic volcanic rocks, mafic and felsic intrusive rocks and sedimentary rocks. The Leadbetter Conglomerate is a sedimentary unit within this belt that was found to contain diamonds. The discovery of diamonds in the Leadbetter Conglomerate has gained much attention in recent years (Stone, 2004; Lefebvre, 2005; De Stefano, 2006; Stachel, 2006; Wyman, 2006), and currently Dianor Resources has 100% undivided ownership interest in the Leadbetter property and is undertaking exploration.

1.2. Objective

The objective of this thesis was to describe the nature of the Leadbetter Conglomerate and to develop a better understanding of how the depositional environment evolved through applying sedimentological and stratigraphical principles. A second objective was to undertake a whole rock geochemical study with the intent of determining the provenance of the sediment and to assess

possible placer accumulation. Along with determining whether placer accumulation occurred there was also an investigation into what possible rock types could have been the source of the diamonds using whole rock major and trace element geochemistry.

1.2. Structure of Thesis

This thesis is organized into seven chapters consisting of: (1) introduction, (2) methodology, (3) regional geology, (4) lithofacies, (5) lithofacies associations and interpretations, (6) clast lithologies, (7) whole rock geochemistry, and (8) conclusions. The methodology chapter summarizes the analytical techniques and field methods used in the gathering of information and processing of data for this study. The regional geology provides a brief summary of the Superior Province, Wawa subprovince and the Michipicoten greenstone belt geology in which the Leadbetter Conglomerate lies. The whole rock geochemistry chapter is divided into four main parts: (1) element immobility, (2) provenance, (3) placer geochemistry, and (4) evaluation of possible source rocks that may have hosted the diamonds. The depositional lithofacies chapter illustrates the types of lithofacies that make up the Leadbetter Conglomerate. This is followed by the lithofacies associations and interpretations chapter, which discusses the depositional environment and how the depositional environment evolved in order to explain the complex nature of the associations between different types of lithofacies. The final chapter summarizes the results of previous chapters and proposes a model for the formation of the Leadbetter Conglomerate.

Chapter 2

Methodology

2.1. Field Methods

Leadbetter Conglomerate

Fieldwork consisted of documenting detailed descriptions of exposures along traverse lines, point counting clast lithologies in conglomerates, sampling, and reconnaissance mapping.

Traverse lines were undertaken by using a survey tape measure and laying it out perpendicular to the strike of bedding so an apparent bed thickness (not true thickness) could be measured (Fig. 2.1). Information collected in each section included the clast-size/grain-size, sorting, bedding structures (if any), and the nature of the matrix.

Point counting was undertaken constructing a grid using two tape measures lying perpendicular to each other. One tape acted as a fixed base line, the other as a mobile traverse line. A five-centimeter spacing was used to traverse across the fixed base line and the type of clast or matrix at the sample points recorded. This was done across roughly 1-2 meters depending on the size of the outcrop, and then moving the traverse line down 10cm to continue another point count traverse across the fixed base line. Where clasts had been recorded, the percentage of each lithology was calculated from 100 point counts.

On select sites with good exposure, and in particular blast pits that have a known diamond content, a detailed stratigraphic section was drawn and

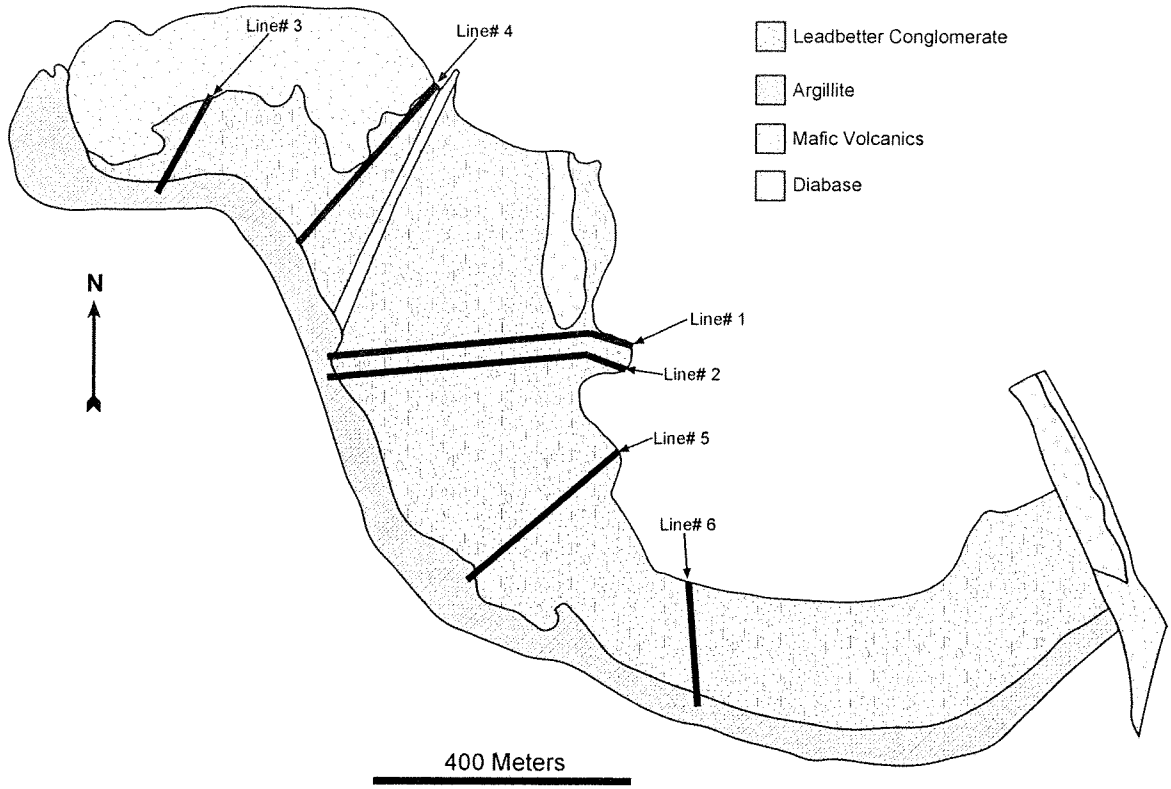

Figure 2.1 Map of the Leadbetter conglomerate showing the location of the six stratigraphic sections that were measured.

measured. Detailed notes on the sedimentology, structure, and stratigraphy of the outcrop were taken as well as representative photographs.

Sampling was undertaken along the traverse lines and at each individual outcrop where a detailed stratigraphic section had been drawn. Selective sampling of only coarse-grained sandstone layers and lenses and coarse-grained sandy matrix material was conducted. This material was used for whole rock geochemistry, because it provides a more representative analysis of source rock compositions than samples containing pebble sized or larger clasts or chemically altered fine-grained sedimentary rocks.

2.2. Analytical Methods

Introduction

The following section outlines the analytical techniques and methodologies utilized in the gathering of data for the Leadbetter Conglomerate. Whole rock geochemical analyses were carried out using an inductively coupled plasma-atomic emission spectrometer (ICP-AES), and an inductively coupled plasma-mass spectrometer (ICP-MS).

ICP-AES

Primary crushing was undertaken using a tungsten carbide mallet and plate, reducing samples to approximately 3-4 mm in size. The metal plate and agate mill cup were cleaned with methanol between each sample to avoid contamination. Secondary crushing was undertaken in an agate rotary mill reducing samples to -200 mesh. Dissolution of samples was carried out as follows: 0.500 grams were weighed out and placed in Teflon crucibles, then 10ml of double distilled deionized water (DDW) and 5ml of nitric acid was added to each sample and left uncovered at 90°C for 12 hours. Crucibles were then filled with 10ml of nitric acid and 5ml hydrofluoric acid and left at low heat for 12 hours (this step was repeated three times). On the last cycle the temperature was increased to 150°C and samples evaporated to dryness. The temperature was then reduced down to 90°C, 5ml of hydrochloric acid was added and simmered for 20 minutes, crucibles were then filled with 10ml DDW and simmered for an

additional 10 minutes. Solutions were transferred to a 100ml volumetric flask and upon cooling made up to 100ml by addition of DDW. For each run three blanks and two internal standards were analyzed to determine the accuracy of the results. Blank preparation involved the same acid digestion process but with no sample, to test for any contamination from the acids. Internal standards from known compositions (MG-8) were prepared by the same acid digestion process together with the samples to evaluate any analytical errors in elemental detection. Analysis of the solution was carried out using a Varian Vista Pro Radial ICP-AES, with a Cetac auto sampler operating at 1100 watts, with a 10 second read-time. Final data processing was carried out using an Excel program developed at Lakehead University which calculates the abundance of elements (except SiO_2), the difference between these and 100 wt.% is assumed to be the abundance of SiO_2. As a result of this processing all ICP-AES results with the addition of CO_2 and H_2O, which was measured by a C-H-N analyzer, will total 100%, which may not be an accurate representation due to the inability to directly measure SiO_2 concentration. Accuracy and precision were assessed by duplicate analysis of known standards with each batch of samples run. Analytical errors were between +/- 2% of the known standards composition as well as duplicate analysis.

ICP-MS

Crushing of 20 samples from the Wawa Leadbetter Conglomerate was done in the same manner as previously described for the ICP-AES method. The powders were analyzed for trace elements and REE by ICP-MS (Inductively Coupled Plasma-Mass Spectrometry) at the Geosciences Laboratories (Geo Labs) of the Ministry of Northern Development and Mines in Sudbury, Ontario. Trace elements and REE were analyzed using a Perkin-Elmer 9000 ICP-MS following a variation on the protocol described by Burnham and Schweyer (2004) and Tomlinson et al. (1998). Twenty four trace elements were determined using a 200 mg aliquot of powder digested by a two stage procedure involving an initial decomposition in a closed beaker by a mixture of HF with lesser HCl and $HClO_4$ followed by a second mixture of dilute HCl and $HClO_4$ as described by Burnham et al. (2002).

Chapter 3

Regional Geology

The Leadbetter Conglomerate lies within the Michipicoten greenstone belt of the Abitibi-Wawa Subprovince in the Superior Province. Below is a brief overview of the Superior Province, Abitibi-Wawa Subprovince, and a more detailed review of the Michipicoten greenstone belt and the Dore metasediments in which the Leadbetter Conglomerate is found.

3.1. Superior Province

Almost a quarter of all exposed Archean crust in the world lies in the Superior Province of North America, the largest Archean craton, covering an area of 1,572,000 km^2 (Goodwin, 1991). The Superior Province contains the longest and broadest exposure of belt-like subprovinces, compared to other exposed areas of Archean crust, in the world, most of which are interpreted as superterranes, dominated or characterized by either volcanic, sedimentary or granitoid plutonic rocks alternating across the craton and ranging in age from 3.1 to 2.7 Ga (Card, 1990).

The Superior Province is subdivided into four basic types of subprovinces (Card and Ciesielski, 1986): (1) volcano-plutonic greenstone belt assemblages, (2) metasedimentary, (3) plutonic, and (4) high-grade gneissic. While this

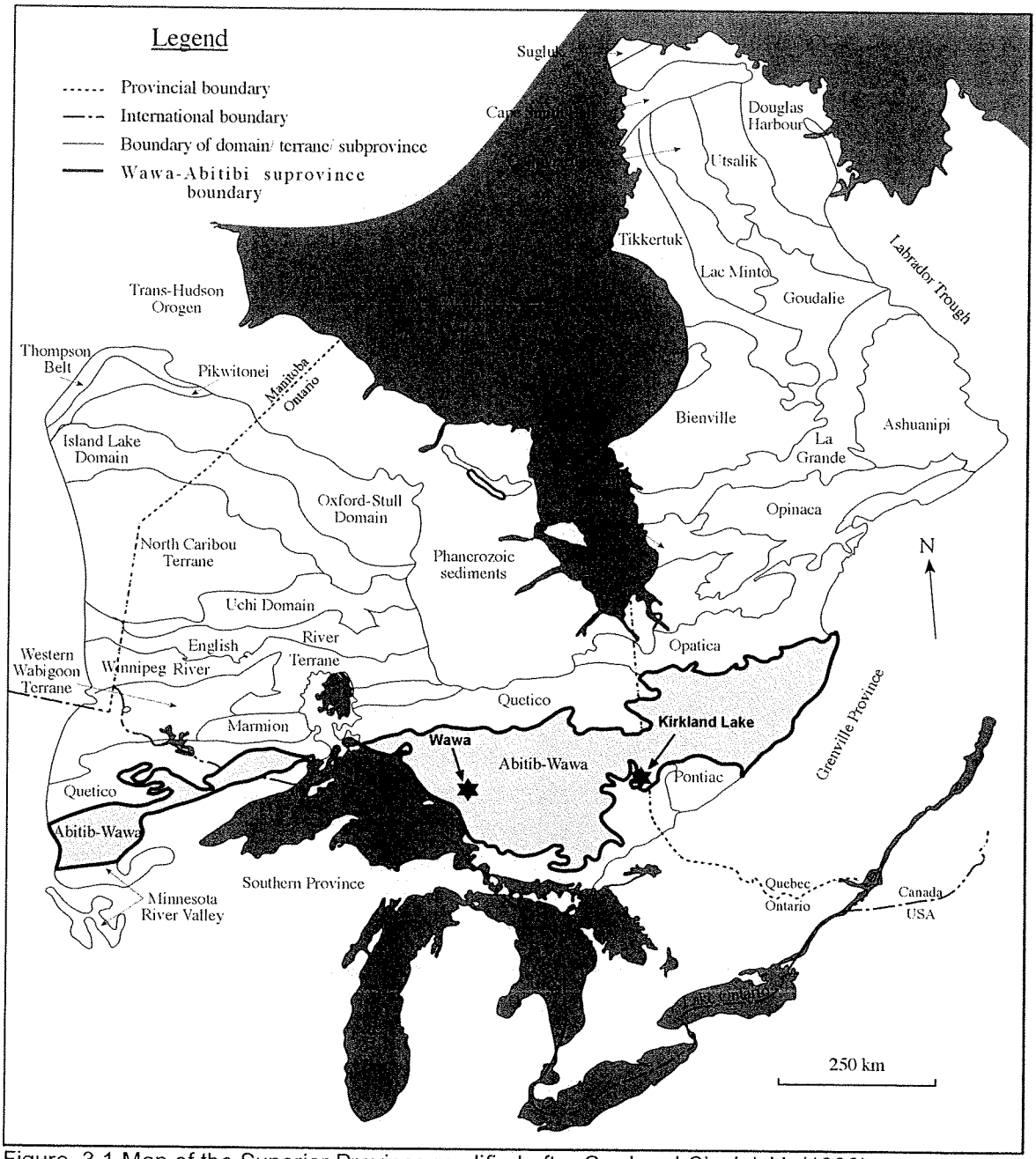

Figure. 3.1 Map of the Superior Province modified after Card and Ciesielski, (1986).

subdivision continues to provide a basic descriptive framework, its value is limited when tectonic analyses have been attempted (Thurston, 1991). Conventional models for Archean continental growth suggest that crust was accreted either by the obduction of oceanic plateau fragments (cf. Desrochers et

al., 1993) or island arc complexes. Current views regard the Superior Province as a collage made up of small continental fragments of Mesoarchean age and Neoarchean oceanic plates, with a complex history of aggregation between 2.72 and 2.68 Ga (Percival, 2004) and subsequent post-orogenic effects.

3.2. Abitibi-Wawa Subprovince:

The Abitibi-Wawa Subprovince is a granite-greenstone terrane in which disparate units, and well-defined greenstone belts of metamorphosed komatiite, basalt, dacite and rhyolite and associated metasedimentary rocks, are dispersed in a sea of granitoid rocks (Williams et al., 1991). Stratigraphic and structural relationships between these units of volcanic and sedimentary rocks are usually unclear and commonly masked by later shearing (Williams et al., 1991).

The Abitibi-Wawa Subprovince is an aggregation of Archean greenstone belts and granitoid plutons (Williams et al., 1991). The northern boundary lies in tectonic contact against structurally overlying metasedimentary rocks of the Quetico and Opatica Subprovinces (Williams et al., 1991). The southern boundary of the Wawa portion of the subprovince is marked by the Montreal River fault in the east, and is hidden beneath Lake Superior and by unconformable Proterozoic supracrustal rocks of the Animikie Basin in the west (Williams et al., 1991). To the south and east the Abitibi portion of the subprovince is bounded by the Paleoproterozoic rift to passive-margin sequence of the Huronian Supergroup (Card et al., 1972; Young, 1983).

The Abitibi and Wawa portions of the subprovince have long been considered part of one volcanic arc with the Abitibi representing a more oceanic sector of the system (e.g., Card, 1990; Wyman et al., 2002). Ketchum et al. (2008) concluded that old crust of the Wawa subprovince may have extended eastward 75 km beneath the western Abitibi belt, which was located in a pericontinental setting relative to the evolving Superior Craton. In this type of scenario, sediments shed from pre-2.75 Ga parts of the nearby Wawa subprovince can also account for some of the >2.75 Ga zircons found in western Abitibi granites and, rarely, in volcanic units (Wyman and Kerrich, 2009).

The Wawa Subprovince and the western Abitibi Subprovince both contain sequences of volcanic rocks consisting of combinations of komatiitic, tholeiitic and calc-alkaline rock types (Wyman et al., 2006). Seven volcanic assemblages in the Abitibi Subprovince record semi-continuous volcanism, with the main phase of tonalite, trondhjemite and granodiorite (TTG) emplacement post-dating the deposition of most supracrustal rocks (Feng and Kerrich, 1992; Corfu, 1993; Sage, 1994). Three volcanic assemblages within the Michipicoten greenstone belt were defined by Williams et al. (1991). The Hawk, Wawa and Catfish assemblages and they correspond to volcanic cycles 1, 2 and 3 described by Sage (1994), and have approximate ages of 2900, 2750, and 2700 Ma (Sage, 1994).

Regional thrusting in Abitibi and Wawa greenstone assemblages was followed by localized crustal extension between 2680 and 2670 Ma (Ayer et al.,

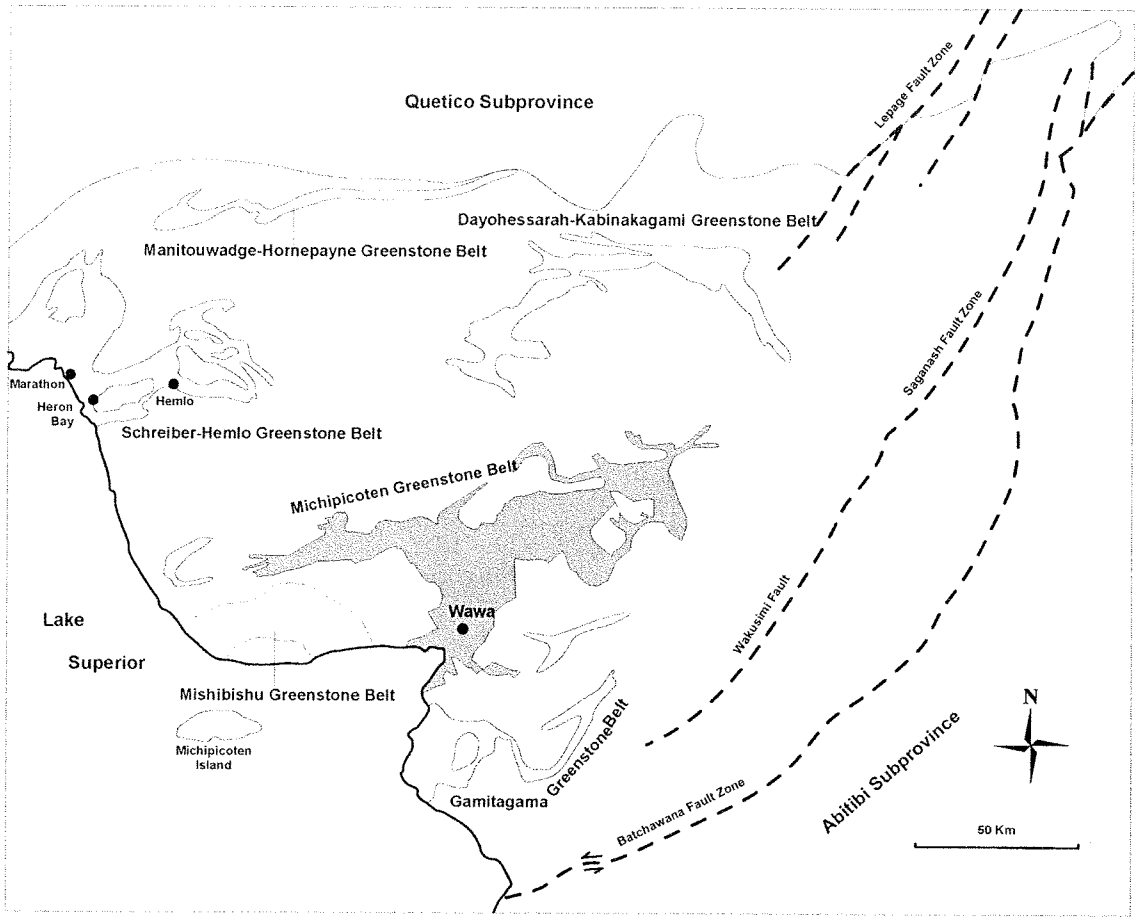

Figure 3.2. Map showing the location of the Michipicoten Greenstone Belt (shaded in grey color) modified after Williams et al (1991).

2002). The late to post-kinematic emplacement of lamprophyres, syenites and associated alkalic rock types in these greenstone belts, and across Superior Province, indicates that the suite of igneous rocks as stated was related to cratonisation (Wyman and Kerrich, 1989, 1993).

3.3. Michipicoten greenstone belt:

The Michipicoten greenstone belt (Fig. 3.2) is present in the eastern part of the Wawa Subprovince (Rice and Donaldson, 1992). It is the largest of eight

greenstone belts within the Wawa Subprovince; it is approximately 140 km long and up to 45 km wide (Williams et al., 1991) (Figure 3.2).

It has been the subject of considerable field, geochemical and geochronological study (Logan, 1847; Goodwin, 1962; Sage, 1985, 1986). Economically, the belt has been of significant importance for iron ore and gold production. Considerable quantities of sideritic iron ore have been recovered in the past from the Helen iron formation and exploration for new sources of gold and other commodities is ongoing (Williams et al., 1991).

The Michipicoten greenstone belt is an Archean volcano-sedimentary sequence that has undergone a complicated history of folding, faulting, granitoid intrusion, and greenschist facies metamorphism (Sylvester et al., 1986). Turek et al. (1982, 1984) dated selected felsic volcanic rock units by the U-Pb zircon method, delineating an age range of 2744-2699 Ma for volcanism within the belt.

Sylvester et al. (1986) determined that there are three time-equivalent stratigraphic sequences of volcanic rocks, the lower, middle, and upper volcanic sequences of the MGB. They further proposed that the tectono-stratigraphic relationships, depositional environments, rock associations, and chemical characteristics of the Michipicoten greenstone belt were analogous to Cenozoic volcanic rocks found at convergent plate margins concluding that the MGB more likely originated from a convergent plate margin rather than in an intercontinental rift.

Sylvester's et al. (1986) three time-equivalent sequences of volcanic rocks are also referred to as cycles by Sage (1986). The oldest cycle one (also known

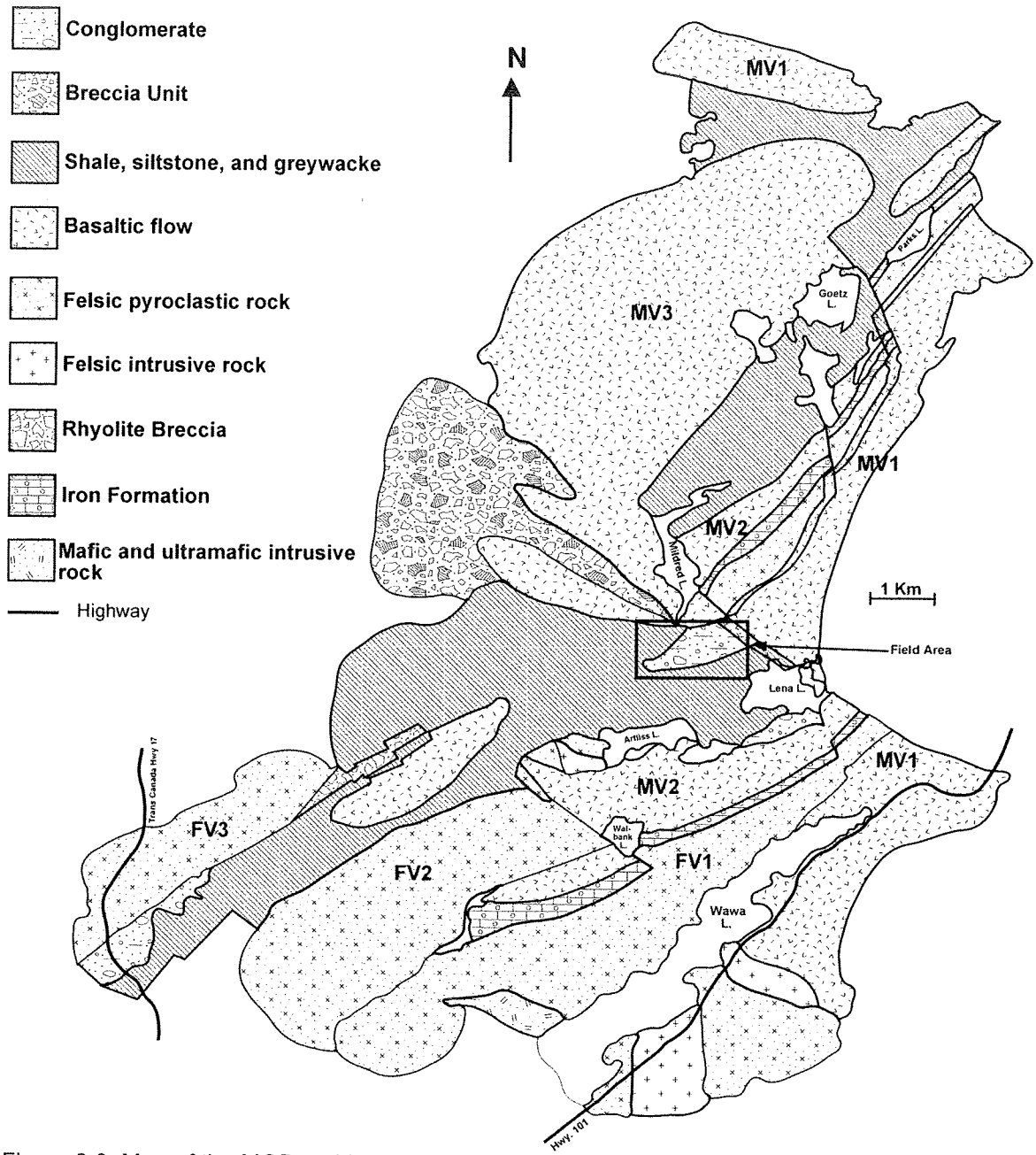

Figure 3.3 Map of the MGB and Leadbetter Conglomerate field area. Modified after Sylvester et al. (1986).

as the Hawk assemblage) is dated at approximately 2889 Ma (Turek et al., 1988), and is followed by cycles two and three (also known as the Wawa and

Catfish assemblages) which are dated at approximately 2750 and 2700 Ma, respectively (Williams et al., 1991).

Goodwin (1964) prepared the first structural synthesis of the MGB, recognizing that the supracrustal rocks were folded around east-trending axes of the Centre and Goudreau anticlines and proposed that they were subsequently refolded about north-west-trending axes. Regional mapping has recently modified the interpretation of Goodwin (1964); detailed structural studies now emphasize the sheared or modified unconformable boundary relations between and within assemblages (McGill and Shrady, 1986; Arias and Heather, 1987; Heather and Arias, 1987; Heather and Buck, 1988; Arias and Helmstaedt, 1990). Structural interpretations currently include recognition of a modified fold-thrust belt geometry for rocks comprising the Wawa and Catfish assemblages to the northeast of Wawa (Arias and Helmstaedt, 1990).

The Leadbetter Conglomerate is part of the Dore metasedimentary rocks in the Arliss Lake area, which unconformably overlie the middle volcanic sequence while mafic flows of the upper volcanic sequence conformably overlie the Dore metasedimentary rocks (Sylvester et al., 1986).

Previous work by Ojakangas (1983) suggested deep-marine and fluvial facies associations for different lithologies in the Dore metasedimentary rocks and proposed that both represented the reworking of island-arc volcanic deposits. Rice and Donaldson (1992) proposed that the Dore metasedimentary rocks predominantly represent submarine-fan sedimentation in mid-to outer-fan

settings; subaerial deposition was rare, occurring in a sandy braided stream environment and as mud-poor debris flows in a probable fan-delta setting.

The Arliss Lake area lies in Chabanel Township; the geology of Chabanel Township is described by Sage et al. (1982). Rice and Donaldson (1992) introduced the term Arliss Lake subbasin to distinguish the paleogeographic setting proposed subsequently for the Arliss Lake area from those proposed for other regions of the Dore basin.

The Arliss Lake subbasin was likely small, and of an irregular configuration, which restricted down-fan sediment distribution, promoting aggradational lobe development; it existed on a convergent plate margin and it has been suggested that the subbasin experienced several episodes of instability, which caused dramatic changes in relative sea level (Rice and Donaldson, 1992).

Donaldson and Rice (1992) made the following assumptions by applying Mutti and Ricci Lucchi's (1972, 1975) model for turbidite facies: *(i)* a fan system existed, as opposed to a non-fan slope apron; *(ii)* the fan system was transverse, as opposed to longitudinal; and *(iii)* the fan system was fed from a point source, as opposed to a line source.

Donaldson and Rice (1992) proposed four successions and seven lithological packages for the Dore metasedimentary rocks and the Leadbetter Conglomerate would lie within their succession one, lithological package seven (130m), described as a conglomerate that overall is fining-upward, predominantly clast-supported and overall sorting is very poor with localized areas of better

sorting. They further described lithological "package seven" as a conglomerate nearly devoid of organization and with poorly developed stratification.

Donaldson and Rice (1992) also point out that the effective absence of organization in the conglomerate makes it very difficult to suggest a stream-flow, or low-density turbidity-current-flow, depositional process. Deposition from cohesion-less debris flows, as proposed by Neale (1981), is therefore suggested for this conglomerate. Neale (1981) also proposed that the debris flows were subaerial, as opposed to subaqueous, based on an absence of interstratified pelite.

The Leadbetter Conglomerate is named after a prospector Mr. Joe Leadbetter, from the town of Wawa, Ontario, who originally staked the property. Initial prospecting during 2002 and 2003 by Mr. Leadbetter followed up on a previous alluvial diamond discovery near the town of Wawa in the early 1990's. This resulted in the discovery of two diamonds, a 1.09 and a 0.25 carat diamond, in the Magpie River, north of Wawa. Follow-up prospecting resulted in the recovery of a 1.39 carat gem quality diamond in December of 2003. Ultimately Mr. Leadbetter followed the tributary upstream to its headwaters and sampled the outcropping rocks, presently known as the Leadbetter Conglomerate, confirming that they contained diamonds. To date, Dianor Resources has 100% undivided ownership interest in the Leadbetter property and is undertaking exploration.

Chapter 4

Lithofacies

4.1. Introduction to Leadbetter Conglomerate

The Leadbetter Conglomerate is roughly 454 meters at its thickest, in what has been called the central area by Dianor Resources. It pinches out in the northern limb of the outcrop area and is faulted and displaced in the south, where it is ~200 meters thick. Both matrix-supported and clast-supported conglomerates characterize the unit.

Dominant clasts include basalt, rhyolite, sandstone, gabbro and diorite. Clasts are generally angular to sub-rounded, and more rarely rounded-to-well rounded with pebble-sized clasts and fine-grained-to-very coarse-grained sand-sized material being more rounded. Matrix compositions and texture are variable: from mud-sized and silt-sized material dominating within the matrix-supported cobble to boulder conglomerates, to fine-grained to very coarse-grained feldspathic, quartz-rich and mafic mineral-rich sand-sized grains forming the majority of the matrix within the clast-supported cobble to pebble conglomerates. Boulder conglomerates are poorly-sorted, while cobble to pebble conglomerates are poorly to moderately-well sorted with a decrease in clast-size and grain-size generally corresponding to better sorting.

In general, units within the Leadbetter Conglomerate fine upward, but commonly can be ungraded to inversely graded near the base of the unit. Sedimentary structures exhibited by the Leadbetter Conglomerate range from

massive to crudely horizontally-stratified, horizontally stratified, trough-crossbedded and planar-tabular cross-bedded. Upwards within the unit the Leadbetter Conglomerate is overlain by a commonly fine-grained to very fine-grained, retrogradational unit of graded and laminated siltstones to mudstones, which indicates a rapid change in depositional environment.

4.2. Introduction to the Leadbetter Lithofacies

Field mapping consisted of measuring and describing six stratigraphic sections with detailed mapping of individual pits (Appendix A). Seven different types of depositional lithofacies were identified using the lithofacies classification scheme developed by Miall (1977) for braided fluvial conglomerates. This chapter will summarize and characterize the types of lithofacies identified.

4.3. Depositional Lithofacies

***Lithofacies Gm**: massive or crudely bedded gravel.* Miall (1977) described lithofacies Gm as pebble or cobble-gravels in which crude horizontal stratification may or may not be apparent. Most gravels are clast-supported, indicating that the matrix (sand and silt) filtered into the interstices following deposition. Some matrix-supported gravels are also present. Impersistent lenticles of clay, silt or cross-bedded sand may be interbedded with the gravels.

Lithofacies Gm is by far the most abundant lithofacies within the Leadbetter conglomerate and most often is a pebble or cobble-conglomerate with

Figure 4.1 Crudely horizontally bedded clast-supported cobble conglomerate of lithofacies Gm.

either crude horizontal stratification that is generally only visible through alternations in clast-size or it can be truly massive in texture. Both clast supported and matrix supported conglomerates were observed. Clast supported conglomerates are poorly to moderately sorted with mud-sized to very coarse-grained matrix material that varies in proportions (Fig. 4.1). Clast supported conglomerates range in thickness from 10cm to 4m and often are laterally continuous, but can be thin and lensy. They commonly contain thin (1-2cm thick) pebble stringers that vary in length along strike from 50cm-4m, often limited by the width that can be seen of the outcrop area. There are a few examples of

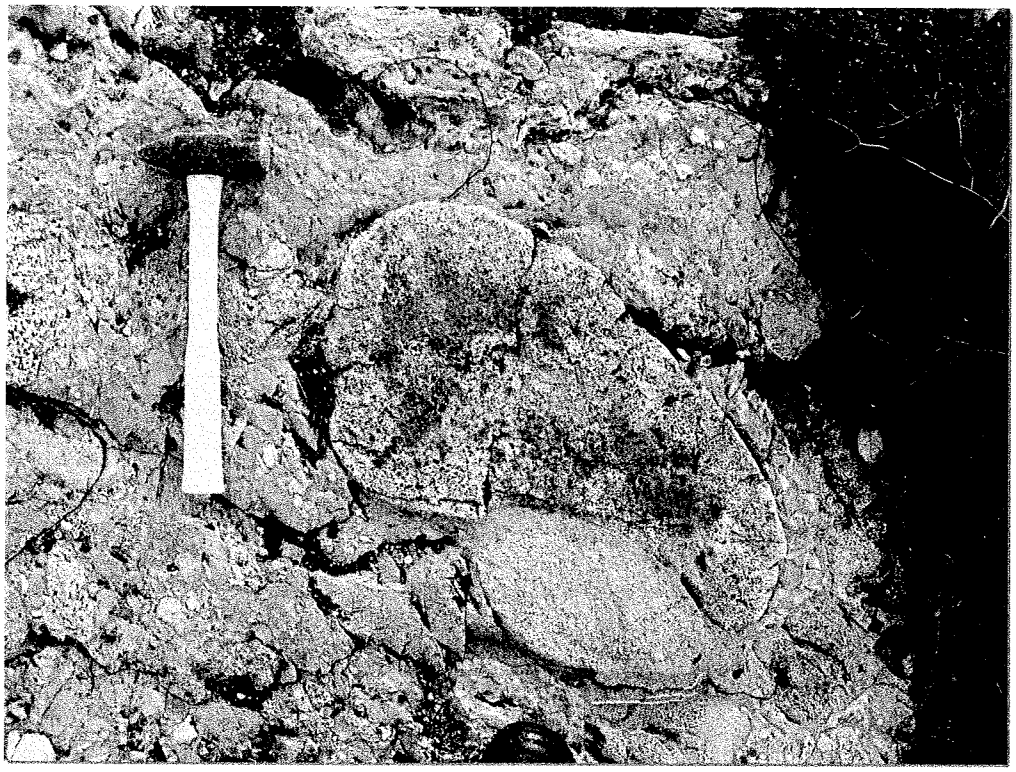

Figure 4.2 Massive matrix-supported cobble to boulder conglomerate of lithofacies Gm.

crossbedded sandstone interbedded with the pebble-cobble conglomerate. They are also commonly ungraded but can have a very diffusive fining upwards trend through the unit, with sharp upper and lower contacts. Rarely are they erosive to units below. Clast supported conglomerates become more prevalent upwards through the succession. Near the base of the Leadbetter Conglomerate matrix supported cobble or boulder conglomerates are more prevalent (Fig. 4.2). Matrix supported conglomerates are characterized by an abundant sericite-chlorite (originally mud) matrix with lesser amounts of very coarse-grained sand. These are poorly sorted and commonly massive and chaotic in structure with a swirled matrix texture. Matrix supported conglomerates can range in thickness from 80cm to 4m and are laterally continuous at the scale of the outcrop. They are

generally ungraded but can more rarely have a diffusive graded contact with units above and sharp lower contacts.

***Lithofacies Gt/St**: trough-crossbedded gravel.* Miall (1977) describes lithofacies Gt as gravels that are distinctly trough cross-stratified, comprising beds of varying grain-size. They form broad, shallow channels, typically 20cm to 3m deep and 1 to 12m wide. The channels commonly cut into each other both laterally and vertically. Each thus has an erosional base, and this may be followed by a lag deposit of coarser grain-size than the overlying trough fill.

Lithofacies Gt is not very common within the Leadbetter Conglomerate, which could be due to deformation from folding, shearing and compaction that may have masked most sedimentary structures that display broad, shallow shapes. The few areas where lithofacies Gt was identified it consisted of moderate to well sorted coarse-grained gravel with either very shallow cross-bedding (Fig. 4.3) or noticeable lag deposit of coarser grained size than the trough-fill. The lags overlie erosional surfaces and exhibit subtle fining upwards. In one outcrop the lag coarsened upwards to the unit above. The lensoid units composing lithofacies Gt can range in thickness from 10cm to 30cm.

Figure 4.3 Trough-crossbedded pebble conglomerate of lithofacies Gt.

***Lithofacies Gp**: planar-crossbedded gravel.* Miall (1977) describes lithofacies Gp as showing distinct stratification, comprising individual sets or cosets of planar crossbedding. Reactivation surfaces may be present. These are surfaces of erosion, which cut across the foresets with the same sense of dip but a lower angle than the foresets (Collinson, 1970).

The one very distinct example of lithofacies Gp within the Leadbetter Conglomerate consists of three thin, 10-15cm thick beds of very coarse-grained pebble conglomerate. They are moderately well-sorted with a fine-grained to coarse-grained matrix. Each conglomerate bed is planar-crossbedded

and the package is interbedded within a crudely horizontally-stratified cobble conglomerate that erodes into the planar-crossbedded sandstone and pebble conglomerates. Reactivation surfaces were not observed.

***Lithofacies St**: trough-crossbedded sand.* Miall (1977) describe lithofacies St as trough cross-stratified sand where the trough crossbedding may consist of solitary scoops with an erosional relationship to underlying planar-bedded units or other sedimentary structures. Grain-size generally is medium to very coarse sand. Pebbles also may be present. The base of the facies commonly consists of an erosion surface, and a thin unit of massive sand with or without intraclasts may occur immediately above the base of the unit.

Lithofacies St is rare within the Leadbetter Conglomerate and is seen as very low angle trough-crossbedding in very coarse-grained sandstone that is moderately well-sorted with a fine-grained matrix (Fig. 4.4). The one distinct example of a trough-crossbedded very coarse-grained sandstone is 20cm thick, lensy in shape and overlies a horizontally-bedded pebble conglomerate. There is an erosional lag deposit of coarser grained pebbles near the base of the unit and the trough-crossbedded very coarse-grained sandstone coarsens upwards to a pebble conglomerate unit above.

Figure 4.4 Trough-crossbedded coarse-grained sandstone of lithofacies St.

***Lithofacies Sp**: planar-crossbedded sand.* Miall (1977) describes lithofacies Sp as having grain-size and sorting characteristics generally similar to those of facies St. Planar-tabular crossbeds are of alpha type (Allen, 1963). They have sharp, flat or slightly scoured bases and tops. Reactivation surfaces may or may not be present.

There are two locations of lithofacies Sp identified within the Leadbetter. One is within stratigraphic section two between 344-352m. The other is within pit# 196 (Appendix A18). Both display a sharp, flat base and top with superimposed planar-crossbeds of coarse to very coarse-grained sandstone.

Figure 4.5 Planar-crossbedded fine-grained sandstone of lithofacies Sp.

They are approximately 20cm thick, moderate to well-sorted with a fine-grained matrix, and do not contain reactivation surfaces. In Pit# 196 planar-crossbedded sandstone lithofacies Sp is underlying a massive coarse-grained sandstone unit, while the Sp lithofacies within stratigraphic section two has two distinct sets of planar-crossbedded, coarse- grained sandstone underlying, and in sharp contact with, a very thin bed of very fine-grained siltstone to mudstone.

Figure 4.6 Horizontally-bedded coarse-grained sandstone of lithofacies Sh interbedded with a pebble conglomerate of lithofacies Gm.

***Lithofacies Sh**: horizontally-bedded sand.* Miall (1977) describes lithofacies Sh as sand that may be laminated to massive, very fine to very coarse-grained or (rarely) pebbly. Lithofacies thickness ranges from a few centimeters to several meters. Parting lineation may be well developed and very small-scale ripple marks with amplitudes of less than 5mm may be present, particularly in the finer-grained sands.

The majority of the Leadbetter Conglomerate fine to very coarse-grained sandstone units are identified as lithofacies Sh. They are most commonly

horizontally to crudely horizontally stratified, moderate to well-sorted, and have a fine-grained matrix (Fig. 4.6). However, due to deformation there is no observable parting lineation, and if there were very small-scale ripple marks they may have been overprinted from compaction and were not observed. Lithofacies Sh can range in thickness from 2cm to 60cm and commonly has sharp contacts with units above and below. Though the basal contact is sharp it rarely shows an irregular erosive surface. They can be laterally continuous at the scale of the outcrop, but more often are lensoid in shape.

***Lithofacies Ss**: scour-fill sand.* Miall (1977) describes lithofacies Ss as consisting of large, asymmetric scours and scour fillings typically up to 45 cm deep and 3m wide. The scour fill comprises fine to coarse, commonly pebbly sand, and the stratification is at a very low angle to the basal erosion surface so that in exposures of limited lateral extent the beds appear to conform to the shape of the scour. Planar beds with parting lineation, trough crossbedding and small-scale cross-stratification may be present. The smaller scours conform in type to eta-cross-stratification of Allen (1963). The cutting and the filling of the structures were probably separate events.

Lithofacies Ss are identified as the many lenses and channel shaped patches of coarse, very coarse and pebbly sandstone that are interstratified ubiquitously throughout the Leadbetter Conglomerate. They are moderate to well-sorted with a coarse-grained to fine-grained matrix. The sandstones generally have a slightly erosive asymmetric shaped base, and if any internal

Figure 4.7 Scour-fill coarse-grained sandstone of lithofacies Ss.

stratification is noticeable it is generally very low angle to the basal erosional surface or planar stratified channel fill (Fig. 4.7). Lithofacies Ss ranges in thickness from 2cm to 15cm on average, but have observed thicknesses of up to 20cm, and range from 80cm to one meter wide.

Lithofacies Fl: *Laminated sand, silt and mud.* Miall (1977) describes lithofacies Fl as being rarely coarser than very fine-grained sand. Interbedding of sand, silt and mud on a fine scale is common. Very small-scale ripple marks, undulating

bedding, and in rocks of appropriate age bioturbation, plant rootlets and coal may all be abundant. The thickness and lateral extent of this facies is variable.

Lithofacies Fl is rarely observed within the Leadbetter Conglomerate except for the transition zone to an argillite facies near the top of the unit. There are three occurrences of lithofacies Fl within the conglomerate; one is in pit# 114 (Appendix A2) consisting of two very thin (1-2cm thick), very finely laminated (1-2mm thick) mud lenses interstratified within a crudely planar stratified, poorly sorted pebble conglomerate with a very coarse-grained to muddy matrix. The second is pit# 169 (Appendix A6) where there are two separate occurrences of lithofacies Fl overlying a massive to crudely horizontally-stratified pebble conglomerate with a very coarse-grained matrix. Both occurrences are very finely laminated and 2-4cm thick with sharp lower and upper contacts. The layers are laterally continuous through the outcrops width (one meter wide). The third observed example of lithofacies Fl is between 384m to 396m within stratigraphic column two and is 12 meters thick with 1-5mm thick thinly laminated mud, silt and very fine-grained sandstone. Individual layers are commonly graded and have sharp contacts between laminae.

Lithofacies Fm: *mud or silt drape.* Miall (1977) describes lithofacies Fm as dark-colored, massive or laminated mud or silt that occurs as lenticles a few millimeters to a few centimeters in thickness. This lithofacies occurs typically as a drape over underlying beds, its lower surface conforming to the shape of any underlying bedform, such as a ripple train.

Figure 4.8 Very fine-grained silt drape of lithofacies Fm.

Lithofacies Fm is only present in the Leadbetter Conglomerate in pit# 169 where there are two channel shaped, very coarse-grained sandstone beds with a very thin 1cm thick dark grey colored mud drape that has a conformable lower contact with the very coarse-grained lense-shaped sandstone beds (Fig. 4.8). The mud drape is confined to the width of the channel shaped sandstone beds. The two lense-shaped very coarse-grained sandstone beds are interstratified within a 30cm thick pebble conglomerate (lithofacies Gm). The only other occurrence of lithofacies Fm is within the argillite lithofacies overlying the Leadbetter Conglomerate.

Chapter 5

Lithofacies Associations and Interpretations

5.1. Introduction

Due to the paucity and randomly located outcrops of the Leadbetter Conglomerate an outline of the vertical lithofacies associations could be made, but observing lateral lithofacies associations was very difficult, due to the lack of outcrops that were well exposed and laterally continuous along strike. The Leadbetter Conglomerate could represent anything from sub-aqueous to sub-aerial deposition. The coarse-grained texture of the unit, general absence of fines in the sandstones and some conglomerates, and mature lithologies suggest vigorous bedload transport and extensive winnowing of fine-grained detritus. The absence of any features or association of features suggestive of marine transport and sedimentation makes it reasonable to assume that the Leadbetter Conglomerate was deposited in a continental setting.

The Leadbetter Conglomerate closely resembles the example of the Scanlan conglomerate described by Middleton and Trujillo (1984) and falls under the Scott type for ancient braided-river deposits (Miall, 1977). The Leadbetter displays three main lithofacies associations with Association One being an alluvial fan-proximal braided system, Association Two being a mid-fan and lower-fan proximal braided system and Association Three representing the upper portion of the Leadbetter Conglomerate that is a transitional zone from alluvial fan to pro-delta facies.

The following discussions will focus on documenting the three lithofacies associations identified and interpretating the processes of sediment transport responsible for deposition of units within the lithofacies associations. This will culminate in the reconstruction of a depositional system for the Leadbetter Conglomerate.

5.2. Lithofacies Association One

Lithofacies Association One is characterized by interbedding of lithofacies Gm with subordinate lithofacies Gt and more rarely Sh. The most abundant lithofacies type within Association One is a massive matrix-supported cobble to boulder conglomerate that is characterized by abundant very fine-grained to muddy matrix. It has a disorganized fabric with a swrily matrix texture (Fig. 5.1). The matrix-supported conglomerate is interbedded with subordinate lithofacies of massive to crudely parallel laminated, and more rarely trough cross-bedded, very coarse-grained sandstone to pebble conglomerate. Contacts between these lithofacies are generally sharp and can be erosive. This lithofacies association is most prevalent near the base of the Leadbetter Conglomerate and more abundant within the central area.

With respect to depositional processes the most important lithofacies within Association One is lithofacies Gm (Fig. 5.1). Significant characteristics of lithofacies Gm are the large size of clasts, angularity of many clasts, poor sorting, fine-grained and muddy matrix support, disorganized fabric and absence of sedimentary structures. Many of the characteristics of lithofacies Gm are

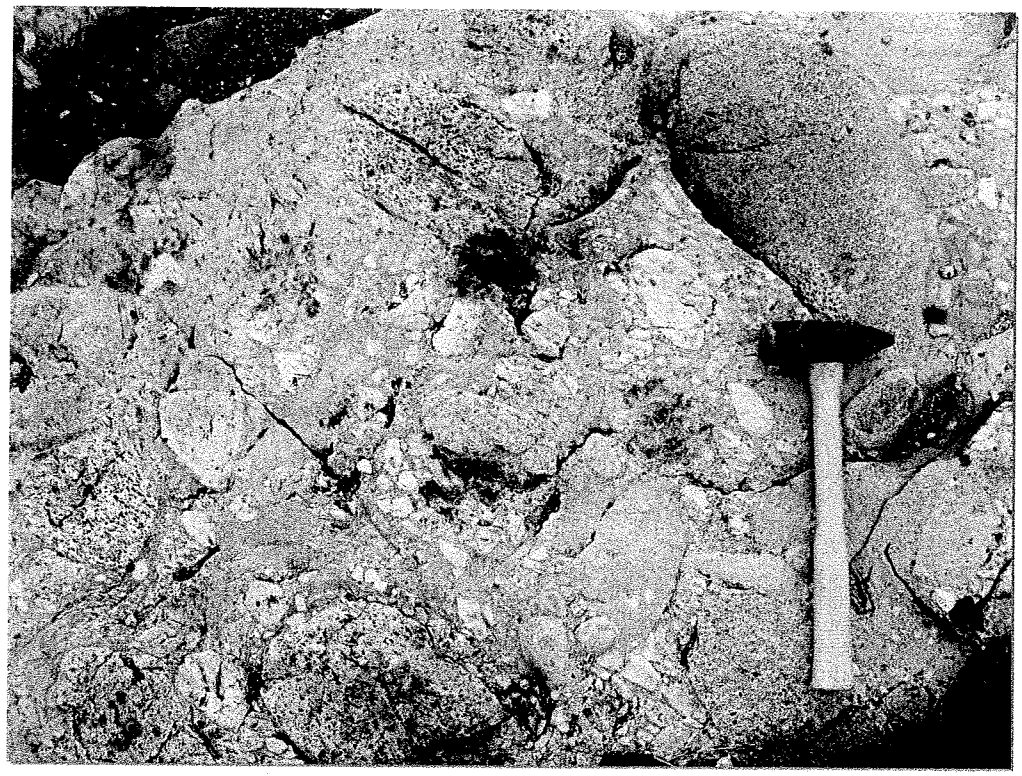

Figure 5.1 Massive matrix-supported cobble to boulder conglomerate that represents a weakly sheared and highly viscous debris-flow of lithofacies association one.

similar to features generally characteristic of debris-flow deposits (Nemec and Steel, 1984; Blair, 1998; Mills, 2000; Kim, 2004; Chakrabarti, 2007) suggesting weakly sheared and highly viscous debris-flows. The most diagnostic feature of this type of debris-flow is disorganized clast fabric, which may simply reflect short travel distance, but also commonly suggests non-sheared (high strength) 'plug' flow, or only weakly sheared (high viscosity) flow (Nemec and Steel, 1984; Kim, 2004). The poor sorting, high mud matrix content, angularity of the clasts and lack of sedimentary structures implies that few grain-to-grain bedload collisions occurred (weakly sheared) and the transportation mechanism was incapable of winnowing fine sediments and sorting clasts. Highly viscous debris-flows are

characterized by a muddy matrix and often occur in the proximal reaches of alluvial fans whereas sandy matrix is typical of less viscous, distal fan debris-flows (Middleton and Trujillo, 1984; Mills, 2000). Therefore, lithofacies Gm of Association One most probably represents weakly sheared and highly viscous debris-flows on the upper reaches of the alluvial fan.

Less commonly, lithofacies Gt interbedded with facies Gm (Fig. 5.2). Important characteristics of facies Gt are moderate to well-sorted, coarse-grained conglomerate, and more rarely pebbly conglomerate, with very shallow cross-bedding and noticeable lag deposits of coarser grain-sized than the trough-fill. It commonly can show minor amounts of erosive scouring at the base of the coarser grained lag deposit with a fining upwards in grain size. More rarely ltihofacies Sh caps lithofacies Gt (Fig. 5.2), which is characterized by being massive to crudely horizontally stratified and moderate to well-sorted. The coarse-grained sandstone layers generally are 2-10cm thick. Contacts between lithofacies Gt and Sh are most commonly sharp, non erosive and sometimes gradational. The more mature fabric and lesser amounts of matrix support between clasts, indicates lithofacies Gt was the product of an active bedload system that was more efficient at winnowing fine sediments and sorting clasts. The presence of an upward-fining sandy cap, sometimes with an erosive base and signs of stratification, may result from turbulent fluidal flow or heavily sediment-laden stream flow following the debris flow (Nemec and Steel, 1984). Lithofacies Gt, where interbedded with lithofacies Gm, in Association One, was probably the result of a fluvial system actively transporting bedload and

Fig. 5.2 Lithofacies Gt and Sh interbedded with lithofacies Gm.

reworking sediment (erosive scouring) on the tops of the debris-flows in the upper proximal reaches of the alluvial fan. Lithofacies Sh is the result of falling flow stage where the water is not flowing strongly enough to transport the gravel load but is still capable of traction transport of coarse sand and granules (Middleton, 1984). Composite units with thick, crude to distinct internal layering or with the presence of thin, discontinuous sandy zones may result from rapidly surging flows (Nemec and Steel, 1984; Mills, 2000).

Lithofacies Association One is the product of proximal alluvial fan debris-flows that would have occurred in a fairly steep gradient environment. The steep gradient would allow for rapidly surging flows to cause an increase in sediment instability causing the coarse-grained sediment and mud charged debris-flow to

rapidly move down the alluvial fan-delta. As the gradient decreased the highly viscous, low sheared debris flow would have deposited very rapidly resulting in the immature nature of the fabric and large boulder-sized clast being left in suspension in the muddy, swirly textured matrix (Blair, 1998; Mills, 2000; Kim, 2004; Nichols, 2005; Chakrabarti, 2007). Once the initial surge of the debris-flow had been deposited the fluvial activity that remained would, on occasion, be strong enough to actively transport bedload material, depositing lithofacies Gt and lithofacies Sh as the stage fell. The rarity of lithofacies Sh being preserved within Association One could be the result of these highly charged surging debris-flows being able to erode previous sandstone caps (lithofacies Sh).

5.3. Lithofacies Association Two

This association dominates in the middle and upper parts of the Leadbetter Conglomerate. There are many variations of the vertical juxtaposition of lithofacies but the most common and abundant lithofacies association within this sequence is interbedding of clast supported conglomerates of lithofacies Gm with subordinate lithofacies Sh and more rarely St. Other minor lithofacies that occur locally are Gt, Gp, Sp, Sr, Ss and more rarely Fl and Fm.

The major difference between lithofacies Gm within Association Two compared to the Association One Gm is the clast size of lithofacies Gm in Association Two is dominated by cobbles and pebbles. As well, lithofacies Gm in Association Two is generally clast-supported with a coarse-grained to granule matrix infill and is, in places, horizontally to crudely horizontally stratified as

opposed to the Gm of lithofacies Association One which is massive and matrix supported with abundant chlorite and sericite (originally mud) forming a very fine-grained matrix.

Lithofacies St is rare within the Leadbetter Conglomerate but when observed it lies within Association Two and is characterized by very low angle trough-crossbedding in very coarse-grained sandstone that is moderately well-sorted with a fine-grained matrix.

There is one local occurrence of lithofacies Gp within Association Two. It is present as three thin, 10-15 cm thick, beds of very coarse-grained sandstone and pebble conglomerate. They are moderately well-sorted with a fine to coarse-grained matrix, planar-crossbedded and interbedded within a crudely parallel bedded cobble conglomerate of lithofacies Gm. Lithofacies Gp probably represents linguoid bars or in channel deltaic growths from older bar remains (Miall, 1977). Lithofacies Sp is seen as superimposed planar-crossbeds of coarse to very coarse-grained sandstone, which are 20cm thick, and moderate to well-sorted with a fine-grained matrix. They do not have reactivation surfaces and appear to represent small linguoid bars or sand waves forming in channels or over bar tops during lower flow regimes.

The majority of the Leadbetter Conglomerate fine to very coarse-grained sandstone units are lithofacies Sh. They are most commonly horizontally to crudely horizontally stratified, moderate to well-sorted and have a fine-grained matrix. They range in thickness from 2cm to 60cm. Lithofacies Ss are identified as the many lenses and channel shaped patches of coarse, very coarse and

pebbly sandstone that is moderate to well-sorted with a coarse-grained to fine-grained matrix. They are interstratified ubiquitously throughout the Leadbetter Conglomerate within Association Two. They generally have a slightly erosive asymmetric shaped base, and if any internal stratification is noticeable it is generally very low angle to the basal erosional surface or represents planar cross-stratification filling the scour.

Lithofacies Association Two has characteristics similar to successions formed by longitudinal bar complexes (Doeglas, 1962; Williams and Rust, 1969; Miall, 1977; Jones, 1989; Burton, 2003). Longitudinal bars can be diamond or lozenge shaped in plan, and are elongate parallel to flow direction (Miall, 1977). They are bounded by active channels on both sides and may, as a result, have partially eroded margins (Miall, 1977). Bars formed in gravel are most commonly of this type (Rust, 1972; N.D. Smith, 1974; Gustavson, 1974; Boothroyd and Ashley, 1975; Jones, 1989; Burton, 2003).

The main characteristic of lithofacies Gm is an interbedding of horizontally bedded clast-supported cobble conglomerates with pebble conglomerates (Fig. 5.3). The cobble conglomerate is probably the result of the coarsest bedload being deposited during waning-flow conditions, and a resultant reduction of competency as a short, submerged, central bar, described as a "diffuse gravel sheet" by Hein and Walker (1977), was deposited during the initial stage of the formation of a longitudinal bar. Thus, the cobble conglomerates being the coarsest material deposited by traction processes, would more commonly represent the bar head.

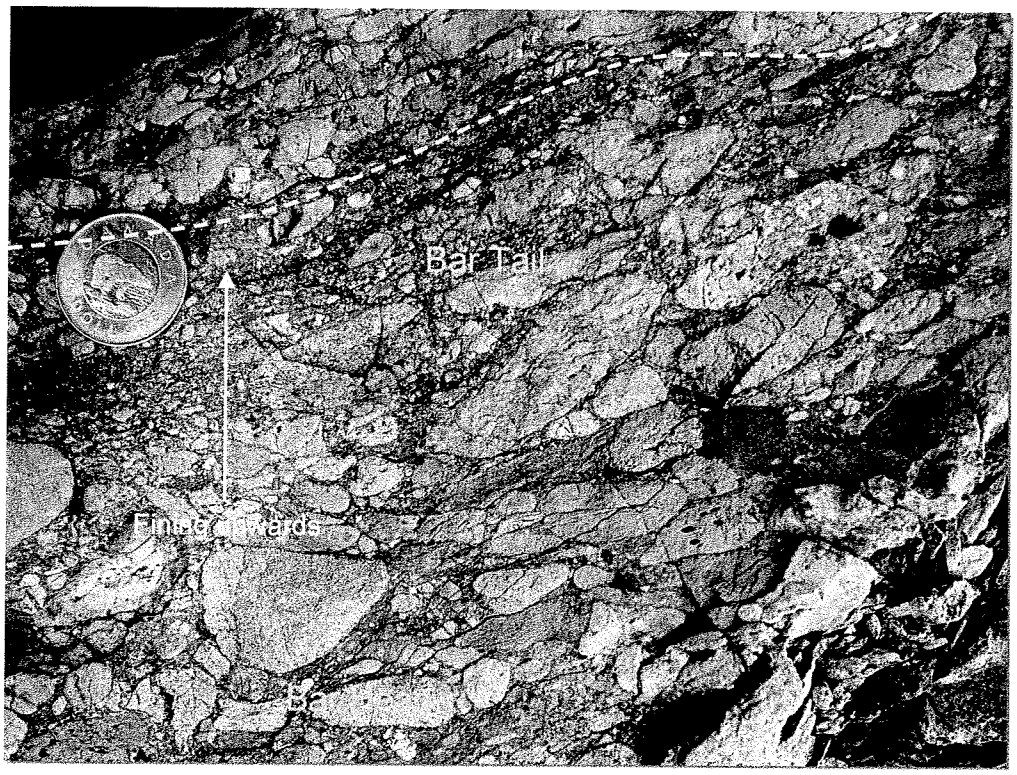

Figure 5.3 Interbedding of a coarse-grained pebble conglomerate with a finer-grained pebble conglomerate of lithofacies Gm representing a longitudinal bar formation with the coarser-grained facies most likely representing the bar head and the finer-grained facies most likely representing the bar tail.

The cobbles were moved and formed the initial deposits sedimented after the highest flood stage and greatest competency of the river to transport the coarsest bedload (Rust, 1972; Smith, 1974; Miall, 1977; Jones, 1989; Burton, 2003). Finer particles are trapped in the interstices of the initial deposit, and more bedload is deposited downstream, in the lee of the bar, so that growth continues (Rust, 1972; Smith, 1974; Miall, 1977). The continued growth in the lee of the bar is probably responsible for deposition of the pebble conglomerates. Pebble conglomerate layers are more likely to represent the bar tail, where a waning in flood stage is no longer able to transport the coarsest bedload of

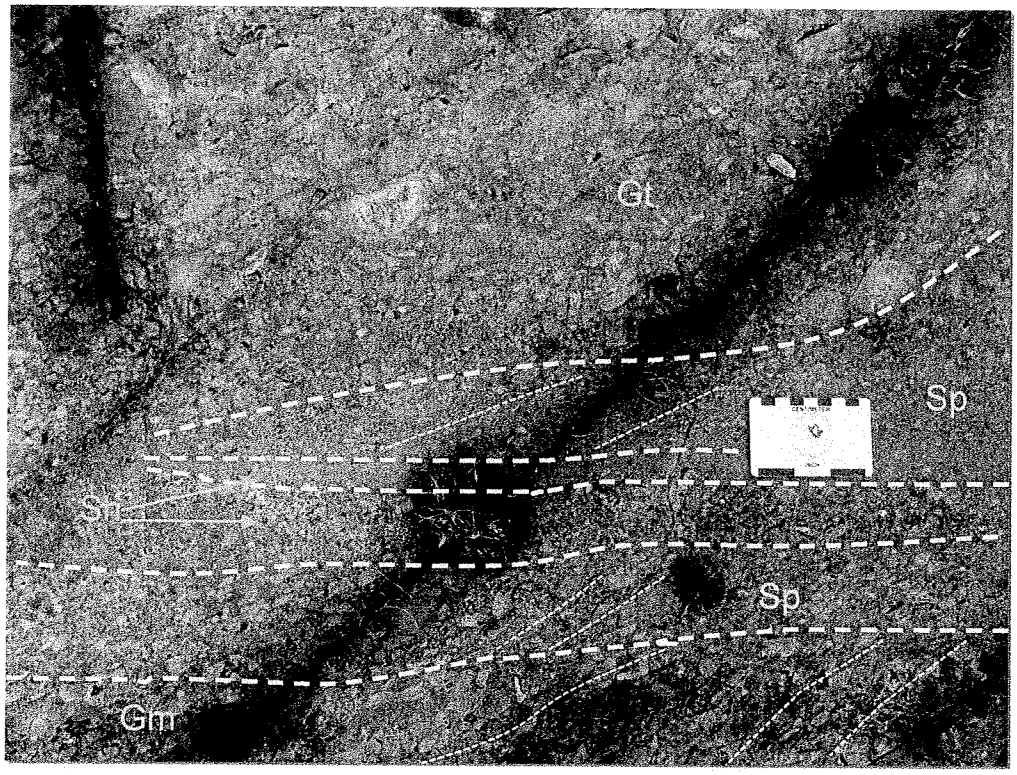

Figure 5.4 Picture of lithofacies Gm, Sp, Sh and Gt with Gm representing longitudinal bar deposition. Sp represents sand waves migrating over the longitudinal bar and being deposited on its top, whereas Sh represents planar bed deposition during upper flow regime and Gt is low stage dissection of longitudinal bar tops and remnants.

cobble sized clasts, whereas pebble sized clasts are still being transported as bedload. Smaller clast migrate over the initial deposit of the bar head where velocities are higher until a reduction in flow caused by the shielding effect of the more highly elevated bar center allows the system to no longer be able to transport the pebble sized clasts and deposition occurs on top of the bar tail (Rust, 1972; Smith, 1974; Miall, 1977; Jones, 1989; Reading, 1996; Burton, 2003). As velocity further drops, due to waning flow, pebbles may also be deposited on the bar head, but have lower preservation potential as they are susceptible to erosion during the next flood event.

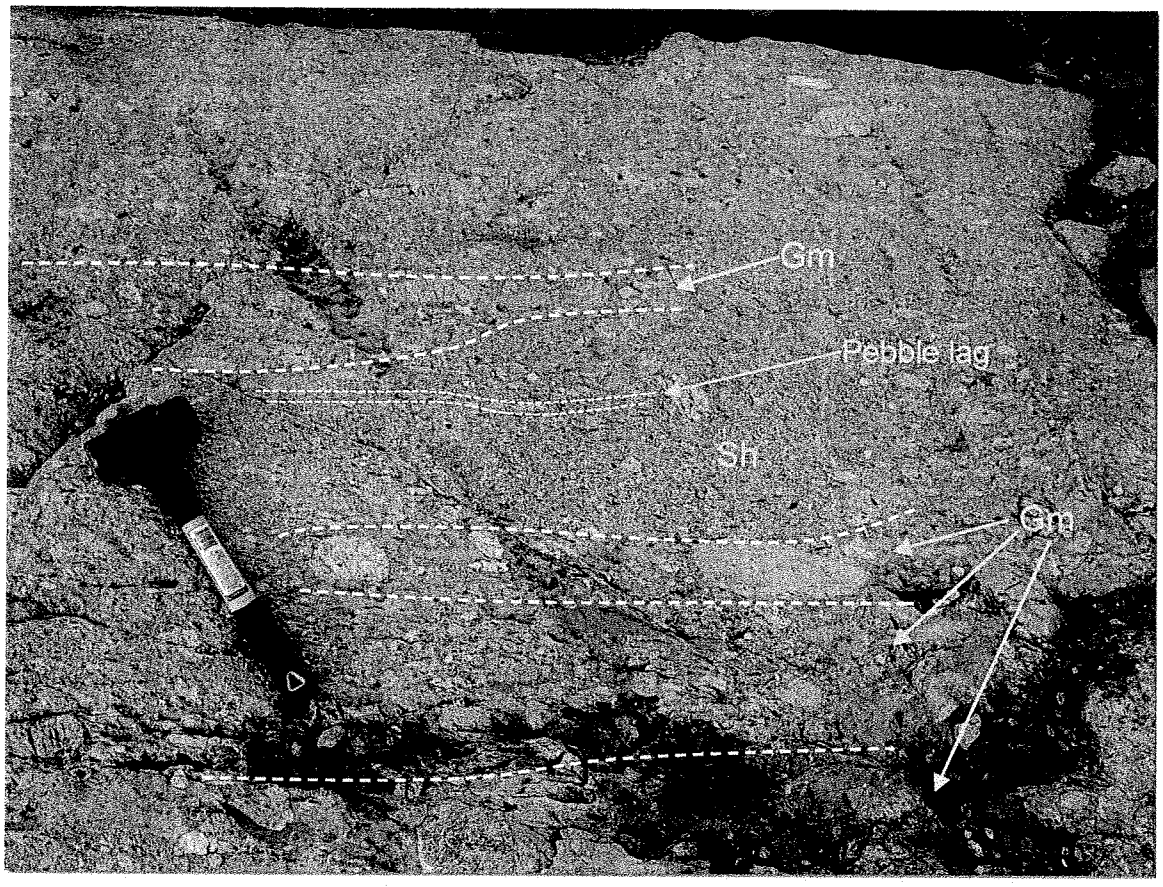

Figure 5.5 Lithofacies Sh interbedded with a clast-supported pebble to cobble conglomerate of lithofacies Gm. The interbedding of a pebble and cobble conglomerate represents longitudinal bar growth and the crudely horizontally bedded sandstone of Sh represents planar bed transport of sand in upper flow regime and deposition on the bar top. There is a minor pebble lag that could be the result of low stage dissection of the longitudinal bar top.

The association of finer lithofacies (Sh, Sp, Sr, Ss, and St) and occasionally trough cross-stratified conglomerates (Gt) is documented in the distal fan/proximal braided reaches of fluvial systems (Rust, 1978; Middleton et al., 1984). The former results during falling stage where the water is not flowing rapidly enough to transport the gravel load but still is capable of traction transport of coarse sand and granules (Middleton et al., 1984). Such conditions are common on bar tops as well as in channels (Bluck, 1979).

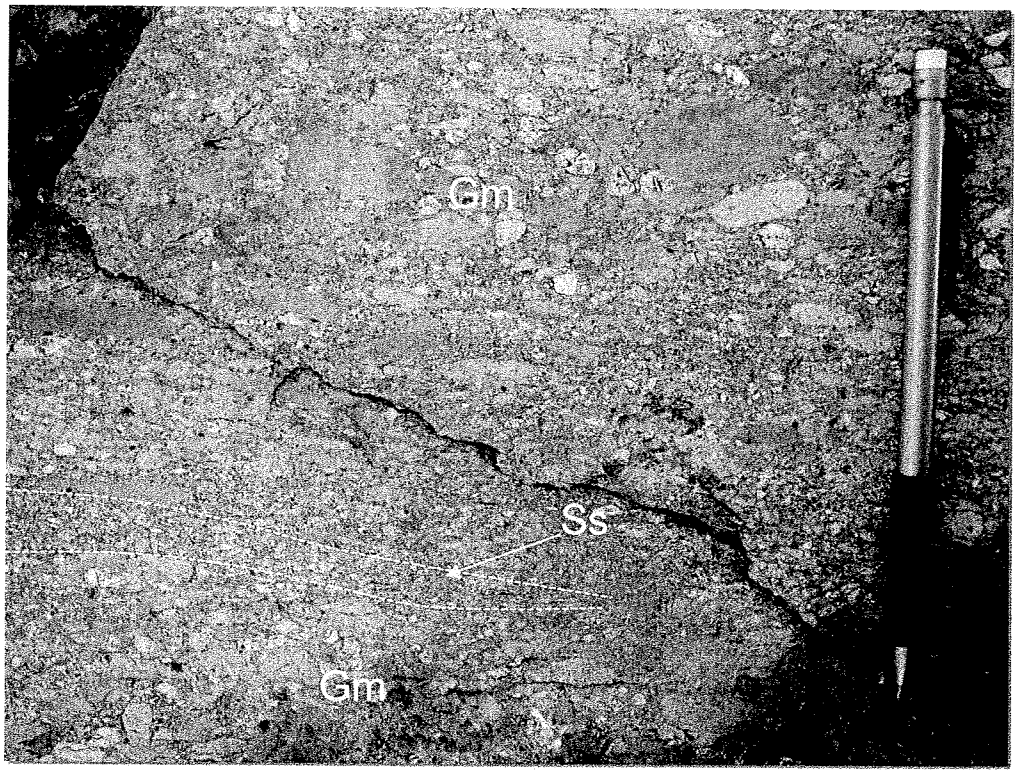

Figure 5.6 Lithofacies Ss interbedded with a massive to crudely horizontally bedded pebble conglomerate of lithofacies Gm. Lithofacies Ss represents low stage dissection of the longitudinal bar top creating minor scour hollows and channels with subsequent infilling during high stage by very coarse sand and granules.

Lithofacies Gt when identified consists of very shallow cross-bedding with lags that overlie an erosional surface and exhibit subtle fining upwards (Fig. 5.4). This lithofacies within Association Two represent low-stage dissection of the bar top and or front and subsequent in-filling of minor channels with rising stage (similar to interpretation put forward by Collinson, 1970).

Lithofacies St, having very low angle trough-crossbedding, is interpreted to represent both in-channel dune migration and in some cases dune migration across the tops of longitudinal bars, as described by Middleton et al. (1984) in the Scanlon Conglomerate.

Lithofacies Sh (Fig. 5.5), horizontally to crudely horizontally stratified sandstone, is interpreted as being the product of plane bed transport of sand over the bars during upper flow regime (Miall, 1977; Bluck, 1979; Middleton et al. 1984). Whereas, lithofacies Ss is interpreted as being the result of low-stage dissection of bar tops and remnants (Fig. 5.6), creating minor channels and scour hollows with subsequent infilling by material moving through them as the stage declines further (Bluck, 1979; Jones, 1989; Burton, 2003). There are a few wedge-shaped occurrences of lithofacies Ss that could be the result of the sand units building out in the lee of the longitudinal gravel bars (Rust, 1972; Boothroyd and Ashley, 1975) or as the infill of erosional channels as discussed previously (Boothroyd and Ashley, 1975).

The last of the fine-grained lithofacies Fl and Fm seen within Association Two are very rare. Lithofacies Fl and Fm are interpreted as thin silt or mud drapes and channel fills in inactive areas cut off from the main flow (Miall, 1977).

The most abundant lithofacies types within this association are Gm, Sh and St and the processes involved in their deposition are dominated by longitudinal bar formation within a braided fluvial system and would be classified as a "Scott type" under Miall's (1977) descriptions of braided river types. The Scott River consists mainly of longitudinal gravel bars with sand lenses formed by infill of channels and scour hollows during low water (Miall, 1977). As stated above, Association One lithofacies Gm is the result of debris-flow deposition, whereas in Association Two Gm is the result of depositional processes associated with longitudinal bar formation.

6.4. Lithofacies Association Three

Lithofacies Association Three occurs near the top of the Leadbetter Conglomerate and is characterized by a very sudden increase of very fine-grained sediment in the form of channel shaped fine-grained sandstone to thinly laminated sandstone, siltstone and mudstone.

The lithofacies types such as Fm and Fl will not be used in interpreting Lithofacies Association Three as the previous lithofacies descriptions were based on Miall's (1977) description of braided fluvial systems and it is unlikely that Lithofacies Association Three represents a braided fluvial system. Instead there is a brief description of the facies within Association Three and an appropriate interpretation of what Lithofacies Association Three represents.

Lithofacies Association Three is mainly characterized by an abundance of thinly bedded and laminated fine-grained sandstone, siltstone, mudstones and minor channel shaped fine to very fine-grained sandstones. Commonly the beds are normally graded, or more rarely inversely graded, from fine-grained sandstone to mudstone in the former and opposite with the later. They are parallel laminated with sharp planar contacts between individual beds. The mudstone and siltstone layers maintain a uniform thickness laterally along strike. The channel shaped fine-to very fine-grained sandstones are generally well-sorted and have a silt to mud sized matrix. The transition from Lithofacies Association Two to Association Three occurs within 2-4 meters defined by the layers of Lithofacies Association Two conglomerates being overlain by very

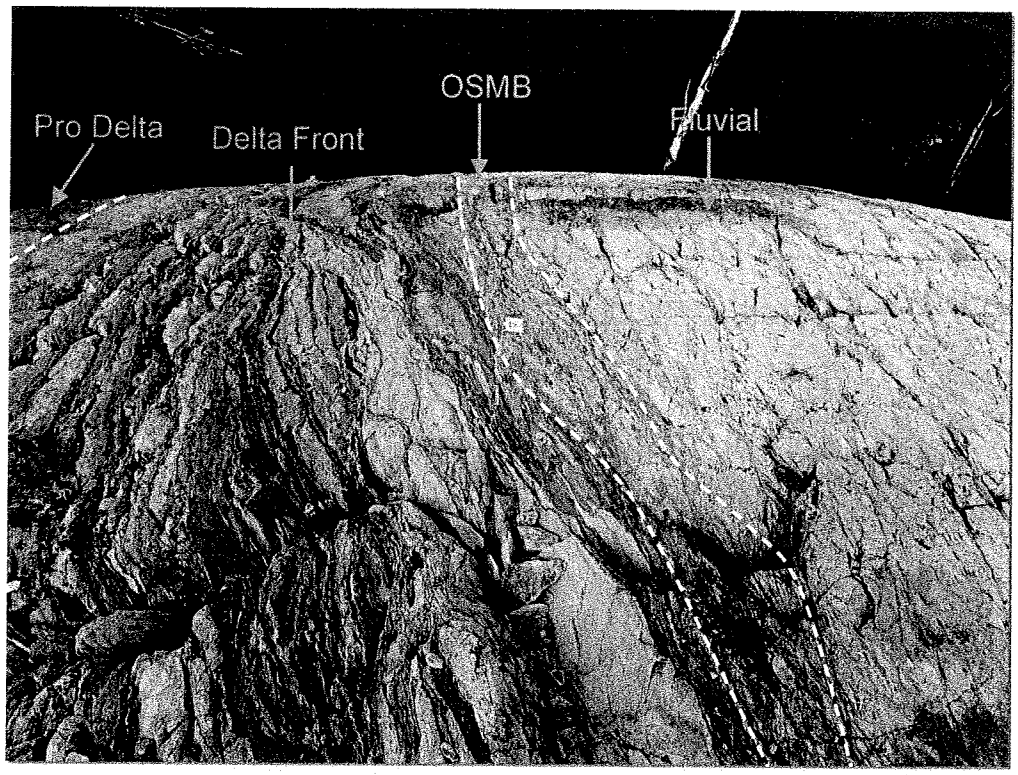

Figure 5.7 Picture showing the transition from lithofacies association two (fluvial conglomerates) into lithofacies association three with possible outer stream mouth bars (OSMB) and channel shaped fine-grained sandstones interbedded with siltstones and mudstones representing the delta front. Lithofacies association three very quickly retrogrades into a pro delta facies with thinly laminated and parallel bedded siltstone and mudstone along with thicker graded beds probably representing turbidite deposition.

subtle trough cross-bedded, fine to medium-grained sandstones that are abruptly overlain by fine-grained to very fine-grained channel shaped sandstones interbedded with thinly laminated very fine-grained siltstone to mudstone beds (Fig. 5.7). Overlying this is dominantly thinly laminated, laterally continuous siltstones and mudstones, which is transitional over two meters into a more mudstone-rich succession.

The subtle trough cross-bedded and thin massive to parallel bedded fine-grained sandstones that directly overlie the conglomerates of Association Two probably represent distributary mouth bars that were deposited within terminal

distributary channels (Fig. 5.7). Distributary mouth-bars described in the literature typically are trough cross-stratified sandy bars with shallow crests, and are cut by sub-aqueous channel levee systems, bordering offshore extensions of the channels (Reading and Collinson, 1996). Because of the stratigraphic location of the trough cross-bedded sandstones, overlying braided fluvial conglomerates and in turn being overlain by thinly laminated and parallel bedded siltstone and mudstone, they most probably represent the area where sediment-laden fluvial currents were interacting with a standing body of water.

Terminal distributary channels are formed within a delta at the very end of a distributary channel system and are intimately associated with mouth bars (Orton and Reading, 1993; Olariu and Bhattacharya, 2006). Mouth-bar deposits form as the flow condition at the channel mouth changes from confined to unconfined and velocity decreases (Albertson et al.1950; Bates, 1953; Wright, 1977). The decrease in velocity and rapid mixing at the river mouth results in immediate deposition of the coarsest part of the load (mainly fine sand) to form distributary mouth-bars (Klein et al., 1972; Orton and Reading, 1993). The initial mouth bar forms close to the channel axis and bifurcates the channel flow. In response to the bifurcating of the channel flow, new terminal distributary channels will be formed by extension of subaqueous channel levees, widening of the channel, and bifurcation of the flows because of mouth-bar formation (Olariu and Bhattacharya, 2006). The growth and migration of the mouth-bar both laterally and upstream accretion, will form terminal distrubutary channels at

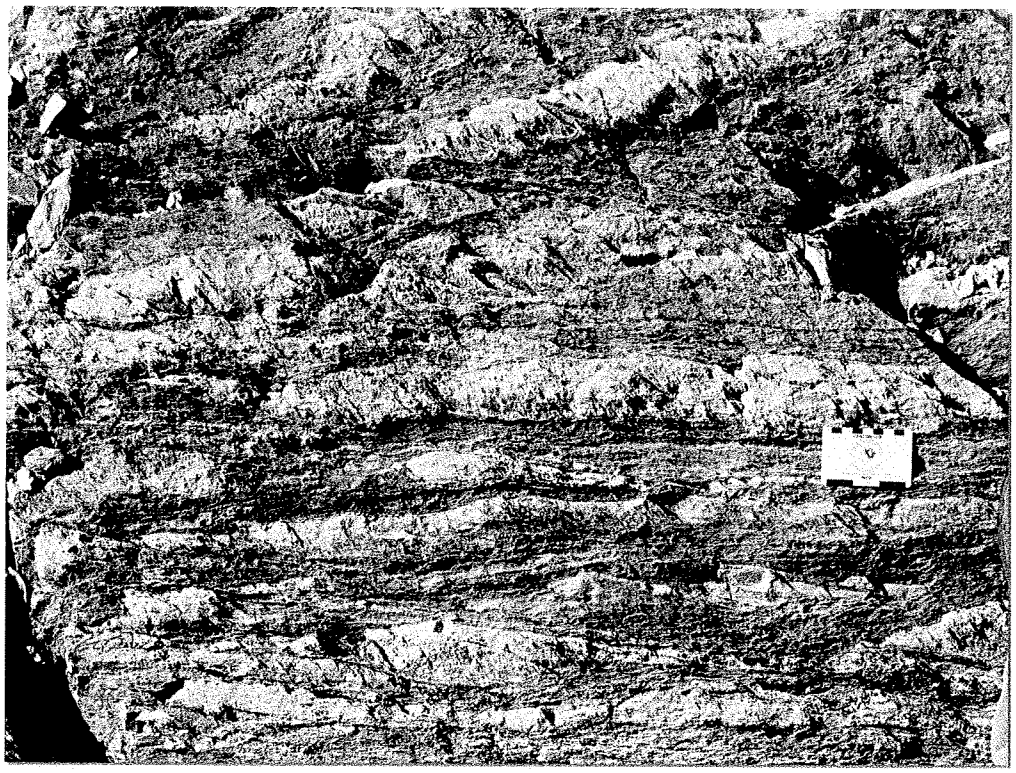

Figure 5.8 A close up picture of the lensoid and channel shaped fine-grained sandstones interbedded with thinly laminated and parallel bedded siltstone and mudstone representing the delta front of lithofacies Association Three.

different scales. Preferential mouth-bar accretion and filling of terminal distributary channels reduces the flow velocity and sediment discharge through that channel, which eventually is abandoned (De Vries Klein et al., 1972; Orton and Reading, 1993; Olariu and Bhattacharya, 2006). This is probably primarily represented in Lithofacies Association Three by the thin parallel bedded, massive, and more rarely graded, fine to very fine-grained sandstones, which were deposited in response to the deceleration and expansion of the river outflow resulting in the deposition of the fine-grained sandstone in the form of distributary mouth-bars. Distributary mouth bars are best developed where aqua-basinal processes are weak and fluvial processes predominate. The interbedding of

channel shaped fine to very fine-grained sandstones with siltstone to mudstone (Fig. 5.8) would represent flooding events where the river mouths were influenced more by frictional and inertial processes during high discharge depositing the fine to very fine-grained sandstones in the form of distributary mouth-bars and channels. During low discharge the river mouth was probably dominated by buoyancy processes depositing the thinly laminated and parallel bedded siltstone and mudstone (Wright & Coleman, 1974). The terminal distributary channels of the Leadbetter Conglomerate would be similar to modern deltas such as the Atchafalaya, Wax Lake and the Mississippi, except for the presence of vegetation. Ancient examples would include the Panther Tongue, Perrin and Ferron deltas.

The thinly bedded and laminated graded beds of fine-grained sandstone to mudstone that overlie the channel-shaped sandstones interbedded with siltstone and mudstone are interpreted to be turbiditic density flows as described by Bouma (1962). Although Bouma's (1962) classification of turbidites is describing mass flows due to slumping events, the turbidites within the Leadbetter are more likely the result from waning flow conditions after an increase in discharge from the river mouth during a flooding event (similar to processes discussed by Olariu and Bhattacharya, 2006). The Leadbetter Lithofacies Association Three turbities are similar to the ones described by Barton (1994) in the Turonian Ferron Delta, which has characteristic delta-associated turbidite deposits, including convoluted strata, massive and thin graded beds exhibiting sharp bases and incomplete Bouma sequences.

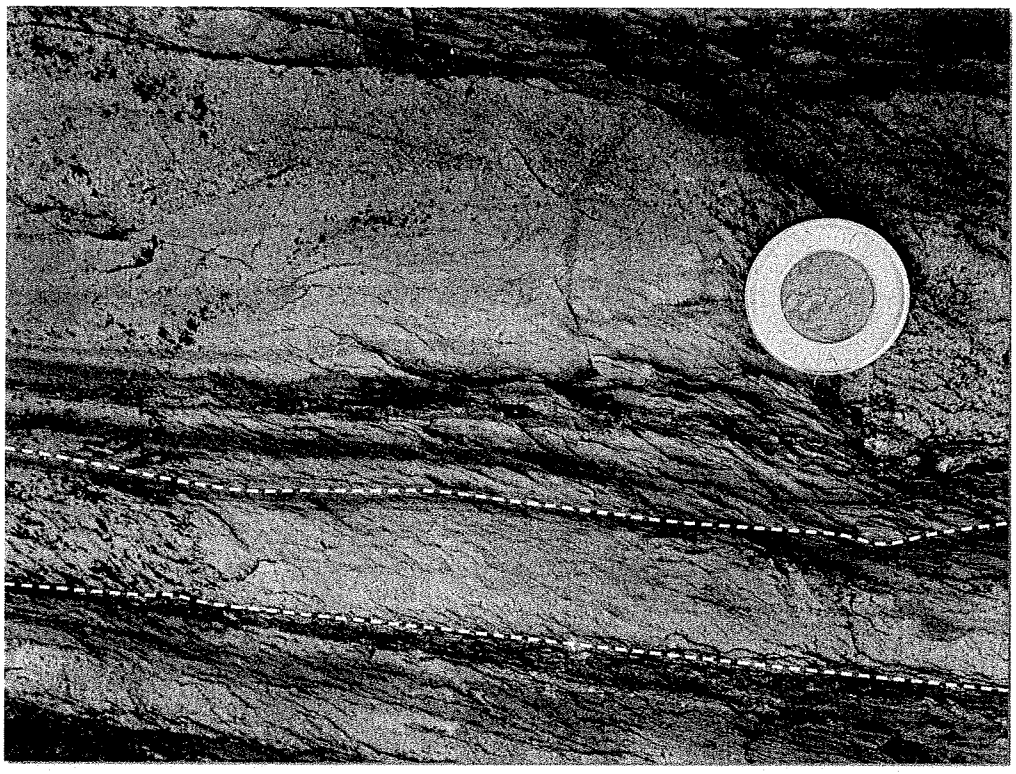

Fig. 5.9 The pro delta facies of lithofacies association three dominated by thinly laminated and parallel bedded siltstone and mudstone interbedded with medium and fine-grained graded sandstones.

The turbidite beds of Lithofacies Association Three are generally between 4 and 10cm thick with the thickest beds near the onset of the transition from the delta front to the pro-delta and a gradual decrease in thickness moving up section. At the outcrop-scale individual beds can be traced laterally without appreciable thickness changes. The layers are commonly composed of the D and E divisions of Bouma (1962). They are characterized by very fine-grained, parallel laminated sandstone and siltstone grading to mudstone. Some beds have a basal unit of massive graded medium to fine sandstone. There were a couple of occurrences where the author observed ripple cross-lamination.

There is a gradual upsection thinning in the basal medium-and fine-grained sandstone portions of beds with a change to thicker siltstone and mudstone portions representing divisions D and E. This is interpreted as a progression into a more distal pro-delta facies with an increase in depth of water and less influx of coarser-grained material.

In summary, Lithofacies Association three probably represents the transformation of the depositional environment from a braided fluvial depositional system within an alluvial fan to a sub-aqueous pro-delta facies. The subtle trough cross-bedded sandstones being distributary mouth bars and the channel shaped sandstones interbedded with thinly laminated siltstone and mudstones representing distributary channels cutting the delta front (Fig. 5.8). Thin beds of turbidites and thinly laminated siltstone to mudstone characterize the pro-delta (Fig. 5.9).

An interesting note of this transitional zone from Lithofacies Association Two to Lithofacies Association Three is the abrupt and fast transition into the pro-delta facies within 2-6 meters. This is interpreted to be the result of a marine or lacustrine environment that quickly transgressed landward and drowned the braided alluvial fan depositional system turning it into a sub-aqueous environment for density flow deposition.

5.5. Summary of the Depositional Environment

Interpretation of the lithofacies associations indicates the Leadbetter Conglomerate represents a high-energy alluvial fan delta succession. For

classification purposes the Leadbetter Conglomerate would fall under a "Scott" type braided fluvial system.

Lithofacies Association One is dominated by weakly sheared and highly viscous debris-flows and represents the upper reaches of the alluvial fan. Association Two is dominated by superimposed longitudinal bars that represent the transformation of the depositional environment to a mid-fan and lower-fan to proximal braided system. Association Three is represented by a transgression and transition to delta front and subsequently pro-delta environment characterized by thinly bedded and graded turbiditic density flows with locally interbedded sandstones that may represent distributary channel mouth bars and flood events with sediment laden stream flow out of the river mouth into the basinal environment.

As stated previously an important feature of the transitional zone from Association Two to Association Three of the Leadbetter Conglomerate is the very abrupt change from braided fluvial dominated facies to a sub-aqueous pro-delta facies implying that there was quick landward transgression of the marine or lacustrine environment that suddenly had a drowning effect on the braided alluvial fan depositional system. The area eventually became a deep-water depositional system with dominantly thinly laminated argillite facies forming throughout the region (Rice and Donaldson, 1992).

Chapter 6

Clast Lithologies

6.1. Introduction

The identification of lithologies that make up the clastic material of the Leadbetter Conglomerate was completed during the fieldwork portion of this study. Pebble counts of the lithologies (Table 6A) were undertaken to: (1) identify the types of lithologies present within the Leadbetter Conglomerate; and (2) to determine if there were any changes in the abundances of lithologies within the Leadbetter Conglomerate. Work was conducted from the base of the succession to the upper part of the succession.

6.2. Clast Lithologies

There were six major types of lithologies identified within the Leadbetter Conglomerate: (1) mafic volcanic (i.e. basalt to intermediate); (2) felsic volcanic (i.e. intermediate to rhyolite); (3) gabbro (or mafic intrusive equivalent); (4) diorite (or intermediate intrusive equivalent); (5) sandstone; and (6) chert (including quartz). Seven outcrops with good exposure were included in the study. Pebble counts were performed on these exposures, which were spaced apart vertically to give a representative sampling from the base to the top of the succession.

Location (up section)	Mafic Volcanic	Felsic Volcanic	Gabbro	Diorite	Sand Stone	Chert	Total
330 meters	19%	65%	5%	2%	5%	4%	100%
317 meters	25%	44%	0%	12%	9%	10%	100%
273 meters	43%	38%	0%	3%	13%	2%	100%
172 meters	50%	35%	0%	3%	5%	7%	100%
153 meters	76%	0%	16%	0%	0%	8%	100%
109 meters	16%	21%	25%	0%	35%	3%	100%
10 meters	86%	0%	1%	0%	0%	13%	100%

Table 6A. The results from seven pebble counts with location referring to the meters up section starting from the base of the succession (0m).

One important observation is the change in percentage of mafic to felsic rock types. Mafic rock types are more abundant near the base of the succession whereas felsic rock types are more abundant near the top of the succession.

6.3. Summary of Clast Lithologies

In general, mafic rock types are more susceptible to chemical weathering and break down faster during bedload transport processes than felsic rock types (Anirban and Krishnaswami, 2007). One possible explanation for the distribution of clast types is that the lower part of the Leadbetter Conglomerate (lithofacies Association One) represents the upper reaches of the alluvial fan-proximal braided system that is dominated by weakly sheared and highly viscous debris flows and few grain-to-grain bedload collisions have occurred. This would allow for mafic rock types to more likely be preserved and deposited due to lesser amounts of exposure to chemical and mechanical weathering processes. The middle and upper parts of the succession (lithofacies Association Two) represent the mid-fan and lower-fan proximal braided system that is dominated by superimposed longitudinal bars and clastic material that has migrated further

downstream as bedload and has undergone reworking by fluvial activity. Felsic rock types contain greater abundance of Si-rich and Mg + Fe poor minerals, which causes them to be more resistant to chemical and mechanical weathering processes. As source material is being eroded and transported downstream there will be a preferential increase in felsic rock types being preserved and deposited. As a consequence, felsic rock types will become more abundant while mafic rock types will erode and break down much faster from chemical and mechanical weathering processes.

The source area was dominated by mafic volcanics and associated gabbros with, subordinate felsic volcanics and diorites, but interestingly no granitic rocks, which indicates that erosion levels were not very deep.

Chapter 7

Whole Rock Geochemistry

7.1. Introduction

Twenty coarse-grained sandstone samples collected in the field were analysed by whole rock geochemistry methods to investigate: element immobility, degree of chemical weathering, provenance, degree of enrichment in heavy minerals, and possible source rocks for the diamonds.

All sandstone samples were taken from either a coarse-grained sandstone lens or the coarse-grained matrix of a pebble to cobble conglomerate. Major elements were measured by ICP-AES while trace and REE's were measured by ICP-MS as described in the methodology chapter. For elemental results refer to Appendix B. Dianor Resources data is from one ton bulk samples and analysed by ICP-MS and ICP-AES. Due to a confidentiality agreement between the author and Dianor Resources, a complete table of results is not presented. Dianor Resources data was used to compare results with the authors data to ensure accuracy and consistency. In the source of diamonds section, some select samples, with diamond content data (carats per ton), were used to evaluate possible source rock types.

Element mobility was assessed using techniques described in Fralick and Kronberg (1997) and Fralick (2003). A chemical index of alteration (CIA) developed by Nesbitt and Young (1984) and described by McLennan and Murray (1999) was used to evaluate the degree of chemical weathering and its effect on

major-element compositions. Ratio plots of immobile element pairs described by Fralick (2008) are used to assess provenance. Another ratio plot adopted from McLennan and Murray (1999) using trace elements was used to investigate the existence of placer accumulation and heavy mineral enrichment as a result of sediment sorting. Investigation of possible source rocks for the diamonds was conducted by comparing known diamond grades from Dianor Resources to inherently unique elements of suspected and common diamond-bearing rock types, (e.g., Cr and V) of diamondiferous lamprophyre dikes and kimberlites (i.e., higher grades should have more diamond bearing rock material which should have some form of geochemical trait).

Discussion of Results

7.2. Element Immobility

Ascertaining provenance of sand-sized material in ancient sedimentary systems is generally difficult because of chemical and physical modification of source materials during weathering, erosion, transport and deposition (Johnsson, 1993). Further compositional changes may occur prior to, as a result of, and during sediment burial and removal from surficial environments, resulting from the isolated or combined effects of lithification, diagenesis, metamorphism and hydrothermal alteration (Fralick and Kronberg, 1997).

The major problem in using sediment geochemistry to infer source area composition is establishing which elements are immobile (Fralick and Kronberg,

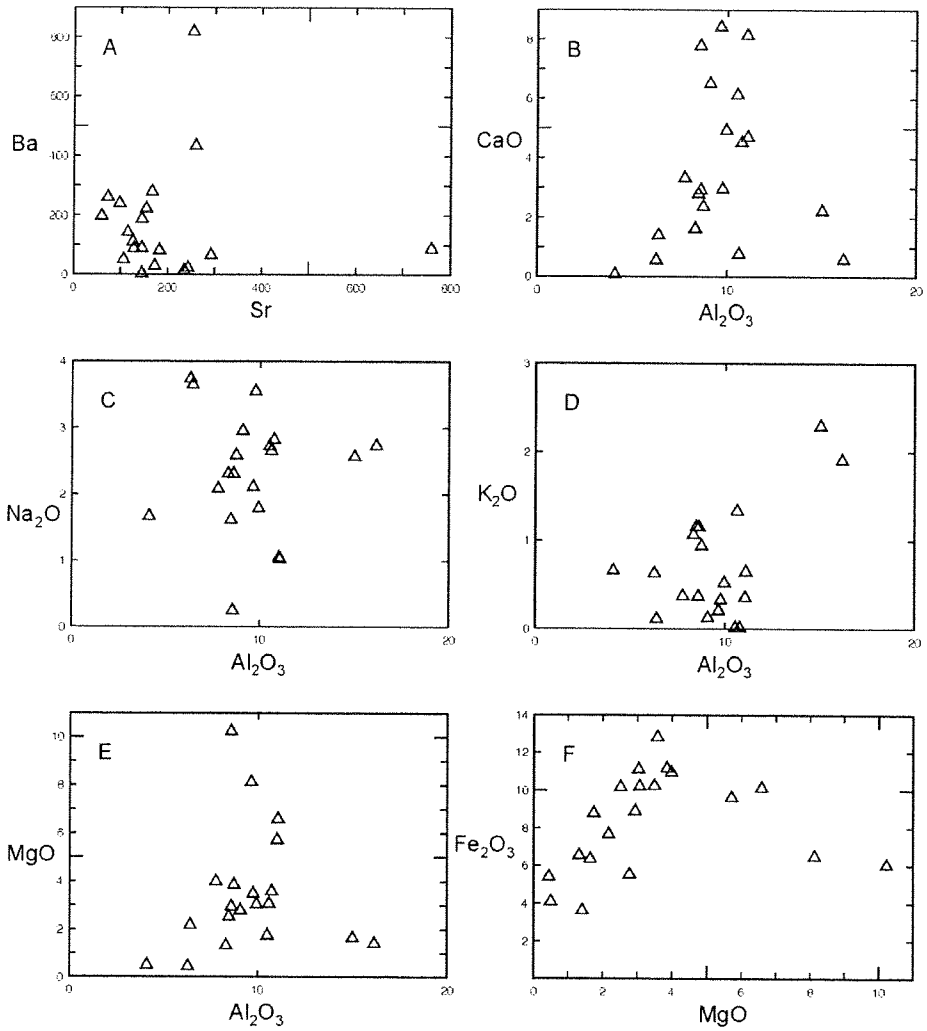

Figure 7.1. Element pairs plotted against each other to test for element immobility. The elements Ba, CaO, Na_2O, K_2O, MgO and Fe_2O_3 all display a scatter of data points indicating that they are mobile during alteration.

1997). The first method of testing element immobility involves plotting pairs of elements, which are suspected of being immobile, e.g., Al, Ti, Zr, Nb, and Y (Fralick, 2003). When multiple sediment samples from the same source terrain are plotted, one of two patterns will develop, depending on chemical immobility and the hydrodynamic behavior of the major mineral phases containing the elements (Fralick, 2003). If both elements plotted were immobile and their major

mineral phases hydrodynamically similar an alignment will develop that trends toward the origin (Fralick, 2003).

Plots shown in Figure 7.1 (A-F), all display a scatter of data points except Ba and Sr, which show a clustering of data points around the point of origin. The apparent clustering is simply the result of having two outlying data points that cause the rest of the data to bunch near the origin. The scatter plots indicate Ca, Na, and K were chemically mobile with some samples having very low concentrations for these elements. Nine of the samples on the K_2O/Al_2O_3 graph define a line extending from the origin, whereas the rest have lower K_2O/Al_2O_3 ratios. The lower K_2O/Al_2O_3 ratios could be due to the removal of K_2O as a result of chemical weathering, or a source with a lower K_2O/Al_2O_3 ratio. Chemical, weathering of feldspars prior to deposition can account for CaO, Na_2O, K_2O, and Sr trends, as CaO, Na_2O and Sr are lost to the weathering solutions and K_2O is commonly retained on clays (Sawyer, 1985). Scattered data points on plots of such elements further show the chemically mobile nature of these elements and discounts their reliability as proxies for determining provenance source compositions.

MgO plotted against Al_2O_3 and Fe_2O_3 shown in Figure 7.1 (E) and (F) shows a scatter of points with four points displaying MgO enrichment relative to the others. This may be due to the addition of a dolomite cement or possibly reflects a more Mg rich source for these samples, an implication that will be discussed in a later section.

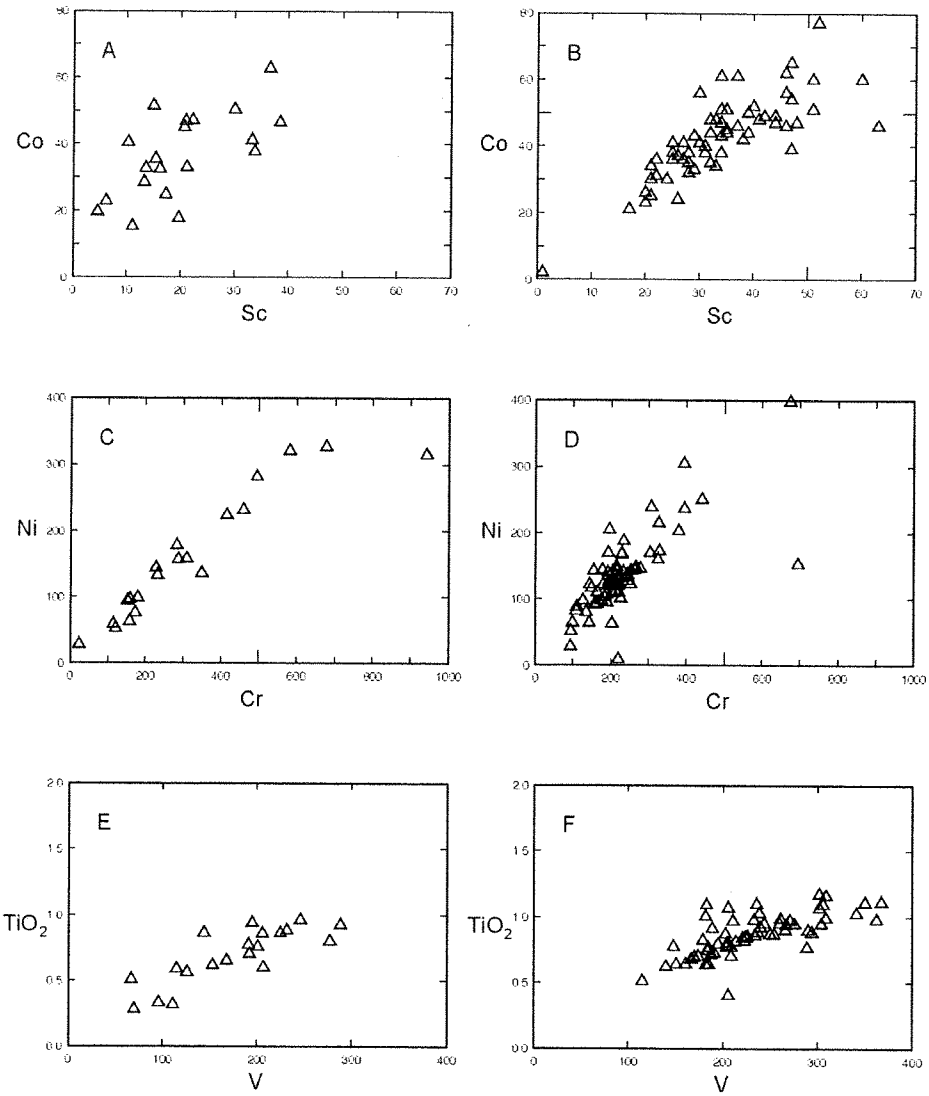

Figure 7.2. Element pairs plotted against each other to asses element immobility. Plots B, C, D, E, F and to a much lesser extent A all trend towards the point of origin implying that they are behaving in a chemically immobile manner.

Plots of Ni, Cr, TiO_2 and V shown in Figure 7.2 (C and E) display a linear array of data points all trending towards the point of origin. The consistent and linear nature of the data points show that Ni, Cr, Ti and V are chemically immobile. Co and Sc in Figure 7.2 (A) display a somewhat linear array but with some deviations from linearity to the point of origin. The scatter around an

imagined line through the cluster of data and the origin may be caused by minor differences in source material, or hydraulic fractionation of the main mineral phases containing Co and Sc (Fralick, 2003). To asses further the chemical immobility of these elements, similar plots (Fig. 7.2, B, D and E) of the same pairs of elements were undertaken using geochemical data obtained from the property (Dianor Resources). As shown in Figure 7.2 (B), (D) and (E) all graphs exhibit a linear array of data points trending towards the point of origin further confirming that the elements Ni, Cr, TiO_2 and V were chemically immobile.

Yttrium plotted against Al_2O_3, and Sc (Fig. 7.3 A and C) all display a very weak linear trend towards the point of origin with the exception that Y and Al_2O_3 trend towards a minor Al_2O_3 enrichment above the point of origin. Plots undertaken with Dianor Resources data are shown in Figures 7.3 (B), and (D) display a clustering of data points rather than a linear array. This clustering of data points can be explained by the main mineral phases containing Y, Al_2O_3, and Sc behaving in a hydrodynamically similar manner and showing no mass loss or gain due to this behavior. The important note is that the data points are grouped rather than scattered and may reflect chemical immobility with the scatter produced by different hydrodynamic behavior of their mineral phases.

Nb plotted against Zr shown in Figure 7.3 (E) displays a linear array of data points with a few very minor deviations showing that they are of a chemically immobile nature. A similar plot of Nb and Zr (Fig. 7.3F) with Dianor Resources data displays similar results.

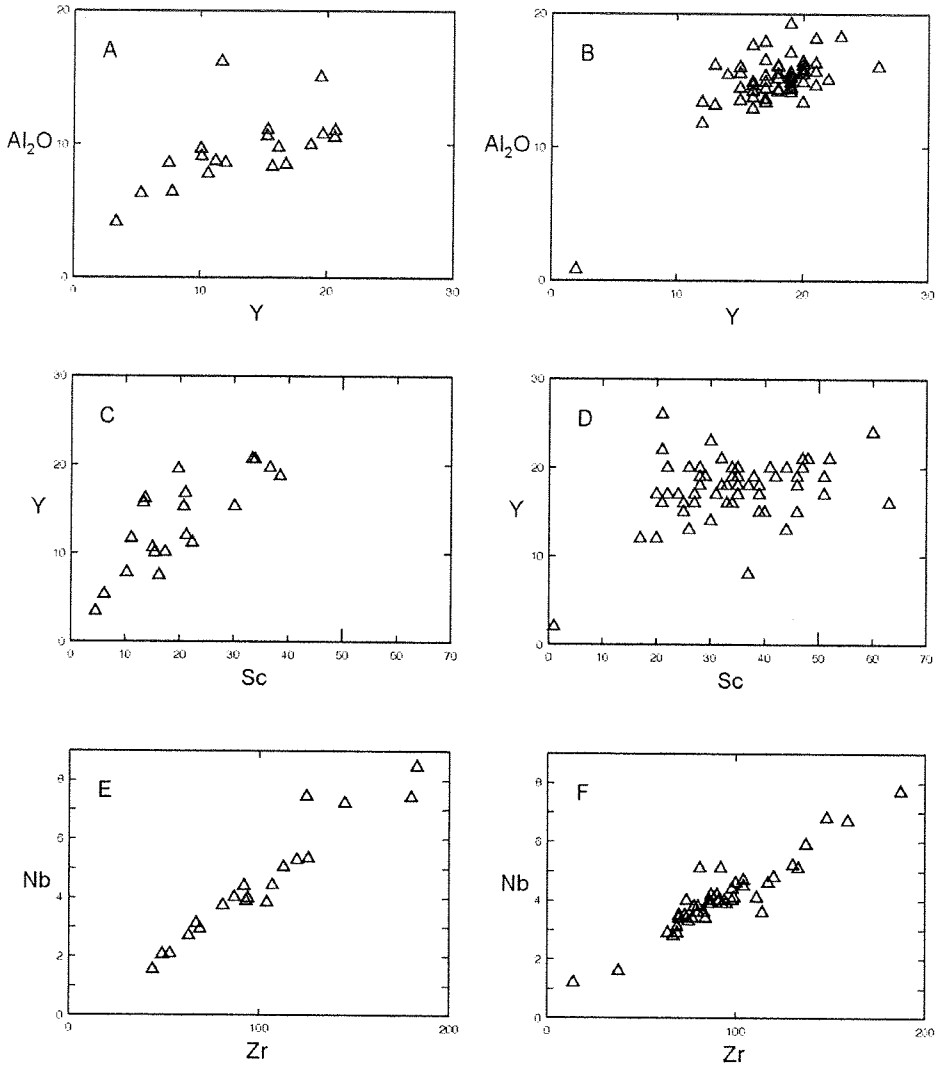

Figure 7.3. Element pairs plotted against each other to asses element immobility. Plots A, B, C, D, E and F all trend towards the point of origin implying that they are all behaving chemically immobile.

K_2O plotted against Ba shown in Figure 7.4 (A) displays a linear array of data points trending towards the point of origin. K_2O and Ba are known to behave in a chemically similar manner and are generally retained on clays (Sawyer, 1985). The linear array of points may correlate to similar mass loss or gain between two chemically similar elements rather than K and Ba being chemically immobile. As Fralick (2003) points out, if elements that behave in a

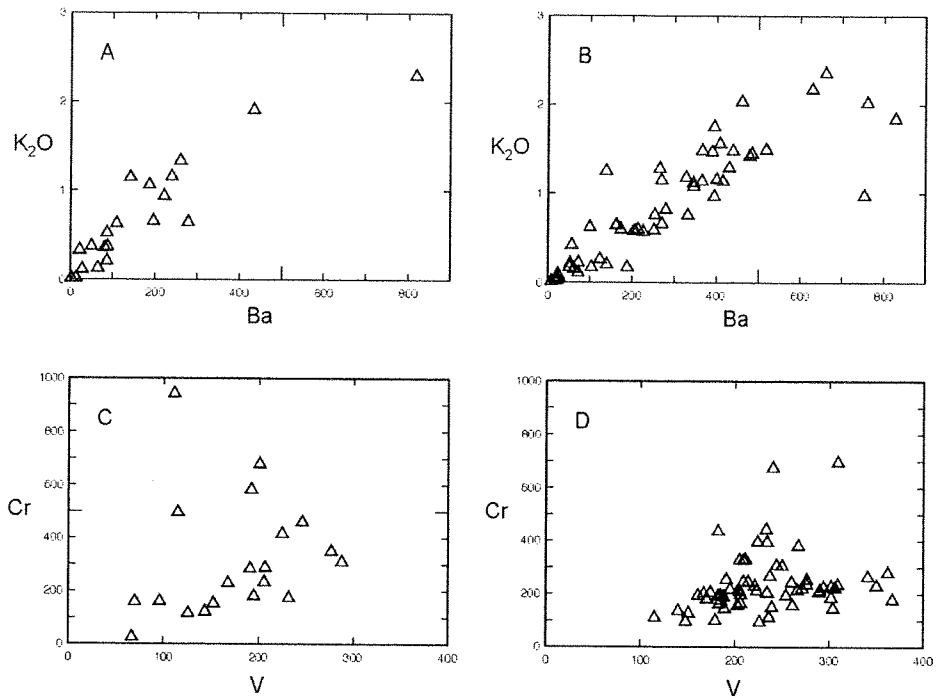

Figure 7.4. Element pairs plotted against each other to asses element immobility. Plots A and B have a trend of data points towards the point of origin implying that they are behaving chemically immobile. Plots C and D have a very subtle trend of data points towards the point of origin with some scatter of data points.

very chemically similar manner are plotted against one another, a linear relationship should develop even if the elements have been chemically mobile. K_2O and Ba enrichment is probably a response to an increase in clay.

Cr plotted against V shown in Figure 7.4 (C) has two trends, one is a linear array of points trending towards the origin, and the other is a few points that show Cr enrichment. As Cr is an incompatible and chemically immobile element, the Cr enrichment is likely related to a difference in source material rather than chemical mobility.

When Hf and Ta are plotted against Zr (Fig. 7.5 A and C) they both display a linear array of data points trending towards the point of origin suggesting that

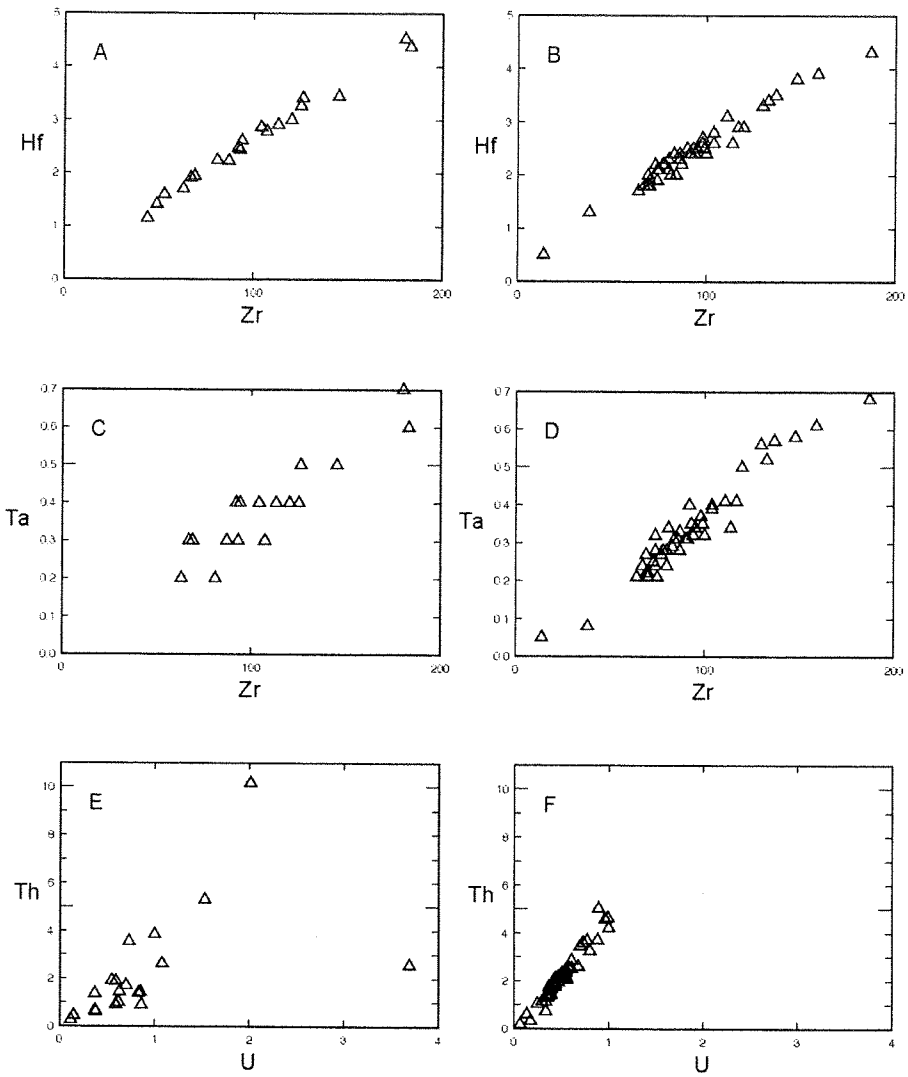

Figure 7.5. Element pairs plotted against each other to asses element immobility. Plots A, B, C, D, E and F all trend towards the point of origin implying that they are all behaving chemically immobile.

they are chemically immobile. Note that Ta plotted against Zr on Figure 7.5 (C) has a horizontal alignment of data points due to measurements in 0.1ppm increments but with company data plotted (Fig. 7.5D), which has a lower measurement increment, the data correlate better forming a linear array of data points trending towards the point of origin, further supporting the chemical immobility of Ta and Hf. Also note that Hf and Zr are primarily incorporated into

zircon and that their ratio in sediments should be constant if all major source rocks containing a significant amount of zircon have a similar ratio or their mixing ratio in the sediment was consistent.

Th plotted against U as shown in Figure 7.5 (E and F) also fits the criteria for these elements being chemically immobile, as it displays a linear array of data points all trending towards the point of origin. One exception is sample number 002-072908 which has enrichment in U. The cause for U enrichment could be due to preferential accumulation of the very dense U-bearing phase uraninite or a nugget effect where the presence of a uraninite grain causes the U concentration to be high due to the otherwise low abundance of U in the samples.

The effects of weathering on the geochemistry of the sandstone samples can also be evaluated using the chemical index of alteration (CIA, Nesbit and Young, 1982). Fresh basalts have CIA values of approximately 0.45, rhyolites 0.50 and secondary clay minerals 0.75-1.00 (Nesbit and Young, 1982). For comparison with sandstones from other Superior Province sedimentary units: the average of the Archean Conley quartzite which has undergone little weathering is 0.52; the Huronian Supergroup with moderate weathering is 0.57, and the Baraboo quartzite with extreme weathering is 0.76. The majority of the sandstone samples range from 0.47-0.76 with an average CIA value of 0.59 indicating that the majority of the samples have undergone moderate chemical weathering with three samples ranging from 0.69-0.76 and showing extreme chemical weathering resulting in considerable depletion in CaO, K_2O and Na_2O, which are susceptible to going into solution. Plots previously presented indicate

other major and minor elements show a minor degree of alteration and the scatter they exhibit is probably more of an affect from sediment sorting, and difference in source rock material.

7.3. Provenance

The distribution of a number of trace elements in terrigenous sedimentary rocks is especially sensitive to the nature of the provenance (McLennan et al., 2003). This is because during most sedimentary processes elements such as Al, Fe, Ti, Mn, Zr, Hf, Nb, Sn, Cr, Ni, V, Co, Y, Sc and the rare-earth elements (La-Lu) are strongly retained in particulate material and not released to solution (McLennan et al. 2003). Analysis of the Leadbetter sandstone samples shows that the elements Co, Ni, Sc, Cr, TiO_2, V, Al_2O_3, Y, Nb, Zr, Hf, Ta, Th and U are immobile, and will be used to investigate further the provenance. The elements Ba, Sr, CaO and Na_2O are found to be very mobile while the elements K_2O, MgO and Fe_2O_3 are found to be somewhat mobile and will not be used to investigate possible provenance.

Since Ni, Al, Cr, V, Zr, Ti and REE's are found to be the most immobile elements they will be used to further investigate provenance source rock composition. The compositions of the sandstones will be investigated using ratio plot techniques described by Fralick (2003) and a ratio plot developed by Winchester and Floyd (1977). REEs will be plotted using Sun & McDonough (1989) chondrite normalizing factors to help further assess the provenance geochemistry. Suspected volcanic source rock compositions will be plotted

using data gathered from various authors (Wyman et al., 1989 and 2006; Sage et al., 1996; and Stone, 2004) from previous work done on the Michipicoten greenstone belt (MGB).

Whole rock geochemical data for the possible volcanic source rocks can be found in Appendix B, and rock type codes are as follows. MVC1, MVC2, and MVC3 are mafic volcanic cycles 1, 2, and 3 as described by Sage et al. (1996). One important note is that MVC1 is classified as a komatitic basalt with elevated Mg-number (0.51-0.83) compared to cycle 2 and 3 tholeiites (Mg-number 0.44-0.56). FVC1, FVC2, and FVC3 are felsic volcanic cycles 1, 2, and 3 as described by Sage et al. (1996). Heterolithic breccias, Sandor dike, and xenolith rich dike are described as being composed of lamprophyric compositions and for further discussion and details refer to Stone (2004). Wawa lamprophyres and Wawa diamondiferous-matrix are lamprophyres described by Wyman et al. (2006), and Wyman and Kerrich (1989). All potential source rocks lie within the MGB and are within 20 Km of the study area. In addition kimberlite compositions from the Jericho Pipe, N.W.T (Price et al., 1999), and average compositions of group I and group II kimberlites of South Africa (Becker and Le Roex, 2005) were also plotted.

A ratio plot (Fig. 7.6A) between Ni, Al, and Cr nicely divides the MGB volcanic rocks into three distinct fields of felsic, mafic, and ultramafic rocks with higher Cr and Ni values in ultramafic rocks, and lower Cr and Ni values in the felsic rocks. A majority of the Leadbetter sandstone samples clearly plot on a

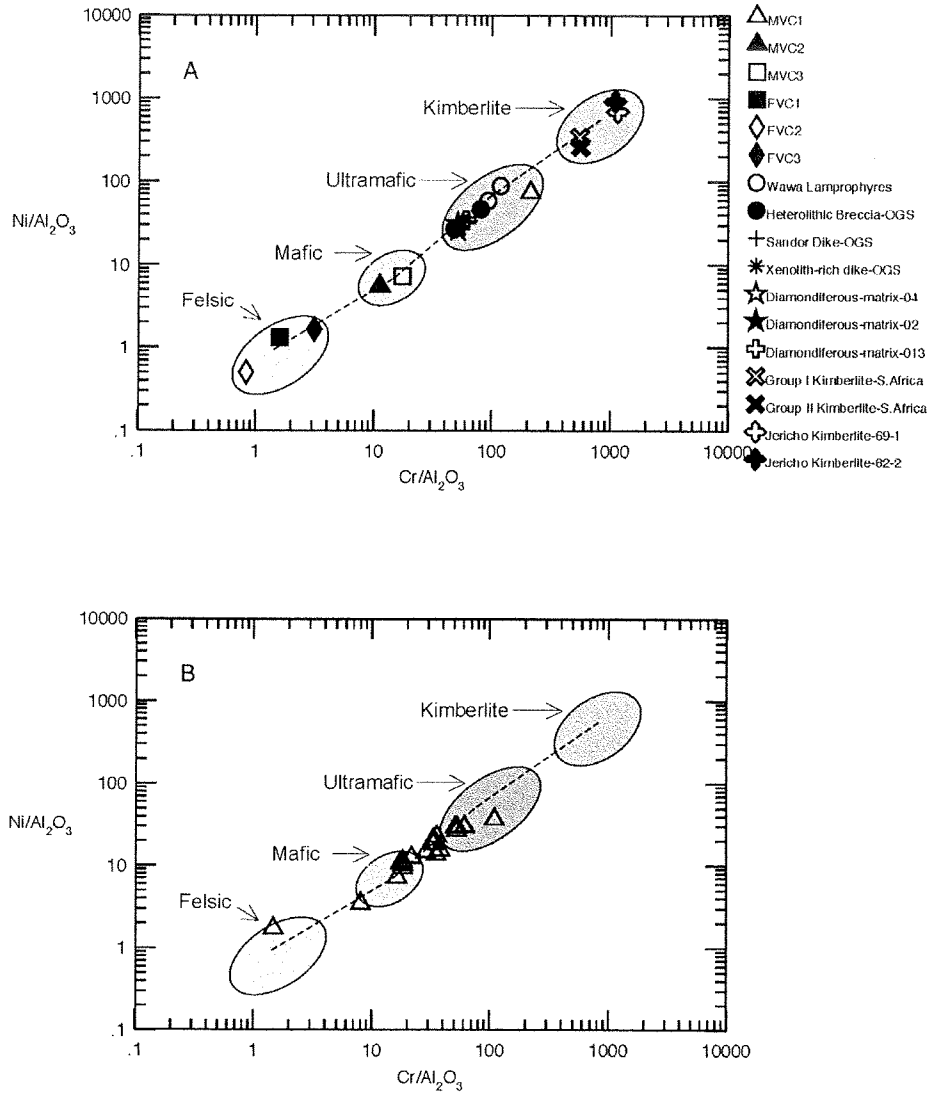

Figure 7.6. Ratio plot between Ni, Al and Cr that divides the MGB volcanic rocks (A) into three distinct fields of felsic, mafic and ultramafic. Leadbetter samples ploted (B) to compare against the MGB volcanic rocks and to assess possible provenance.

mixing line between the kimberlite plus the ultramafic rocks and the mafic plus felsic volcanic rocks with two plotting much closer to the felsic volcanic rocks (Fig. 7.6B). This would imply that a significant amount of the sediment is being derived from mafic and ultra-mafic source rocks and possible kimberlite source rocks. In order for Cr and Ni values to plot outside of the mafic field, towards Cr

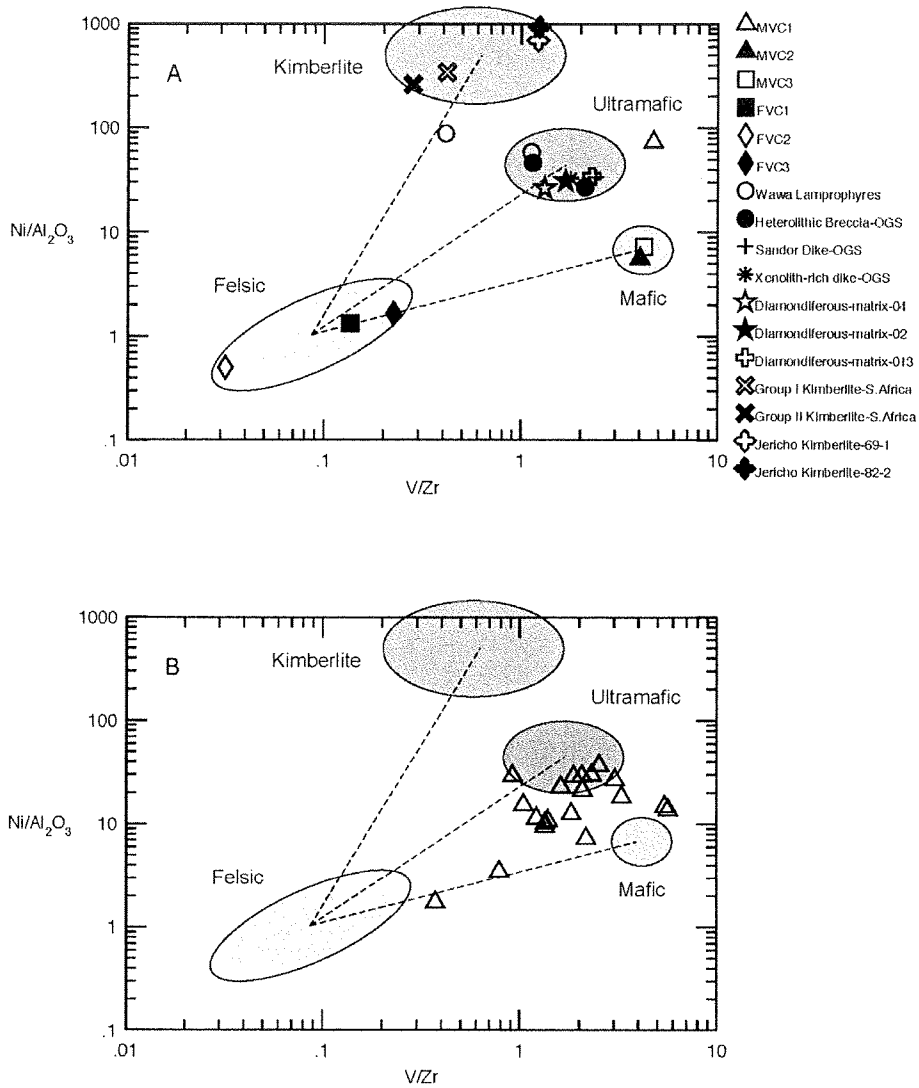

Figure 7.7. Ratio plot between Ni, Al, V and Zr developed by Fralick et al. (2008) that divides the MGB volcanics (A) into four distinct groupings, felsic, mafic, ultramafic lamprophyres and kimberlites. Leadbetter samples plotted (B) to compare against the MGB volcanic rocks and to assess possible provenance.

and Ni enrichment of the ultramafic field, there must be significant ultra-mafic derived sediment contributing to the depositional environment. Another possibility is that there was a significant amount of heavy mineral accumulation that contained Cr and Ni (see below).

A ratio plot (Fig. 7.7A) between Ni, Al, V and Zr developed by Fralick et al. (2008) divides the MGB volcanics into four distinct groupings, felsic, mafic, ultramafic lamprophyres, and kimberlites. When compared to the MGB volcanic rocks, the Leadbetter samples plot in the triangular area defined by the ultramafic, mafic and felsic end members (Fig. 7.7B). This denotes mixing between mafic, ultramafic and felsic source rock compositions. It can be assumed that all three variables of mafic, ultramafic and felsic MGB igneous rocks play a role in contributing sediment to the depositional environment. Most of the points group in or are in close proximity to the mafic and ultramafic fields implying that these source rock compositions played a more significant role in contributing sediment to the depositional environment. There is a possibility that kimberlitic material was present in the source area, but it was not a dominant contributor to the sediment.

When plotted against Ti, Al and V the MGB volcanic rocks are divided into three distinct groupings of felsic, mafic and ultramafic (Fig. 7.8A). Note that six out of the seven lamprophyre samples plot with the mafic volcanics due to low Ti values; only the Wawa lamprophyres (Wyman and Kerrich, 1989) plot in the ultramafic field with high Ti values. This discrepancy needs to be taken into account in that samples that plot within the mafic field could also imply a mixing of lamprophyre and mafic volcanic material. Samples of the Leadbetter sandstone plotted against the same elements (Fig. 7.8B) clearly show a tendency to plot within the mafic composition field implying mafic igneous rocks

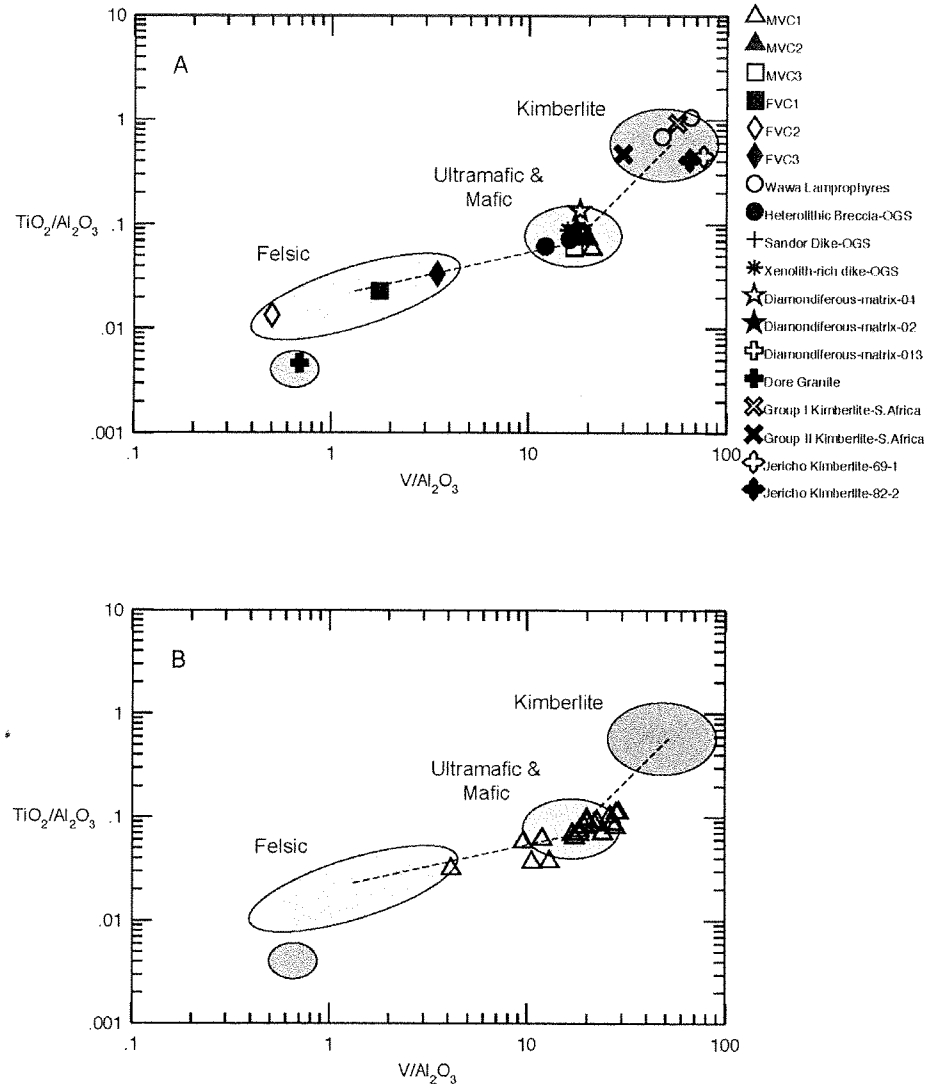

Figure 7.8. Ratio plot between Ti, Al and V that divides the MGB volcanic rocks (A) into three distinct groupings of felsic, mafic and ultramafic. Leadbetter samples plotted (B) against to compare and assess for provenance.

were a major source of the sediments. A few of the samples plot with a trend towards or within the felsic compositional field.

Using a ratio plot for discriminating rock types developed by Winchester and Floyd (1977) the MGB volcanics, heterolithic breccia and diamondiferous matrix (02 and 013) all plot on a well defined linear trend within the fields

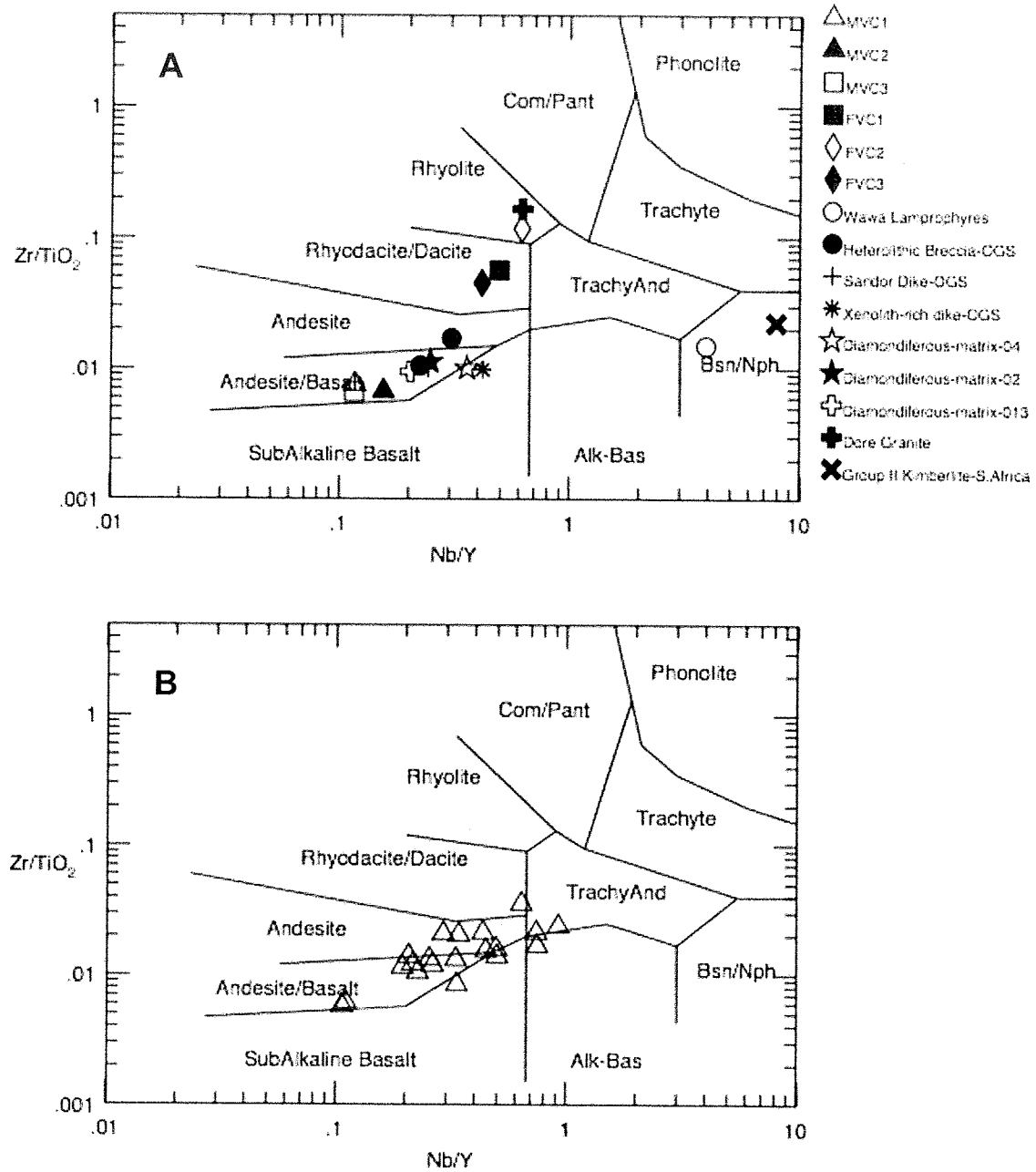

Figure 7.9. Ratio plot for discriminating rock types developed by Winchester and Floyd (1977). The MGB source rocks are plotted in diagram (A), and the Leadbetter samples are plotted in diagram (B).

of basalt, andesite and rhyolite (Fig. 7.9A). Diamondiferous matrix-04, xenolith-rich dike and Wawa lamprophyres and group II kimberlites all plot trending towards a more alkalic composition. This plot can also be used to interpret the

provenance of sedimentary rock samples, as discussed by Fralick (2003). This allows a direct comparison between the geochemistry of possible source rocks and the sandstones. When this is done a considerable number of the Leadbetter sandstone samples are pulled off of the linear trend and scatter towards a more alkalic composition defined by the volcanic, breccia and two diamondiferous matrix samples (Fig. 7.9B). The Wawa lamprophyre sample from Wyman (1989) plots within the basanite/nephelinite field and it would appear that the ultramafic lamprophyres are contributing some material to the system allowing a few of the Leadbetter sandstone samples to trend towards the Bsn/Nph field. This is significant since the Wawa lamprophyres are described to be diamondiferous by previous workers (Stone, 2004; Wyman, 2003 and 1989; Lefebvre, 2005; De Stefano, 2006; Stachel, 2006) and could be acting as a source for the diamonds being deposited within the Leadbetter sandstone. However, as the kimberlites are alkalic, and similar in composition to the Wawa lamprophyres, a kimberlitic source cannot be ruled out. The only conclusive inference that can be drawn is that a more alkalic source than the mafic volcanic rocks is also contributing sediment to the depositional system.

REEs were plotted using chondrite normalized REE curves (Sun and McDonough, 1989). The suspected source rocks can be divided into four distinct sub-groups; one being the mafic volcanic rocks of MVC1, MVC2 and MVC3 which have a near flat pattern (Fig 7.10A), the second being felsic volcanic rocks of FVC1, FVC2 and FVC3 having a steep LREE slope with LREE enrichment and then a near flat HREE slope (Fig. 7.10B). The third sub-group is the

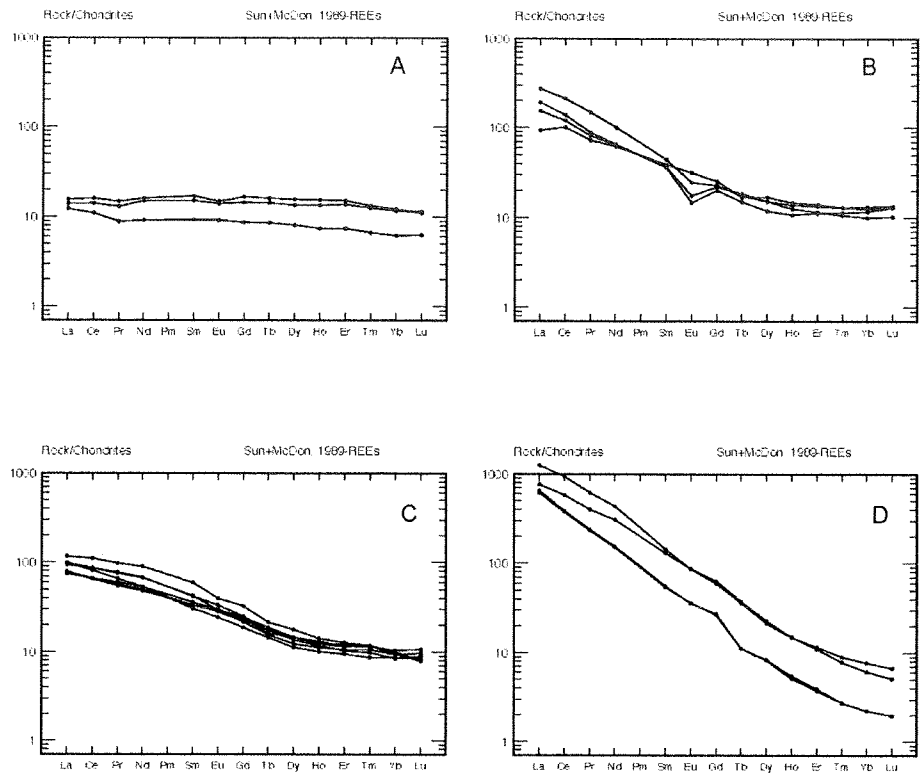

Figure 7.10. Chondrite normalized REE curves (Sun & McDonough, 1989) plotted using suspected MGB source rocks. A) mafic, B) felsic rocks, C) ultramafic lamprophyric rocks and D) kimberlite rocks for reference.

ultramafic rocks that consist of the lamprophyre dikes, which have a moderately steep LREE slope that resembles a concave down slightly curved pattern and then a near flat HREE pattern very similar to the other two sub-groups (fig. 7.10C). The fourth sub-group consists of examples of kimberlites that display an overall steep slope.

The sandstone samples have been divided into four sub-groups with respect to possible source rock sub-groups. The criteria for deciding on what sub-group an individual sandstone sample was placed in was based on how well

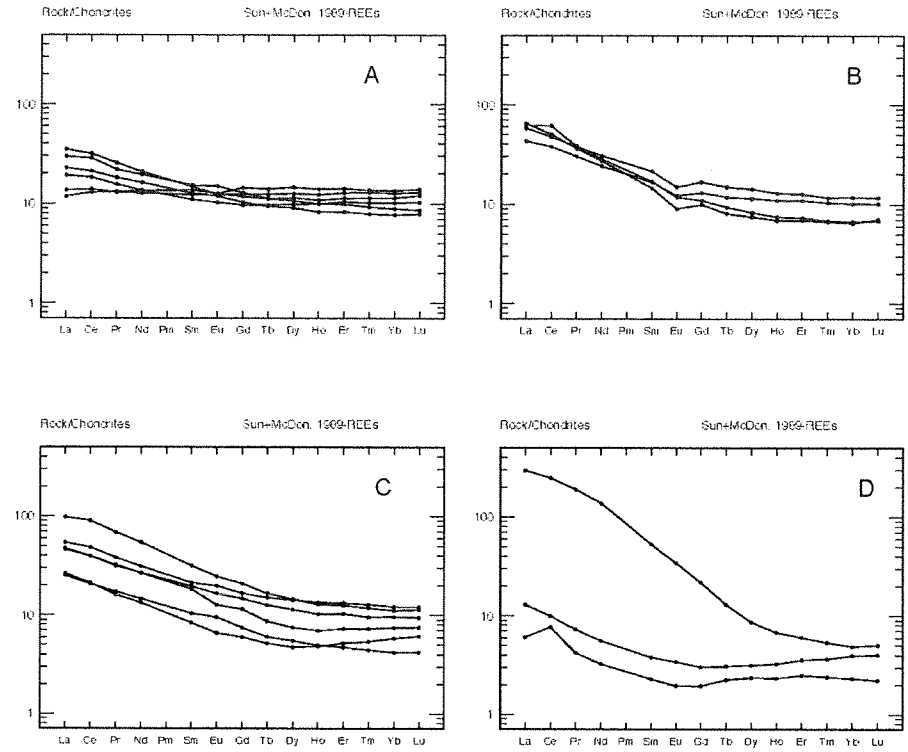

Figure 7.11. Chondrite normalized REE curves (Sun & McDonough, 1989) plotted using Leadbetter sandstone samples. Samples are grouped into subgroups that they most closely resemble from the previous possible source rock chondrite plot (Fig. 7.10). The subgroups are group A) mafic rocks, B) felsic rocks, C) ultramafic lamprophyric rocks and D) kimberlite rocks or some other unknown.

the characteristics of the shape and pattern of the slope displayed a resemblance to a particular source rock type. The members of the sub-group in Figure 7.11A all have a fairly well developed flat slope and shape much like the REE slope of the mafic volcanics (Fig. 7.10A). The members of the sub-group in Figure 7.11B all have a moderately steep LREE slope with a near flat HREE slope very similar to the REE curve shape of the felsic volcanics in Figure 7.10B. In Figure 7.11C, this sub-group of samples all display a moderately steep, in some instances curved LREE slope and flat HREE slope. They most resemble the REE curve shape of the lamprophyre dikes (Fig. 7.10C). The important differences between

this sub-group (Fig 7.11C) and the felsic volcanic sub-group (Fig 7.11B) are the absence of the negative Eu anomaly in 7.11C and the slightly concave curvature of the LREE slope in this sub-group that most resembles the lamprophyre dikes (Fig. 7.10C). The last sub-group in Figure 7.11D are anomalous samples that do not correlate well with the other three sub-groups. Sample DC-002 (Fig. 7.11D) displays a higher overall slope than the felsic volcanic rocks (Fig 7.10B) and more closely resembles the shape and pattern of the kimberlites (Fig 7.10D). One major difference between sample DC-002 and the kimberlites is that DC-002 has a relatively flatter HREE slope compared to the more moderately steep HREE slope that the kimberlites display.

By dividing the sandstone samples into sub-groups it is more clearly shown that a mixture of source rocks, mafic, felsic, lamprophyre, and possibly kimberlites, all contributed sediment to the depositional system.

7.4. Placer Geochemistry

Investigating the possibility that the Leadbetter conglomerate's depositional system was efficient at sorting heavy minerals through hydraulic sorting and accumulating placer deposits; two ratio plots were used to find evidence of such a process.

A ratio plot using Cr/V and Y/Ni (Fig. 7.12) to show if chromite is progressively added to a sample (McLennan et al., 1993) was used to see if there is evidence of chromite enrichment and placer accumulation. If chromite enrichment occurred the samples would plot along the Y-axis with a higher Cr/V

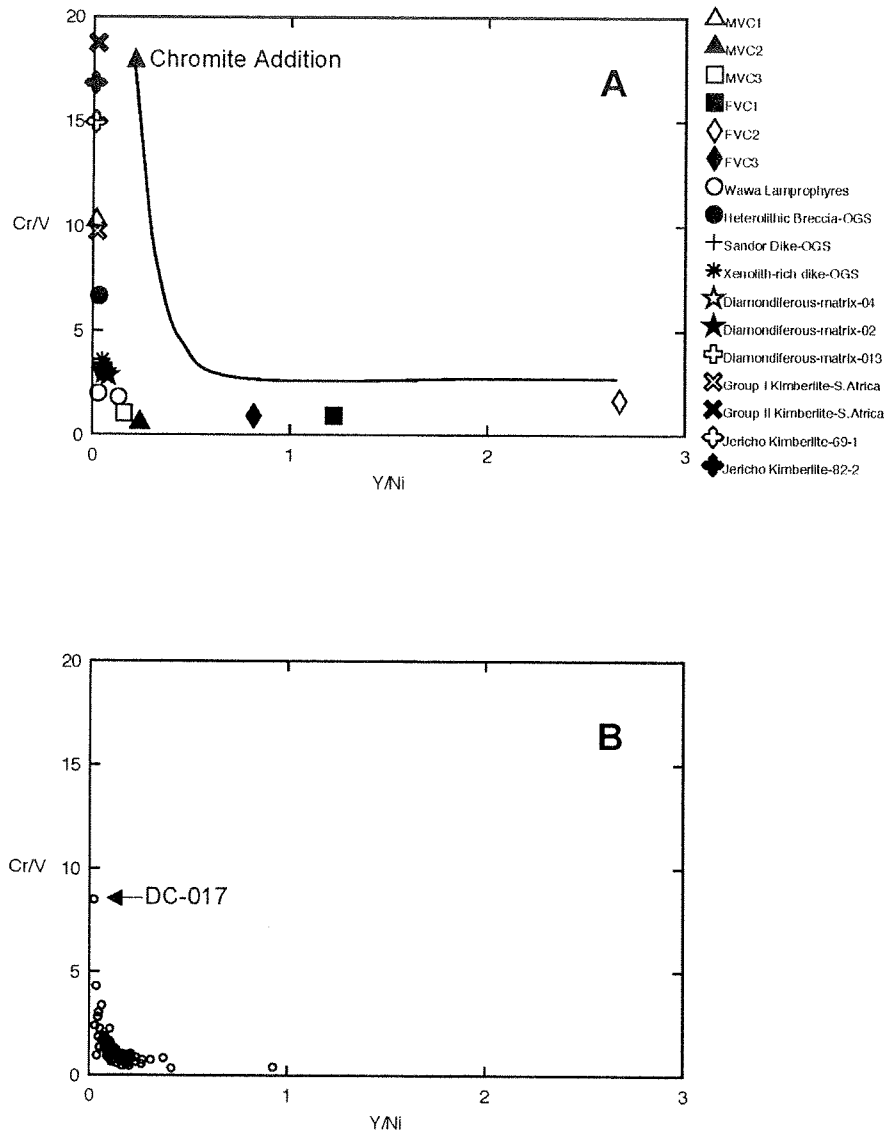

Figure 7.12. Ratio plot between Cr/V and Y/Ni to show if chromite is progressively added to a sample (McLennan et al., 1993). Diagram A is of possible MGB source rocks and diagram B is of the Leadbetter sandstone samples. Sample DC-017 appears to display chromite enrichment.

value compared to the source rock plots and would imply that enrichment of chromite has occurred. Sample DC-017 stands out from the rest of the samples in having a much higher Cr/V value then any of the other samples and needs further investigation. One of two scenarios could explain the higher Cr/V value compared to the other samples. One is that the MVC1, found in the region, is a

komatiitic basalt that plots just above sample DC-017 on the Cr/V axis. It is possible that it is the main source of material for this sample allowing an enrichment of chromite to occur. The other scenario is that hydraulic fractionation of the mineral chromite created a heavy mineral placer accumulation. If the first scenario were true then by looking at the whole rock geochemistry you would expect DC-017 to be very similar to the MVC1 volcanic chemistry because of the close proximity of each other in the plot. The best way to compare would be to look for similarities in ratios of similar elements, i.e. TiO_2/Cr, Fe_2O_3/Cr and Zr/Cr. This method should help eliminate any dilution effect caused by quartz being added to the sandstone sample and lead to a more reliable comparison in geochemistry. The ratios of elements are calculated and compared between MVC1 and sample DC-017. The most notable differences are between MgO/Cr, Zr/Cr, Nb/Cr, Zr/V and Nb/V with MVC1 having values almost twice as much in DC-017. If chromite enrichment was to occur one would suspect enrichment in zircon (incorporating Zr), due to a similar density to chromite and both being susceptible to heavy mineral enrichment through hydraulic fractionation. The higher Zr/Cr and Zr/V ratios of DC-017 could support this observation. The same is true with Nb/Cr and Nb/V with Nb commonly incorporated into monazite and is commonly concentrated through hydraulic fractionation and would create a higher ratio percent compared to MVC1. The other notable ratio difference with MgO/Cr could be explained with enrichment between chrome diopside or chromite creating a higher ratio percent and could also support the idea of heavy mineral accumulation through hydraulic

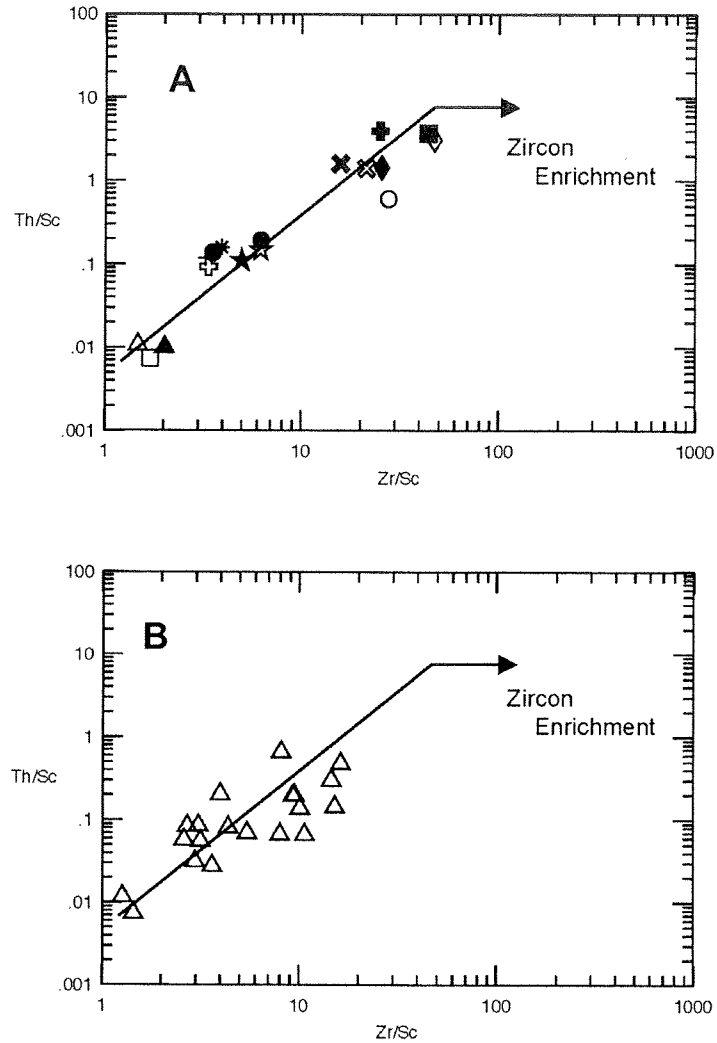

Figure 7.13. Ratio plot between Th/Sc and Zr/Sc to see if zircon enrichment has occurred (McLennan et al., 1993). Diagram A is a plot using possible MGB source rock data. Diagram B is a plot using the Leadbetter sandstone samples data. There is no evidence of zircon enrichment as shown in diagram A. If zircon enrichment had occurred, points will be pulled off the line and significantly to the right.

fractionation. However, this evidence is not conclusive but does allow for some suspicion on whether placer accumulation has occurred and also that only one sample has shown some evidence of placer accumulation does not support a highly efficient depositional environment for placer accumulation to occur.

A plot of Th/Sc and Zr/Sc (Fig. 7.13) designed to test whether zircon enrichment has occurred (Mclennan et al., 1993) does not show any positive results for zircon enrichment. Note also that the sample set to area ratio is small and it could be that zircon enrichment has occurred in areas that the researcher was not able to sample.

7.5. Source of Diamonds

The data used to investigate the source of diamonds were gathered by previous property owners (Dianor Resources) and is a different data set then was used in the previous sections. The methods used for analizing elements is the same as the previous data set, the only difference is that the data originates from samples that were also analysed for diamonds (carats per ton) together with major, trace elements and REE. The symbols used for data points are based on quantity of diamonds per sample; i.e. the top 33% are represented by the white triangles, the middle 33% are represented by the black triangles and the lower 33% of the results are represented by the white squares.

In assessing possible source rocks for diamonds the first step involves using scatter plots of the number of diamonds in a sample from a test pit and plotting individual elements analyzed in a sample from that test pit; i.e. Cr, V and Co, etc. If a significant amount of the element was derived from the diamond-bearing source rock, the plot should show an enrichment of the element with an

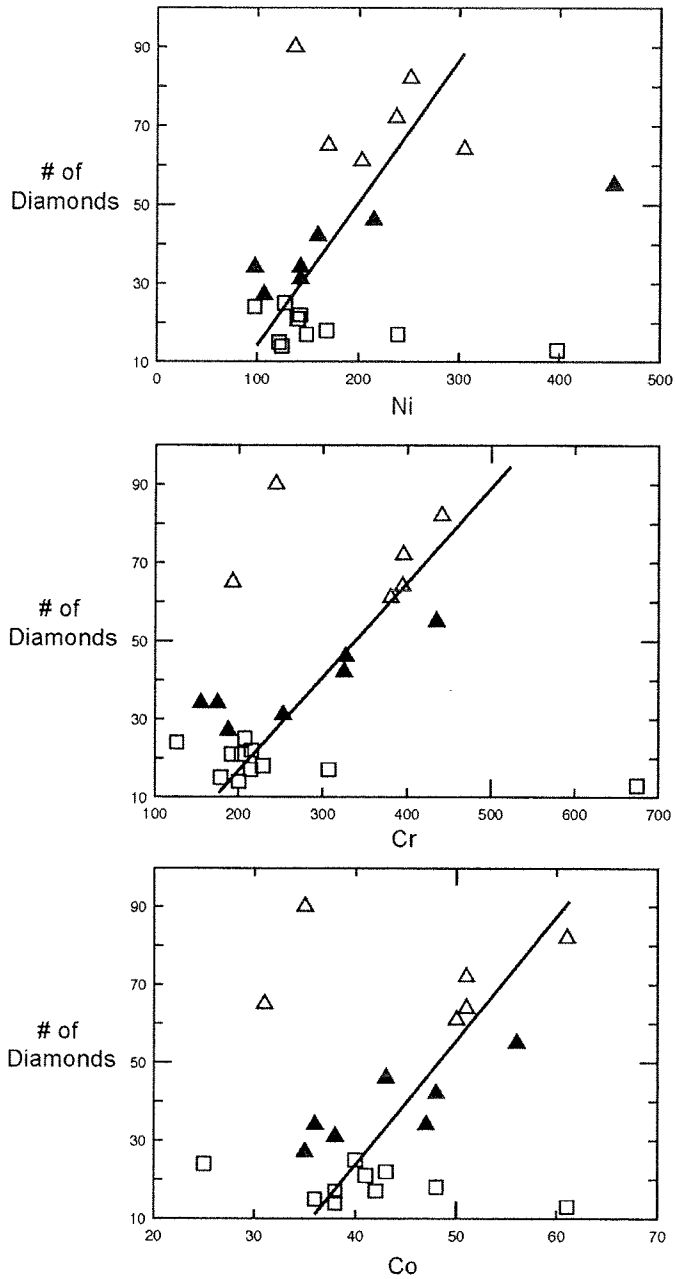

Figure 7.14. Scatter plot of number of diamonds compared to an abundance of the individual elements Ni, Cr and Co. All plots appear to show a slightly positive correlation with an increase in the elements Ni, Cr and Co with an increase in the number of diamonds per sample.

increase in diamond concentration. Two plots that displayed a positive result were Ni and Cr (Fig 7.14). All three appear to have the same correlation

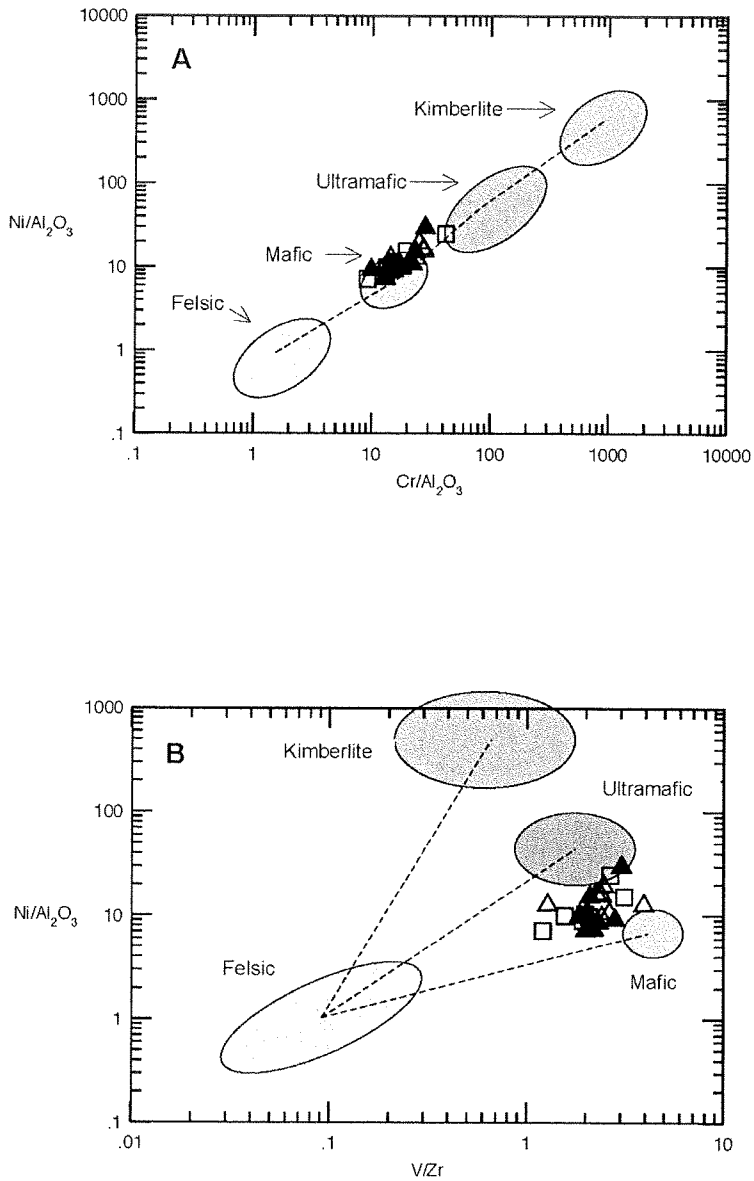

Figure 7.15. Previous ratio plots depicting source rock geochemistry compared to concentration of diamonds to see if any correlations exist between higher diamond results to suspected source rocks. Diagram A displays data points mostly within the mafic rock type area, while diagram B displays data points on a mixing line between mafic and ultramafic rock types.

between increasing amounts of Ni, Cr and Co and increasing amounts of diamonds.

Previously presented ratio plots depicting source rock geochemistry were also used to explore correlations of higher CPHT (Carats per ton) with any of the suspected source rocks. In Figure 7.15 ratio plots of Ni/Al_2O_3 against Cr/Al_2O_3 and Ni/Al_2O_3 against V/Zr show no correlation with higher CPHT plotting in a particular source rock area, but do however show that the majority of samples plot within the mafic volcanic or on a mixing line between mafic volcanic and ultra-mafic lamprophyres (Fig. 7.15B).

Using REE to asses source of diamonds the samples were grouped into three categories, high CPHT, medium CPHT and low CPHT. In Figure 7.16 the high CPHT samples were then further sub-divided into four groups that displayed similar patterns in their slopes. In Figure 7.16A all the samples display an enrichment of LREE with a near flat HREE similar to the lamprophyres. The samples in Figure 7.16B are very similar to sub-group (A) but with a slight negative Eu anomaly that is characteristic of the felsic volcanic rocks in the area. Figure 7.16C is made up of samples similar to (A) but with a slight positive Eu anomaly and Figure 7.16(D) both depicts two samples that have a slight convex downward shape in their LREE slope with a near flat HREE slope.

When REE of samples with moderate CPHT are plotted (Figure 7.17) two sub-groups, (A) and (B) are distinguishable. Both are enrichment in LREE with a near flat HREE pattern. Sub-group (B) displays a higher slope.

In Figure 7.18, REE plots of the samples with low CPHT, there are three sub-groups (A, B and C). Sub-group (A) displays enrichment of LREE and near flat HREE. Sub-group (B) is very similar to sub-group (A) except with a slight

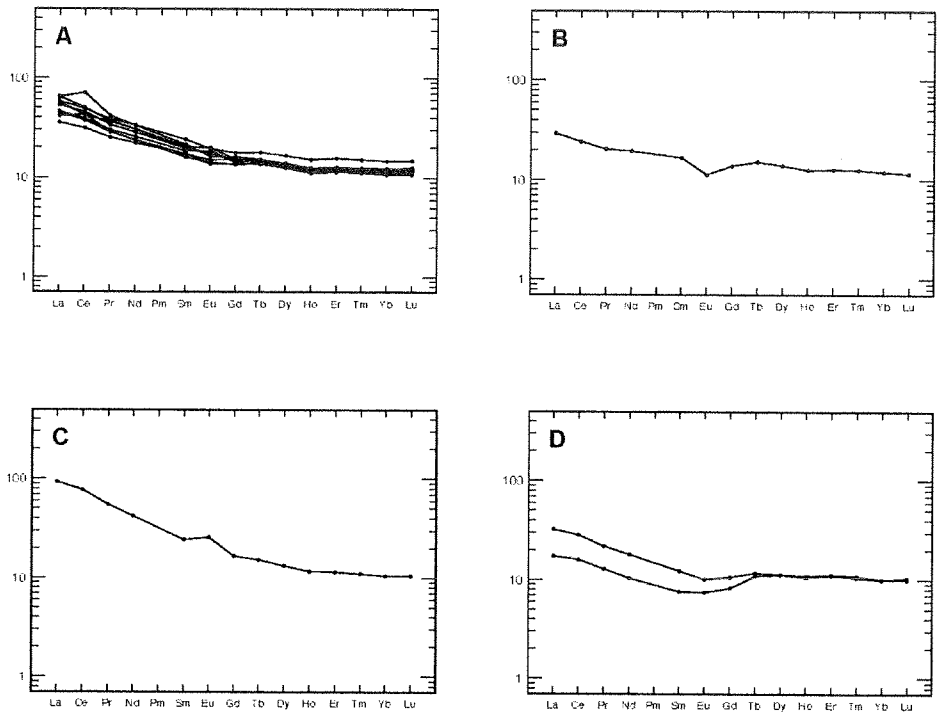

Figure 7.16. REE chondrite plots (Sun and McDonough, 1989) of the upper 33% of diamond concentration results to asses source of diamonds. Samples are divided into four sub-groups that they most likely represent. A) lamprophyres, B) felsic, C) similar to (A) but with a positive Eu anomaly and D) is unknown.

negative Eu anomaly. Subgroup (C) displays a depletion of LREE with a near flat HREE pattern.

When comparing the REE plots with REE plots of possible source rocks (Fig. 7.10) the majority of the samples are more similar to the felsic volcanic and lamprophyre REE patterns. Since the felsic volcanic and lamprophyres display similar patterns and slopes the one notable difference between the two is a negative Eu anomaly. The majority of the samples do not display the negative Eu anomaly and fit the shape and pattern of the lamprophyres. This evidence is not conclusive, but when also comparing the curve to the REE slopes and

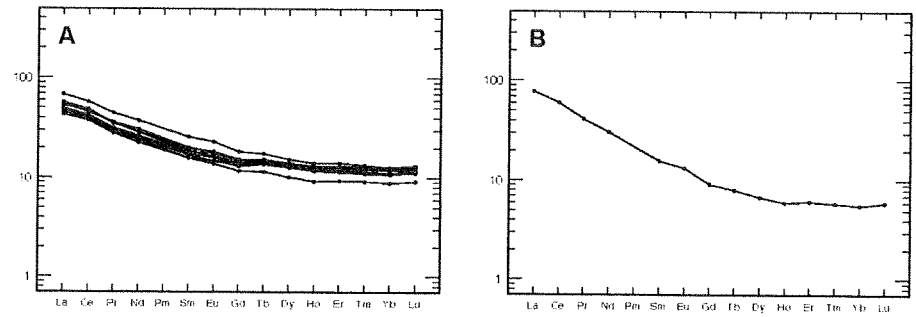

Figure 7.17. REE chondrite plots (Sun and McDonough, 1989) of the middle 33% of diamond concentration results to asses source of diamonds.

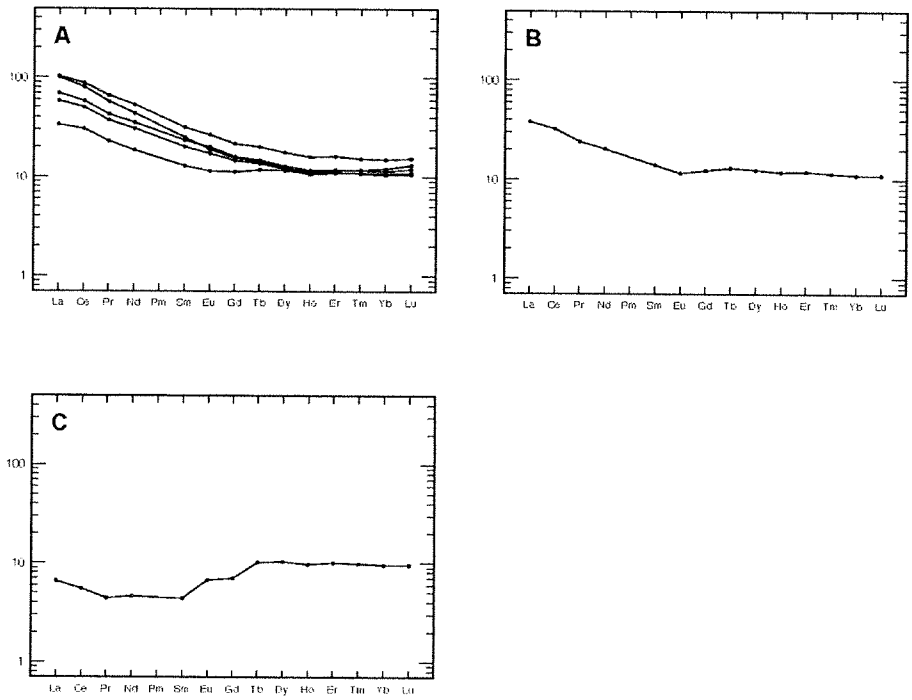

Figure 7.18. REE chondrite plots (Sun and McDonough, 1989) of the lower 33% of diamond concentration results to asses source of diamonds.

patterns of the kimberlite examples (Fig. 7.10D) there is no evidence of the amount of LREE enrichment as seen in the kimberlites.

7.6. Summary of Results

Using scatter plots the elements Co, Ni, Sc, TiO_2, V, Al_2O_3, Y, Nb, Zr, Hf, Ta, Th and U are found to be immobile. The elements Ba, Sr, CaO and Na_2O are found to be very mobile while the elements K_2O, MgO and Fe_2O_3 are found to be somewhat mobile.

The most immobile elements Ni, Al, Cr, V, Zr, Ti and REE's were then used to investigate provenance source rock compositions. No distinct singular source rock could be delineated from the provenance studies, but did show that there is a mixture of source rocks, mafic, felsic, lamprophyre, and possible kimberlites that all contributed sediment to the depositional system.

Ratio plots using the elements Cr, V, Y, Ni, Th, Sc and Zr to determine if there was placer accumulation of the heavy minerals chromite and zircon was not conclusive. However there was some evidence that allows for suspicion on whether placer accumulation has occurred with one sample showing possible chromite accumulation, but only one sample is not enough evidence to suggest that the Leadbetter was a highly efficient depositional environment for placer accumulation to occur.

The investigation of possible source rocks of the diamonds showed that the elements Ni, Cr and Co display moderate to weak positive correlation with an increase in diamond concentration. This is significant because Ni, Cr and Co in particular are generally associated with either mafic, or ultramafic rock types, and the two possible sources of diamonds are either ultramafic lamprophyres or

kimberlite. The ratio plots (Fig. 7.15) correlate well with all samples plotting either in the mafic to ultra-mafic sub-groups or on a mixing between the two. Combining the data from the REE plots would suggest that an ultra-mafic lamprophyre source is more likely because none of the samples displayed a near flat REE pattern similar to the mafic volcanics. Instead they display an LREE enrichment similar to the felsic volcanic rocks or lamprophyres. Keeping in mind that there is direct evidence of diamond-bearing lamprophyres within the field area and no known physical evidence of kimberlites one could assume that the lamprophyres are more likely the contributor of the diamonds within the Leadbetter conglomerate.

Chapter 8

Summary and Conclusions

8.1. Introduction

The application of a number of different techniques (sedimentology, stratigraphy and whole rock geochemistry) have been applied to the Leadbetter Conglomerate. The following will summarize chapter four through seven results, with a conclusion at the end.

Using a lithofacies classification scheme developed by Miall (1977) for braided fluvial conglomerates, seven different types of depositional lithofacies were identified. Lithofacies Gm is the most abundant lithofacies within the Leadbetter Conglomerate followed by minor lithofacies Gt/St, Gp, Sh, Sp, Ss and more rarely (nearly absent) is lithofacies Fl/Fm.

Three lithofacies associations are identified within the Leadbetter Conglomerate. Lithofacies Association One is characterized by a massive matrix-supported cobble to boulder conglomerate of lithofacies Gm. This can be interbedded with subordinate lithofacies Gt and more rarely Sh. Contacts between these lithofacies are generally sharp and can be erosive. This lithofacies association is most prevalent near the base of the Leadbetter Conglomerate.

Lithofacies Association Two is characterized by the interbedding of clast supported conglomerates of lithofacies Gm with subordinate lithofacies Sh and more rarely St. Other minor lithofacies that occur locally are Gt, Gp, Sp, Ss and

more rarely Fl and Fm. This lithofacies association dominates in the middle and upper parts of the Leadbetter Conglomerate.

Lithofacies Association Three occurs near the top of the Leadbetter Conglomerate and is characterized by a very sudden increase of very fine-grained sediment in the form of channel shaped fine-grained sandstones to thinly laminated sandstones, siltstone and mudstones. The channel shaped fine-grained sandstones are often interbedded with a thinly laminated or parallel-bedded very fine-grained sandstone, siltstones and mudstone. Contacts between these lithofacies are often sharp and planar. Overlying this is dominantly thinly laminated and parallel-bedded siltstones and mudstones, which is transitional into an argillite with significantly less siltstone layers.

Six types of clast lithologies are identified within the Leadbetter Conglomerate, 1) mafic volcanic (i.e. basalt to intermediate), 2) felsic volcanic (i.e. intermediate to rhyolite), 3) gabbro (or mafic intrusive equivalent), 4) diorite (or intermediate intrusive equivalent), 5) sandstone and 6) chert (including quartz). Using the application of pebble counts, mafic rock types are more abundant near the base of the succession while felsic rock types are more abundant near the top of the succession.

Interpretation of scatter plots of the elements Co, Ni, Sc, TiO_2, V, Al_2O_3, Y, Nb, Zr, Hf, Ta, Th and U indicated they were immobile. The elements Ba, Sr, CaO and Na_2O were found to be very mobile whereas the elements K_2O, MgO and Fe_2O_3 were found to be somewhat mobile.

The most immobile elements Ni, Al, Cr, V, Zr, Ti and REE were then used to investigate provenance source rock compositions. No distinct singular source rock could be delineated from the provenance studies, but they did show that there is a mixture of source rocks, i.e., mafic, felsic, lamprophyre, and possible kimberlites that all contributed sediment to the depositional system.

Ratio plots using the elements Cr, V, Y, Ni, Th, Sc and Zr to investigate if there was placer accumulation of the heavy minerals chromite and zircon did not indicate significant enrichment of these heavy minerals. However, one sample showed possible chromite enrichment. One sample is certainly not enough evidence to support the hypothesis that the Leadbetter was a highly efficient depositional environment for placer accumulation to occur in.

The investigation of possible source rocks to the diamonds showed that the elements Ni, Cr and Co display moderate to weak positive correlation with an increase in diamond concentration. The ratio plots (Fig. 7.15) correlate well with most samples plotting either in the mafic to ultra-mafic sub-groups or in a mixing zone between the two. None of the samples displayed a near flat REE pattern similar to the mafic volcanics. Instead they display a LREE enrichment similar to the felsic volcanic rocks or lamprophyres.

8.3. Conclusions

Of the seven different types of depositional lithofacies identified within the Leadbetter Conglomerate, three lithofacies associations were recognized. Interpretation of the lithofacies associations clearly indicates that the Leadbetter

Conglomerate represents a high-energy alluvial fan delta succession. Lithofacies Association One is dominated by weakly sheared and highly viscous debris-flows and represents the upper reaches of the alluvial fan. Lithofacies Association Two is dominated by superimposed longitudinal bars that represent the transformation of the depositional environment to a mid-fan and lower-fan proximal braided system. Lithofacies Association Three is dominated by distributary channel mouth-bars, graded turbiditic density flows and argillite facies, which represents a transgression and transition to delta front and subsequently pro-delta environment.

The very quick and sudden transition from a braided fluvial dominated facies of Lithofacies Association Two to a sub-aqueous pro-delta facies of Association Three implies that there was a quick landward transgression of the marine or lacustrine environment that suddenly had a drowning effect on the braided alluvial fan depositional system.

After investigating clast lithology types that make up the lithofacies within the Leadbetter Conglomerate, it is apparent that mafic rock types are more abundant near the base of the succession while felsic rock types are more abundant near the top of the succession. One possible explanation for the distribution in rock types is that mafic rock types are more susceptible to chemical weathering and break down faster during bedload transport processes than felsic rock types. As source material is being eroded and transported downstream there will be a preferential increase in felsic rock types being preserved and deposited as clasts. As a consequence, felsic rock types will

become more abundant near the top of the succession (which represents a more distal environment from source) and mafic rock types will be more abundant near the base of the succession (which represents a more proximal environment to source).

Through whole rock geochemistry studies of the Leadbetter Conglomerate, immobile elements (Co, Ni, Sc, TiO_2, V, Al_2O_3, Y, Nb, Zr, Hf, Ta, Th and U) were used to investigate provenance source rock compositions. There is a mixture of source rocks, mafic, felsic, lamprophyre, and possible kimberlites that all contributed sediment to the depositional system of the Leadbetter Conglomerate. Since felsic clast types are more abundant near the top of the succession, one could suspect that there should be a clear fractionation pattern of the plots trending towards a more felsic end member. The Leadbetter Conglomerate clearly does not display this pattern and instead displays a scatter of plots that group dominantly between the mafic and ultramafic rock types. This can be explained by mafic rock types breaking down and weathering into clay material due to the exposure of erosional and depositional processes that formed the Leadbetter Conglomerate. Since there was a significant amount of matrix infill made up of clay-sized material observed within the Leadbetter Conglomerate samples commonly plot within the mafic to ultramafic rock fields on geochemical diagrams. Ratio plots used to investigate whether placer accumulation of the heavy minerals chromite and zircon occurred indicated that significant placer accumulation was not indicated.

Possible source rocks to the diamonds could either be ultramafic lamprophyre dikes and breccias, which have been observed and described near the Leadbetter Conglomerate, or a more commonly diamond-associated rock type such as kimberlites, which have yet to be observed and described near the Leadbetter Conglomerate. The presence of kimberlites could be investigated by a study of mineral chemistry, but that was beyond the scope of this thesis. There is a moderate to weak correlation of Ni, Cr and Co with an increase in diamond concentration. This is significant because Ni, Cr and Co in particular are generally associated with either mafic, or ultramafic rock types such as lamprophyres and kimberlites. The data from the REE plots would suggest that an ultra-mafic lamprophyre source is more likely because none of the samples displayed a near flat REE pattern similar to the mafic volcanics. Instead they display LREE enrichment similar to the felsic volcanic rocks or lamprophyres. Being that there is direct evidence of diamond-bearing lamprophyres within the field area and no known physical evidence of kimberlites one could assume that the lamprophyres are more likely the contributor of the diamonds within the Leadbetter Conglomerate.

8.4. Future Work

A general study of the lithofacies, lithofacies associations, clast lithologies and whole rock geochemistry of the Leadbetter Conglomerate has been completed. The following are some suggestions for questions that should be addressed with future work.

- The question of whether placer accumulation occurred within the Leadbetter Conglomerate should be further investigated by a more intensive sampling program. Sampling should be done keeping different lithofacies in mind, and trying to delineate a correlation (if any) of what lithofacies is associated with diamond accumulation (if any occurred).

- The source of diamonds should be more thoroughly investigated. One possible way of addressing this question could be to compare the diamonds found within the Leadbetter Conglomerate with known diamonds found in the lamprophyre dikes and breccias, near the Leadbetter Conglomerate. This could possibly answer whether the diamonds are derived from the lamprophyres or not; if not then there will need to be a further investigation into other nearby diamond bearing rock types. Another line of investigation is to study the geochemistry of minerals associated with the diamonds.

References

Allen, J. R. L., 1963. The classification of cross-stratified units, with notes on their origin. Sedimentology, Vol. 2, p93-114.

Arias, Z. G., and Heather, K. B., 1987. Regional structural geology related to gold mineralization in the Goudreau-Lochalsh area, District of Algoma. Ontario Geological Survey Miscellaneous Paper 137, p146-154.

Arias, Z. G., and Helmstaedt, H., 1990. Early thrust faults in the Archean Michipicoten greenstone belt, Superior Province, central Ontario. In, Program with Abstracts-Geological Association of Canada; Mineralogical Association of Canada; Joint Annual Meeting, Vol. 15, p4.

Arias, Z. G., 1990. Structural evolution of the Michipicoten (Wawa) greenstone belt, Superior Province; evidence for an Archean fold and thrust belt. Ontario Geological Survey Miscellaneous Paper 150, p107-114.

Ayer, J., Amelin, Y., Corfu, F., and Kamoet, S., 2002. Evolution of the southern Abitibi greenstone belt based on U-Pb geochronology; autochthonous volcanic construction followed by plutonism, regional deformation and sedimentation. Precambrian Research, Vol. 115, p63-95.

Barton, M. D., 1994. Outcrop characterization of architecture and permeability structure in fluvial-deltaic sandstones, Cretaceous Ferron Sandstone, Utah. Unpublished PhD. Thesis, University of Texas, Austin, TX, United States.

Bates, C. C., 1953. Rational theory of delta formation. Bulletin of the American Association of Petroleum Geologists, Vol. 37, p2119-2162.

Becker, M., and Le Roex, A. P., 2006. Geochemistry of South African on- and off-craton, Group I and Group II kimberlites; petrogenesis and source region evolution. Journal of Petrology, Vol. 47, p673-703.

Bhatia, M. R., 1983. Plate tectonics and geochemical composition of sandstones. Journal of Geology, Vol. 91, p611-627.

Bhatia, M. R., and Crook, K. W., 1986. Trace element characteristics of graywackes and tectonic setting discrimination of sedimentary basins. Contributions to Mineralogy and Petrology, Vol. 92, p181-193.

Blair, T. C., and Mcpherson, J. G., 1998. Recent debris-flow processes and resultant form and facies of the Dolomite alluvial fan, Owens Valley, California. Journal of

Sedimentary Research, Vol. 68, p800-818.

Bluck, B. J., 1979. Structure of coarse grained braided stream alluvium. Transactions - Royal Society of Edinburgh, Vol. 70, p181-221.

Boothroyd, J. C., and Ashley, G. M., 1975. Processes, bar morphology, and sedimentary structures on braided outwash fans, northeastern Gulf of Alaska. In Glaciofluvial and glaciolacustrine sedimentation, Special Publication 30, Society of Economic Paleontologists and Mineralogists, p193-222.

Bouma, A. H., 1962. Sedimentology of some Flysch deposits; a graphic approach to facies interpretation. Amsterdam-New York, Elsevier Pub. Co.

Burnham, O. M., Hechler, J. H., Semenyna, L., and Schweyer, J., 2002. Mineralogical controls on the determination of trace elements following mixed acid dissolution. Open File Report 6100 - Ontario Geological Survey, p36.1-36.12.

Burnham, O. M., and Schweyer, J., 2004. Trace element analysis of geological samples by inductively coupled plasma mass spectrometry at the Geoscience Laboratories; revised capabilities due to improvements to instrumentation. Open File Report 6145 - Ontario Geological Survey, p54.1-54.5.

Burton, J. P., and Fralick, P., 2003. Depositional placer accumulations in coarse-grained alluvial braided river systems. Economic Geology, Vol. 98, p985-1001.

Card, K. D., 1990. A review of the Superior Province of the Canadian Shield, a product of Archean accretion. Precambrian Research, Vol. 48, p99-156.

Card, K. D., Church, W. R., Franklin, J. M., Frareyet, Robertson, J. A., West, G. F., and Young, G. M., 1972. The Southern Province. In, Variations in tectonic styles in Canada, Special Paper 11, Geological Association of Canada, p335-380.

Card, K. D., and Ciesielski, A., 1986. Subdivisions of the Superior Province of the Canadian Shield. Geosciences Canada, Vol. 13, p5-13.

Chakrabarti, U., and Roy, A., 2007. Sedimentary processes and facies of upper Pleistocene alluvial fans in the Purna Valley basin of central India. Journal of the Geological Society of India, Vol. 69, p916-924.

Collinson, J. D., 1970. Bedforms of the Tana river, Norway. Geografiska Annaler. Series A: Physical Geography, Vol. 52, p31-56.

Corfu, F., and Stott, G. M., 1993. Age and petrogenesis of two late Archean magmatic suites, northwestern Superior Province, Canada; zircon U-Pb and Lu-Hf isotopic

relations. Journal of Petrology, Vol. 34, p817-838.

Das, A., and Krishnaswami, S., 2007. Elemental geochemistry of river sediments from the Deccan Traps, India; implications to sources of elements and their mobility during basalt-water interaction. Chemical Geology, Vol. 242, p232-254.

Desrochers, J., Hubert, C., Ludden, J., and Pilote, P., 1993. Accretion of Archean oceanic plateau fragments in the Abitibi greenstone belt, Canada. Geology (Boulder), Vol. 21, p451-454.

De Stefano, A., Lefebvre, N., and Kopylova, M., 2006. Enigmatic diamonds in Archean calc-alkaline lamprophyres of Wawa, southern Ontario, Canada. Contributions to Mineralogy and Petrology, Vol. 151, p158-173.

Doeglas, D. J., 1962. The structure of sedimentary deposits of braided rivers. Sedimentology, Vol. 1, p167-190.

Feng, R., and Kerrich, R., 1992. Geodynamic evolution of the southern Abitibi and Pontiac terranes; evidence from geochemistry of granitoid magma series (2700-2630 Ma). Canadian Journal of Earth Sciences, Vol. 29, p2266-2286.

Fralick, P., Hollings, P., and King, D., 2008. Stratigraphy, geochemistry, and depositional environments of Mesoarchean sedimentary units in western Superior Province; implications for generation of early crust. In, edited by Condie, K., and Pease, V., When did plate tectonics begin on planet Earth?, Special Paper 20, Geological Society of America, Vol. 440, p77-96.

Fralick, P. W., and Kronberg, B., 1997. Geochemical discrimination of clastic sedimentary rock sources. Sedimentary Geology, Vol. 113, p111-124.

Fralick, P. W., Hollings, P., Metsaranta, R., and Heaman, L., 2009. Using sediment geochemistry and detrital zircon geochronology to categorize eroded igneous units; an example from the Mesoarchean Birch-Uchi greenstone belt, Superior Province. Precambrian Research, Vol. 168, p106-122.

Goodwin, A. M., 1962. Structure, stratigraphy, and origin of iron formations, Michipicoten area, Algoma District, Ontario, Canada. Geological Society of America Bulletin, Vol. 73, p561-585.

Goodwin, A. M., 1991. Precambrian geology; the dynamic evolution of the continental crust. United States: Acad. Press: San Diego, CA.

Gustavson, T. C., 1974. Sedimentation on gravel outwash fans, Malaspina Glacier Foreland, Alaska. Journal of Sedimentary Petrology, Vol. 44, p374-389.

Heather, K. B., and Arias, Z. G., 1987. Geological setting of gold mineralization in the Goudreau-Lochalsh area, District of Algoma. Ontario Geological Survey Miscellaneous Paper, 137, p155-162.

Hein, F. J., and Walker, R. G., 1977. Bar evolution and development of stratification in the gravelly, braided, Kicking Horse River, British Columbia. Canadian Journal of Earth Sciences, Vol. 14, p562-570.

Hollings, P., and Kerrich, R., 2000. An Archean arc basalt-Nb-enriched basalt-adakite association; the 2.7 Ga Confederation assemblage of the Birch-Uchi greenstone belt, Superior Province. Contributions to Mineralogy and Petrology, Vol. 139, p208-226.

Jones, D. A., 1989. Braided stream deposition and provenance of the Late Cretaceous-Paleocene Canaan Peak Formation, Table Cliff and Kaiparowits plateaus, southwestern Utah. Unpublished Master's. Thesis, University of Nevada, Las Vegas, NV, United States.

Ketchum, J., Ayer, J., Van Breemen, O., Pearson, N., and Becker, J., 2008. Pericontinental crustal growth of the southwestern Abitibi Subprovince, Canada; U-Pb, Hf, and Nd isotope evidence. Economic Geology and the Bulletin of the Society of Economic Geologist, Vol. 103, p1151-1184.

Kim, B. C., and Lowe, D. R., 2004. Depositional processes of the gravelly debris flow deposits, South Dolomite alluvial fan, Owens Valley, California. Geosciences Journal [Seoul], Vol. 8, p153-170.

Klein, G. d. V., De Melo, U., and Della, J., 1972. Subaqueous Gravity Processes on the Front of Cretaceous Deltas, Reconcavo Basin, Brazil. Geological Society of America Bulletin, Vol. 83, p1469-1491.

Lefebvre, N., Kopylova, M., and Kivi, K., 2005. Archean calc-alkaline lamprophyres of Wawa, Ontario, Canada; unconventional diamondiferous volcaniclastic rocks. Precambrian Research, Vol. 138, p57-87.

Logan, W. E., 1847. On the geology and economic minerals of the north shore of Lake Superior. Progress Report - Geological Survey of Canada, 1846-1847.

Marzo, M. and P. Anadon., 1988. Anatomy of a conglomeratic fan-delta complex; the Eocene Montserrat Conglomerate, Ebro Basin, northeastern Spain. In, edited by Nemec, W., and Steel, R. J., Fan deltas; sedimentology and tectonic settings, Blackie and Son: Glasgow, United Kingdom.

McGill, G. E. and Shrady, C. H., 1986. Evidence for a complex Archean deformational

history, southwestern Michipicoten greenstone belt, Ontario. Journal of Geophysical Research, Vol. 91, p281-289.

Miall, A. D., 1977. A review of the braided-river depositional environment. Earth-Science Reviews, Vol. 13, p1-62.

Middleton, L. T., and Trujillo, A. P., 1984. Sedimentology and depositional setting of the upper Proterozoic Scanlan Conglomerate, central Arizona. In, edited by Koster, E. and Steel, R. J., Sedimentology of gravels and conglomerates, Memoir 10, Canadian Society of Petroleum Geologists, p189-201.

Mills, H. H., 2000. Controls on form, process, and sedimentology of alluvial fans in the Central and Southern Appalachians, Southeastern U.S.A. Southeastern Geology, Vol. 39, p281-313.

Nemec, W., and Steel, R. J., 1984. Alluvial and coastal conglomerates; their significant features and some comments on gravelly mass-flow deposits. In, edited by Koster, E., and Steel, R., Sedimentology of gravels and conglomerates, Memoir 10, Canadian Society of Petroleum Geologists, p1-31.

Nemec, W., and Steel, R. J., 1984. Domba Conglomerate, Devonian, Norway; process and lateral variability in a mass flow-dominated, lacustrine fan-delta. In, edited by Koster, E., and Steel, R., Sedimentology of gravels and conglomerates, Memoir 10, Canadian Society of Petroleum Geologists, p295-320.

Nemec, W. and Steel, R. J., 1988. Fan deltas; sedimentology and tectonic settings, Blackie and Son: Glasgow, United Kingdom.

Nichols, G., 2005. Tertiary alluvial fans at the northern margin of Ebro Basin; a review. In, edited by Harvey, A., Mather, A., and Stokes, M., Alluvial fans; geomorphology, sedimentology, dynamics, Geological Society, Special Publication 251, p187-206.

O'Neill, C., and Wyman, D. A., 2006. Geodynamic modeling of late Archean subduction; pressure-temperature constraints from greenstone belt diamond deposits. Geophysical Monograph, Vol. 164, p177-188.

Olariu, C., and Bhattacharya, J. P., 2006. Terminal distributary channels and delta front architecture of river-dominated delta systems. Journal of Sedimentary Research, Vol. 76, p212-233.

Orton, G. J., and Reading, H. G., 1993. Variability of deltaic processes in terms of sediment supply, with particular emphasis on grain size. Sedimentology, Vol. 40, p475-512.

Percival, J. A., 2004. Insights on Archean continent-ocean assembly, western Superior Province; from new structural, geochemical and geochronological observations. Precambrian Research, Vol. 132, p209-326.

Polat, A., and Kerrich, R., 2002. Nd-isotope systematics of approximately 2.7 Ga adakites, magnesian andesites, and arc basalts, Superior Province; evidence for shallow crustal recycling at Archean subduction zones. Earth and Planetary Science Letters, Vol. 202, p345-360.

Rice, R. J., and Donaldson, J. A., 1992. Sedimentology of the Archean Dore metasediments, Arliss Lake area, southern Michipicoten greenstone belt, Superior Province. Canadian Journal of Earth Sciences, Vol. 29, p2558-2570.

Rust, B. R., 1972. Structure and process in a braided river. Sedimentology, Vol. 18, p221-245.

Rust, B. R., 1978. Depositional models for braided alluvium. In, edited by Miall, A. D., Fluvial sedimentology, Memoir 5, Canadian Society of Petroleum Geologists, p605-625.

Sage, R. P., 1994. Geology of the Michipicoten greenstone belt. Open File Report number 5888, Ontario Geological Survey.

Sage, R. P., Lightfoot, P., and Doherty, W., 1996. Bimodal cyclical Archean basalts and rhyolites from the Michipicoten (Wawa) greenstone belt, Ontario; geochemical evidence for magma contributions from the asthenospheric mantle and ancient continental lithosphere near the southern margin. Precambrian Research, Vol. 76, p119-153.

Sage, R. P., Lightfoot, P., and Doherty, W., 1996. Geochemical characteristics of granitoid rocks from within the Archean Michipicoten greenstone belt, Wawa Subprovince, Superior Province, Canada; implications for source regions and tectonic evolution. Precambrian Research, Vol. 76, p155-190.

Sawyer, E. W., 1986. The influence of source rock type, chemical weathering and sorting on the geochemistry of clastic sediments from the Quetico metasedimentary belt, Superior Province, Canada. Chemical Geology, Vol. 55, p77-95.

Smith, N. D., 1974. Sedimentology and bar formation in the upper Kicking Horse River, a braided outwash stream. Journal of Geology, Vol. 82, p205-223.

Stachel, T., Banas, A., Muehlenbachs, K., Kurszlaukis, S., and Walker, E., 2006. Archean diamonds from Wawa (Canada); samples from deep cratonic roots predating cratonization of the Superior Province. Contributions to Mineralogy and Petrology, Vol. 151, p737-750.

Stone, D., and Semanyna, L., 2004. Petrography, chemistry and diamond characteristics of heterolithic breccia and lamprophyre dikes at Wawa, Ontario. Open File Report number 6134, Ontario Geological Survey, Canada.

Stott, G. M., 1997. The Superior Province, Canada. Oxford Monographs on Geology and Geophysics, Vol. 35, p480-507.

Sylvester, P. J., Attoh, K., and Schulz, K., 1987. Tectonic setting of late Archean bimodal volcanism in the Michipicoten (Wawa) greenstone belt, Ontario. Canadian Journal of Earth Sciences, Vol. 24, p1120-1134.

Thurston, P. C., Williams, H., Sutcliffe, R., and Stott, G., 1991. Geology of Ontario. Ontario Geological Survey Special Volume Vol. 4.

Tomlinson, K. Y., Stevenson, R., Hughes, D., Hall, P., Thurston, P., and Henry, P., 1998. The Red Lake greenstone belt, Superior Province; evidence of plume-related magmatism at 3 Ga and evidence of an older enriched source. Precambrian Research, Vol. 89, p59-76.

Turek, A., Smith, P., and Van Schmus, W., 1982. Rb-Sr and U-Pb ages of volcanism and granite emplacement in the Michipicoten Belt; Wawa, Ontario. Canadian Journal of Earth Sciences, Vol. 19, p1608-1626.

Turek, A., Smith, P., and Van Schmus, W., 1984. U-Pb zircon ages and the evolution of the Michipicoten plutonic-volcanic terrane of the Superior Province, Ontario. Canadian Journal of Earth Sciences, Vol. 21, p457-464.

Vos, R. G., 1981. Sedimentology of an Ordovician fan delta complex, western Libya. Sedimentary Geology, Vol. 29, p153-170.

Williams, H. R., Stott, G., Heather, K., Muir, T., and Sage, R., 1991. Wawa Subprovince. In, edited by Thurston, P. C., Williams, H., Sutcliffe, R., and Stott, G., Geology of Ontario, Ontario Geological Survey Special Volume 4, p485-539.

Williams, P. F., and Rust, B. R., 1969. The sedimentology of a braided river. Journal of Sedimentary Petrology, Vol. 39, p649-679.

Wright, L. D., 1977. Sediment transport and deposition at river mouths; a synthesis. Geological Society of America Bulletin, Vol. 88, p857-868.

Wyman, D., and Kerrich, R., 2009. Plume and arc magmatism in the Abitibi Subprovince; implications for the origin of Archean continental lithospheric mantle. Precambrian Research, Vol. 168, p4-22.

Wyman, D. A., Kerrich, R., and Polat, A., 2002. Assembly of Archean cratonic mantle lithosphere and crust; plume-arc interaction in the Abitibi-Wawa subduction-accretion complex. Precambrian Research, Vol. 115, p37-62.

Wyman, D. A., and Kerrich, R., 1993. Archean shoshonitic lamprophyres of the Abitibi Subprovince, Canada; petrogenesis, age, and tectonic setting. Journal of Petrology, Vol. 34, p1067-1109.

Wyman, D. A., Ayer, J., Conceicao, R., and Sage, R., 2006. Mantle processes in an Archean orogen; evidence from 2.67 Ga diamond-bearing lamprophyres and xenoliths. Lithos, Vol. 89, p300-328.

Wyman, D. A., and Kerrich, R., 1989. Archean lamprophyre dikes of the Superior Province, Canada; distribution, petrology, and geochemical characteristics. Journal of Geophysical Research, Vol. 94, p4667-4696.

Young, G. M., 1983. Tectono-sedimentary history of early Proterozoic rocks of the northern Great Lakes region. In, edited by Medaris, L. G., Early Proterozoic geology of the Great Lakes region, Memoir 160, Geological Society of America, p15-32.

Appendix A

Stratigraphic Sections of Bulk Sample Pits

F M C P Cb B

Pit# 108

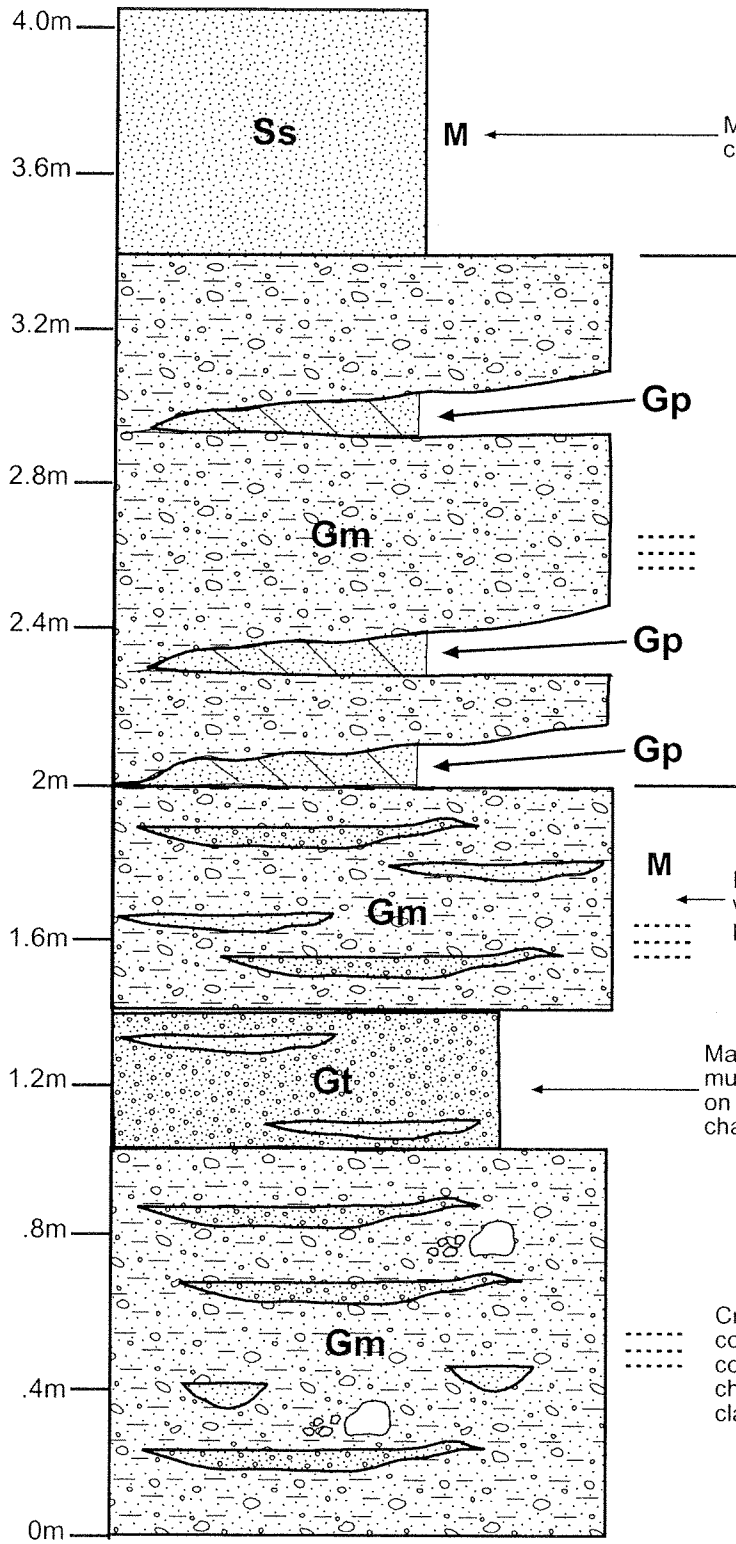

Massive very coarse-grained sandstone with a few pebble sized clasts. No apparent grading and sharp lower contact.

Crudely planar stratified cobble conglomerate interbedded with thin beds of planear cross-stratifed very coarse-grained sandstone. Cobble conglomerate is erosive and slightly truncating thin beds of very coarse-grained sandstone.

Massive to curdely planar stratified poorly sorted cobble conglomerate with a very coarse-grained to muddy matrix. A few thin lenses of pebble conglomerate and patches of very coarse-grained sandstone.

Massive pebble conglomerate with a very coarse-grained to muddy matrix. Laterally (along strike) there is a cobble conglomerate on both sides, the pebble conglomerate bed looks to be a narrow channel.

Crudely planar stratified poorly sorted cobble conglomerate with a very coarse-grained to muddy matrix interbedded with thin lenses of pebble conglomerate. Patches of very coarse-grained sandstone, with some channel shaped (facies Ss). A few pebble shadows behind larger sized clasts.

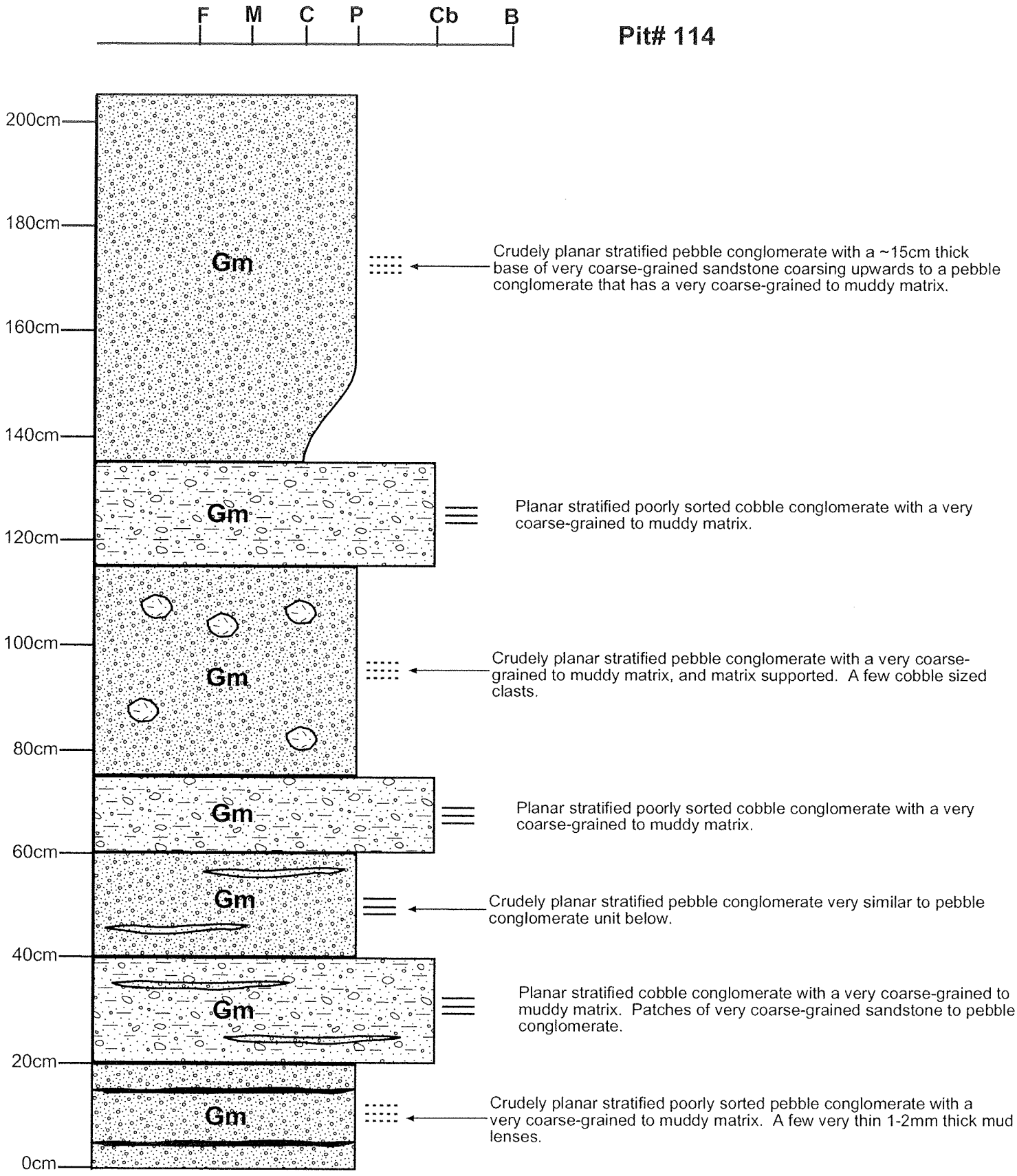
F
M
C
P
Cb
B
Pit# 114
200cm
180cm
160cm
140cm
120cm
100cm
80cm
60cm
40cm
20cm
0cm
Gm
Gm
Gm
Gm
Gm
Gm
Crudely planar stratified pebble conglomerate with a ~15cm thick base of very coarse-grained sandstone coarsing upwards to a pebble conglomerate that has a very coarse-grained to muddy matrix.
Planar stratified poorly sorted cobble conglomerate with a very coarse-grained to muddy matrix.
Crudely planar stratified pebble conglomerate with a very coarse-grained to muddy matrix, and matrix supported. A few cobble sized clasts.
Planar stratified poorly sorted cobble conglomerate with a very coarse-grained to muddy matrix.
Crudely planar stratified pebble conglomerate very similar to pebble conglomerate unit below.
Planar stratified cobble conglomerate with a very coarse-grained to muddy matrix. Patches of very coarse-grained sandstone to pebble conglomerate.
Crudely planar stratified poorly sorted pebble conglomerate with a very coarse-grained to muddy matrix. A few very thin 1-2mm thick mud lenses.

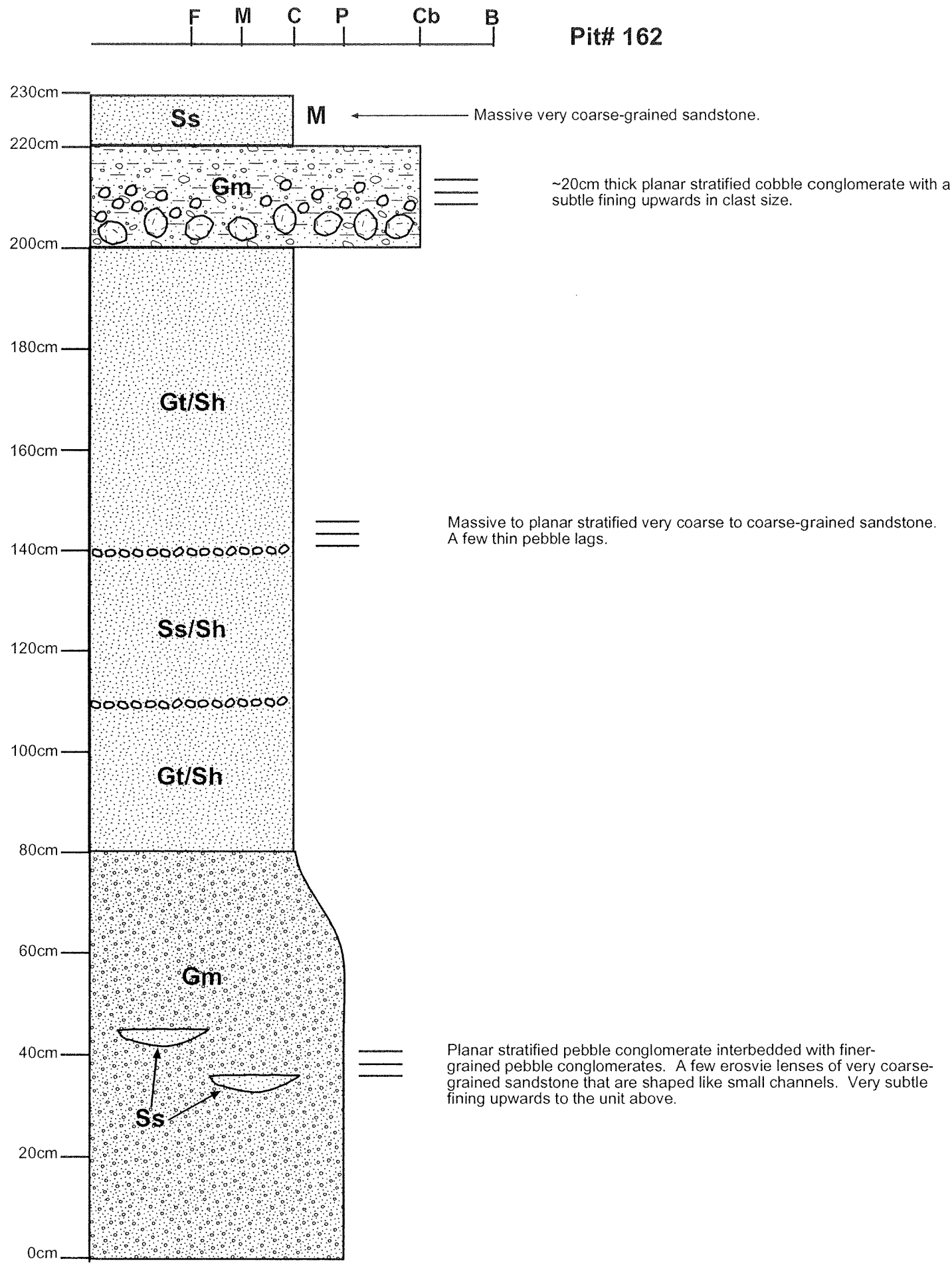
F M C P Cb B
Pit# 162
230cm
220cm
200cm
180cm
160cm
140cm
120cm
100cm
80cm
60cm
40cm
20cm
0cm
Ss
M
Massive very coarse-grained sandstone.
Gm
~20cm thick planar stratified cobble conglomerate with a subtle fining upwards in clast size.
Gt/Sh
Massive to planar stratified very coarse to coarse-grained sandstone. A few thin pebble lags.
Ss/Sh
Gt/Sh
Gm
Ss
Planar stratified pebble conglomerate interbedded with finer-grained pebble conglomerates. A few erosvie lenses of very coarse-grained sandstone that are shaped like small channels. Very subtle fining upwards to the unit above.

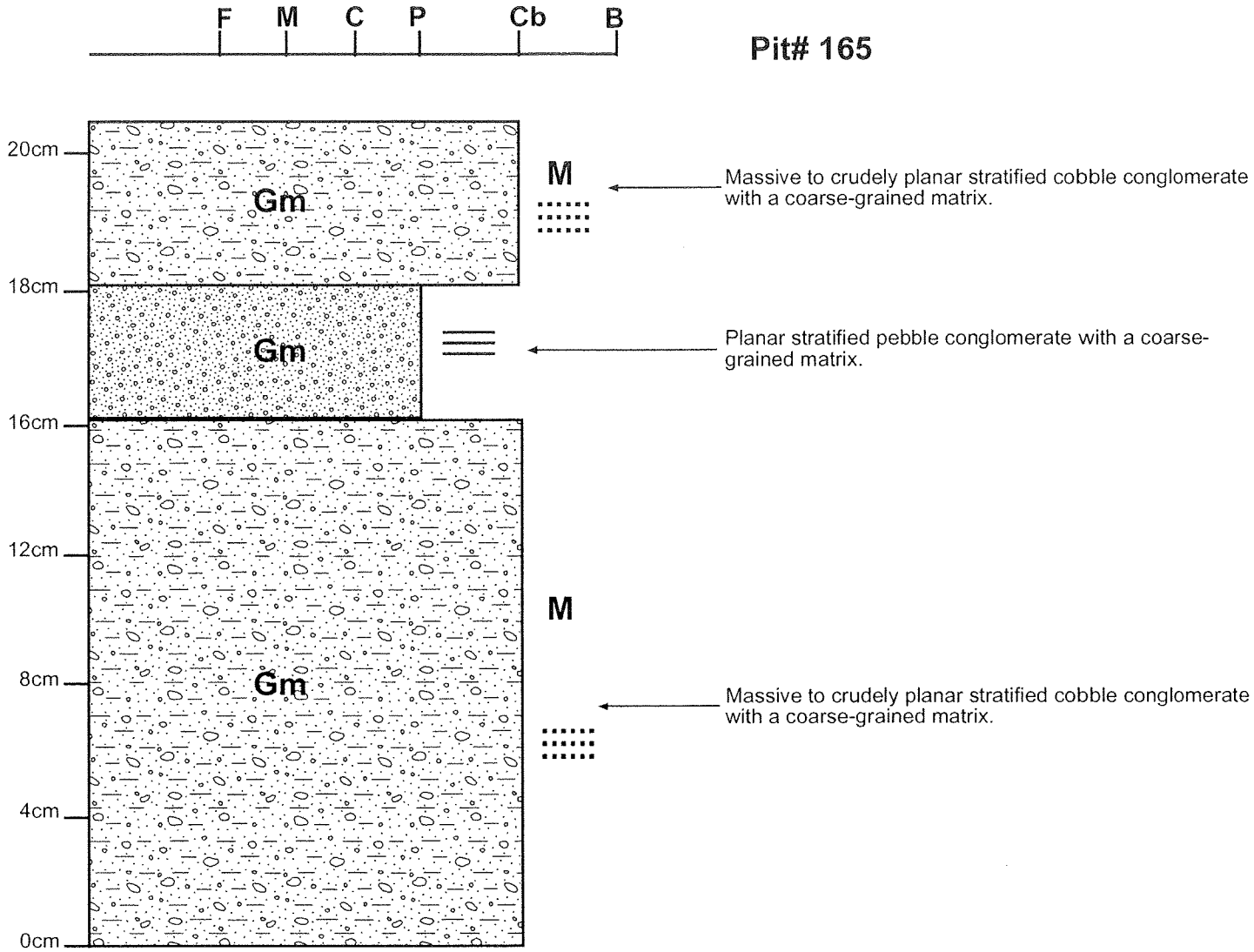
F
M
C
P
Cb
B
Pit# 165
20cm
18cm
16cm
12cm
8cm
4cm
0cm
Gm
Gm
Gm
M
M
Massive to crudely planar stratified cobble conglomerate with a coarse-grained matrix.
Planar stratified pebble conglomerate with a coarse-grained matrix.
Massive to crudely planar stratified cobble conglomerate with a coarse-grained matrix.

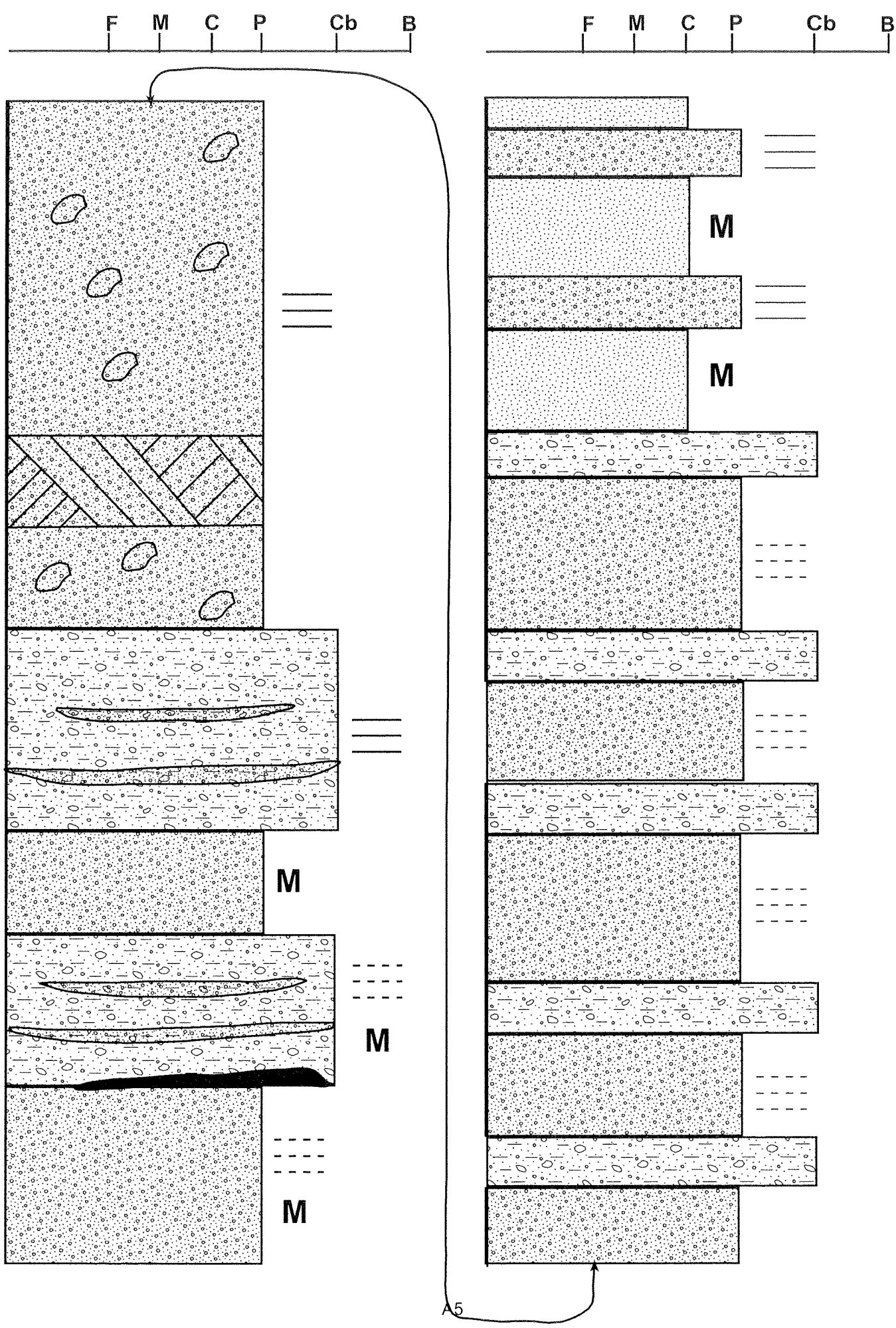
F
M
C
P
Cb
B
M
M
M
M
M
A5

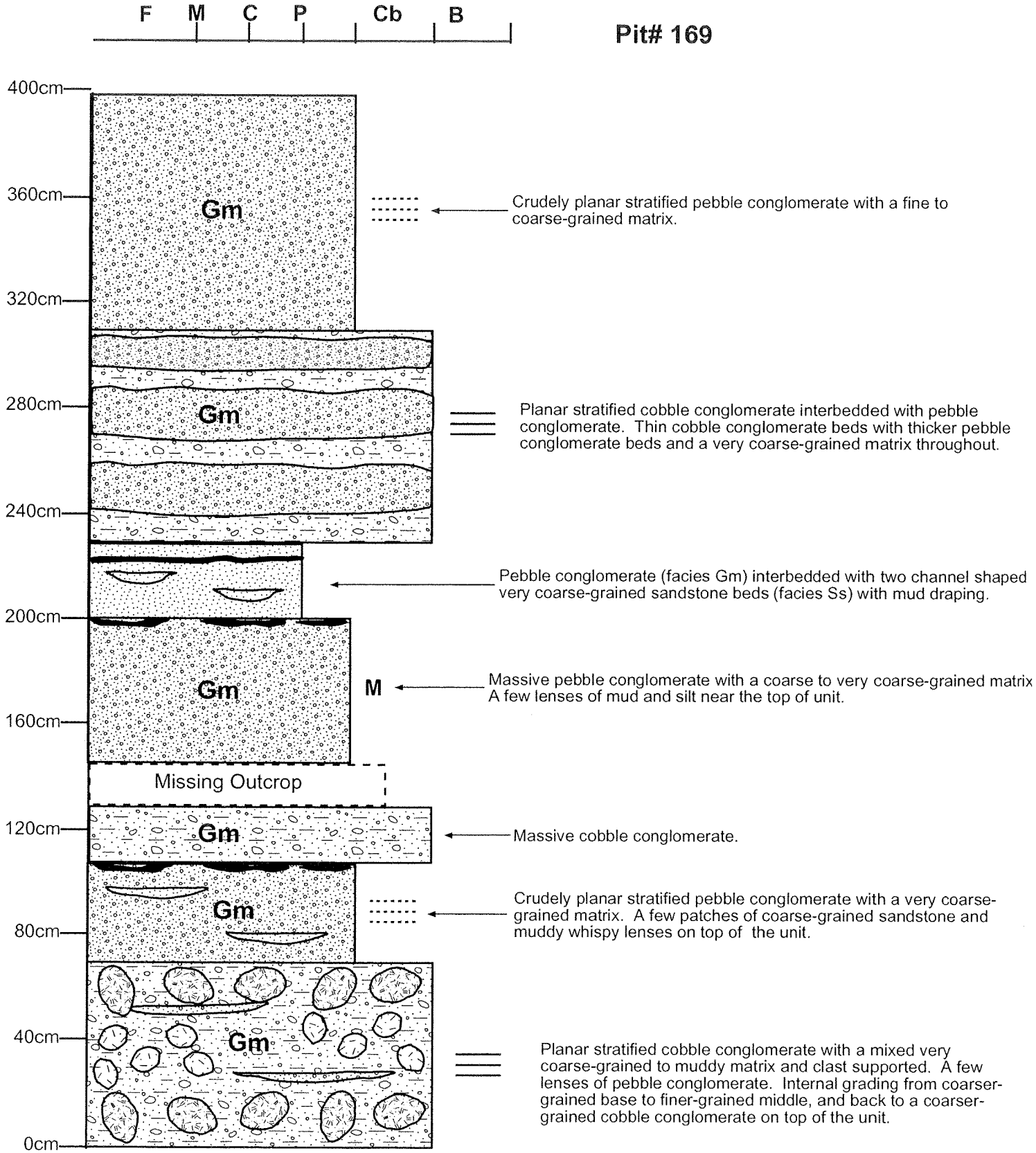
F M C P Cb B
Pit# 169
400cm
360cm
320cm
280cm
240cm
200cm
160cm
120cm
80cm
40cm
0cm
Gm
Gm
Gm
M
Missing Outcrop
Gm
Gm
Gm
Crudely planar stratified pebble conglomerate with a fine to coarse-grained matrix.
Planar stratified cobble conglomerate interbedded with pebble conglomerate. Thin cobble conglomerate beds with thicker pebble conglomerate beds and a very coarse-grained matrix throughout.
Pebble conglomerate (facies Gm) interbedded with two channel shaped very coarse-grained sandstone beds (facies Ss) with mud draping.
Massive pebble conglomerate with a coarse to very coarse-grained matrix A few lenses of mud and silt near the top of unit.
Massive cobble conglomerate.
Crudely planar stratified pebble conglomerate with a very coarse-grained matrix. A few patches of coarse-grained sandstone and muddy whispy lenses on top of the unit.
Planar stratified cobble conglomerate with a mixed very coarse-grained to muddy matrix and clast supported. A few lenses of pebble conglomerate. Internal grading from coarser-grained base to finer-grained middle, and back to a coarser-grained cobble conglomerate on top of the unit.

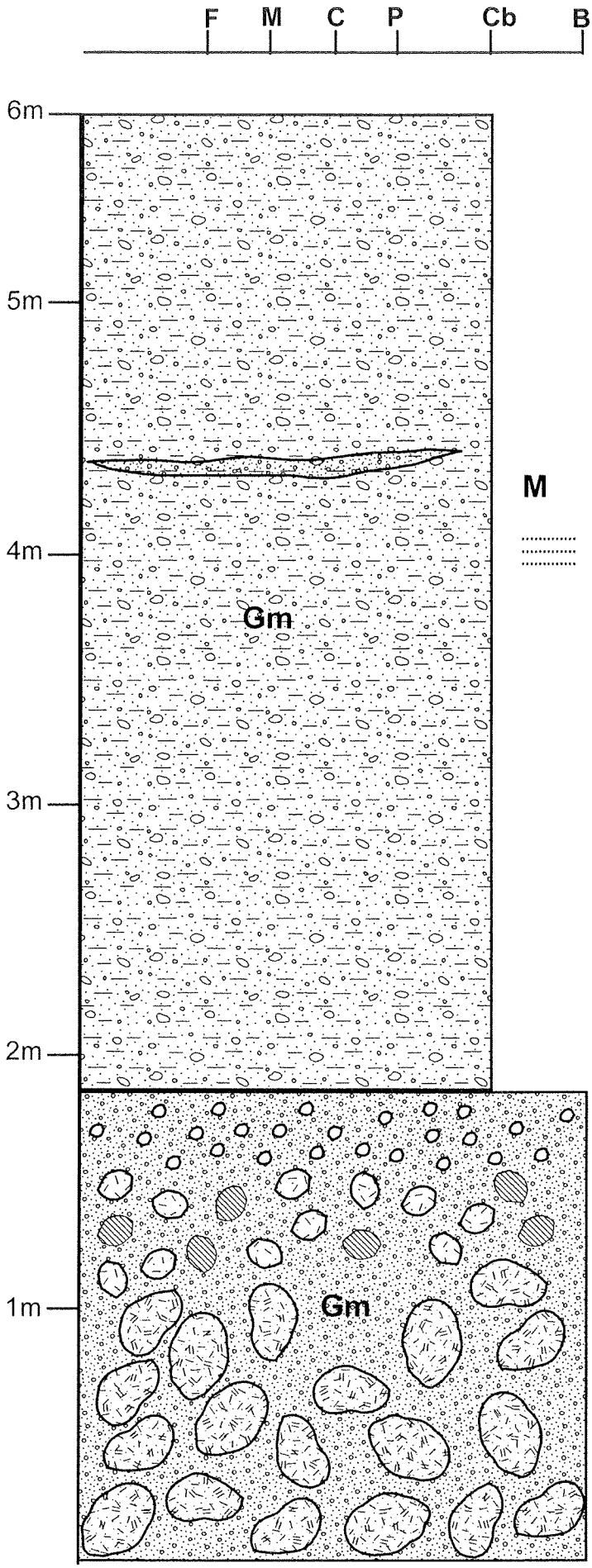

Pit# 170

M

Massive to very crudely planar stratified cobble conglomerate with a mixture of pebble size clast, very coarse sand and mud matrix. Absent of fine to very fine-grained matrix. Clast of coarse-grained sandstone.

M

Massive Boulder conglomerate or debris flow. No sedimentary structure except a very subtle decrease in clast size upwards. Mixture of pebbles, very coarse sand and mud matrix infill.

Pit# 171

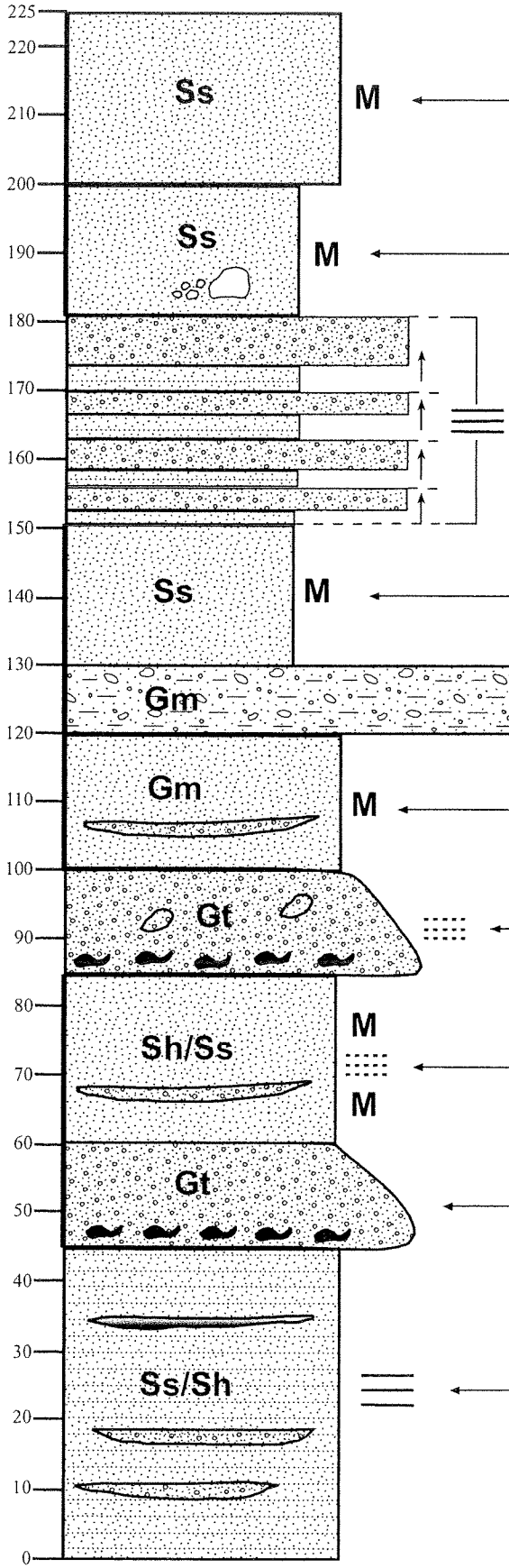

Massive moderately sorted very coarse-grained sandstone with a very fine-grained matrix.

Massive coarse-grained sandstone with a few pebble to cobble sized clasts. Observed cobble clast with a pebble shadow behind it.

~4 sequences of planar stratified very coarse-grained sandstone coarsing upwards to a pebble conglomerate. Clast are rounded to sub-rounded. (facies Sh)

Massive coarse-grained sandstone with a very fine-grained matrix. 50/50 mix of quartz and felsic grains.

Massive cobble conglomerate with clast sizes 10-15cm in diameter.

Massive very coarse-grained sandstone to pebble conglomerate. A few thin 2-3cm thick lenses of pebble conglomerate. Sharp upper contact with cobble conglomerate unit above.

Crudely planar stratified pebble conglomerate with a few cobble sized clasts. A subtle fining upwards to a coarse-grained sandstone unit above. Rip up clast near base of unit.

Crudely planar stratified very coarse-grained sandstone with a fine grained matrix. A thin lense of pebble conglomerate ~5cm thick interstratified within the coarse-grained sandstone.

Pebble conglomerate with a mixture of fine/coarse/mud grained matrix. Mud rip up clast and a subtle fining upwards to the unit above.

Planar stratified very coarse-grained sandstone with thin lenses 2-3cm thick of pebble conglomerate. From 20-28cm there is an increase in mud matrix, from 28-43cm is mainly coarse-grained to fine-grained matrix, very little mud, massive and no grading. Subtle coarsing upwards within the mud unit.

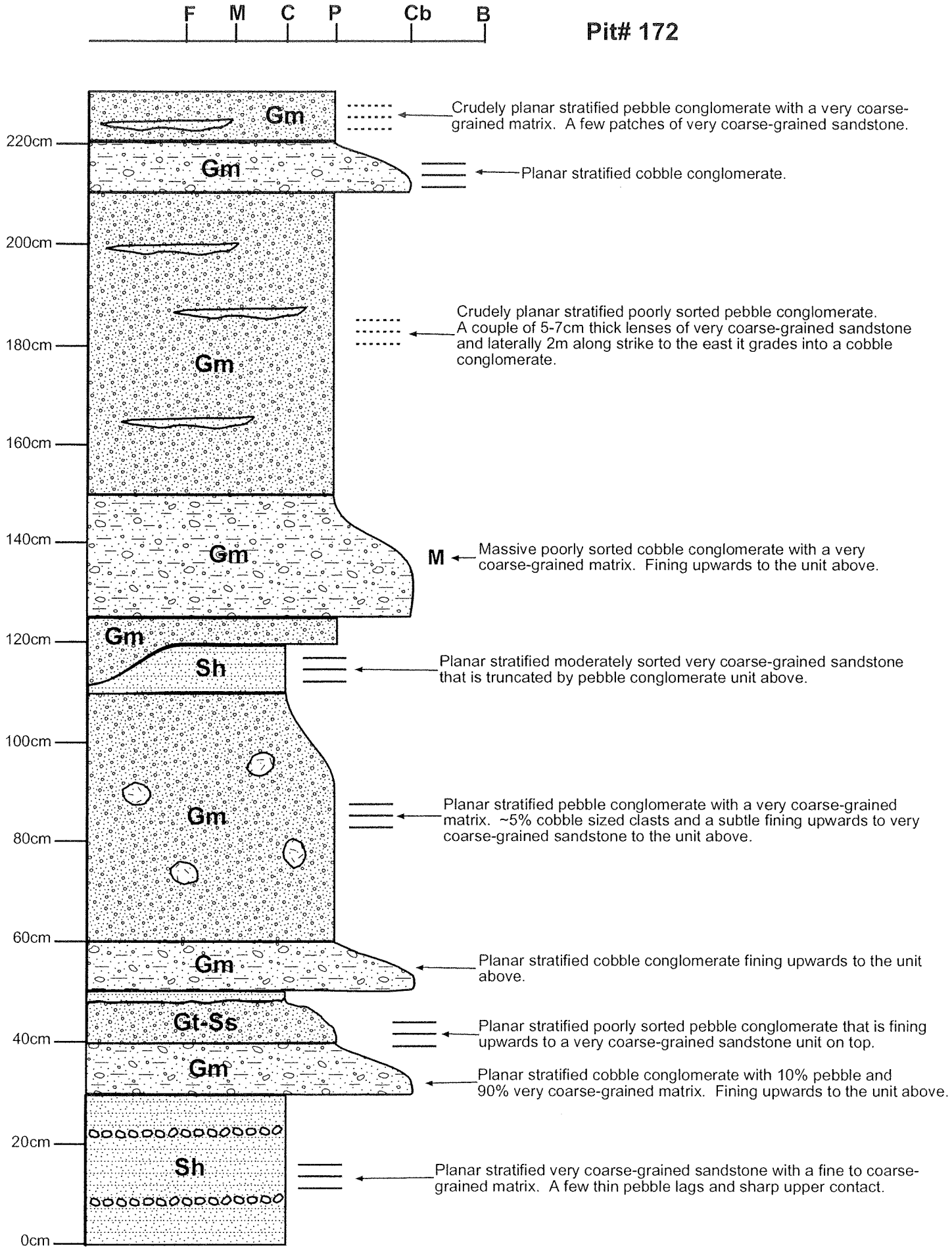
F M C P Cb B
Pit# 172
220cm
200cm
180cm
160cm
140cm
120cm
100cm
80cm
60cm
40cm
20cm
0cm
Gm
Gm
Gm
Gm
Gm
Sh
Gm
Gm
Gt-Ss
Gm
Sh
Crudely planar stratified pebble conglomerate with a very coarse-grained matrix. A few patches of very coarse-grained sandstone.
Planar stratified cobble conglomerate.
Crudely planar stratified poorly sorted pebble conglomerate. A couple of 5-7cm thick lenses of very coarse-grained sandstone and laterally 2m along strike to the east it grades into a cobble conglomerate.
M
Massive poorly sorted cobble conglomerate with a very coarse-grained matrix. Fining upwards to the unit above.
Planar stratified moderately sorted very coarse-grained sandstone that is truncated by pebble conglomerate unit above.
Planar stratified pebble conglomerate with a very coarse-grained matrix. ~5% cobble sized clasts and a subtle fining upwards to very coarse-grained sandstone to the unit above.
Planar stratified cobble conglomerate fining upwards to the unit above.
Planar stratified poorly sorted pebble conglomerate that is fining upwards to a very coarse-grained sandstone unit on top.
Planar stratified cobble conglomerate with 10% pebble and 90% very coarse-grained matrix. Fining upwards to the unit above.
Planar stratified very coarse-grained sandstone with a fine to coarse-grained matrix. A few thin pebble lags and sharp upper contact.

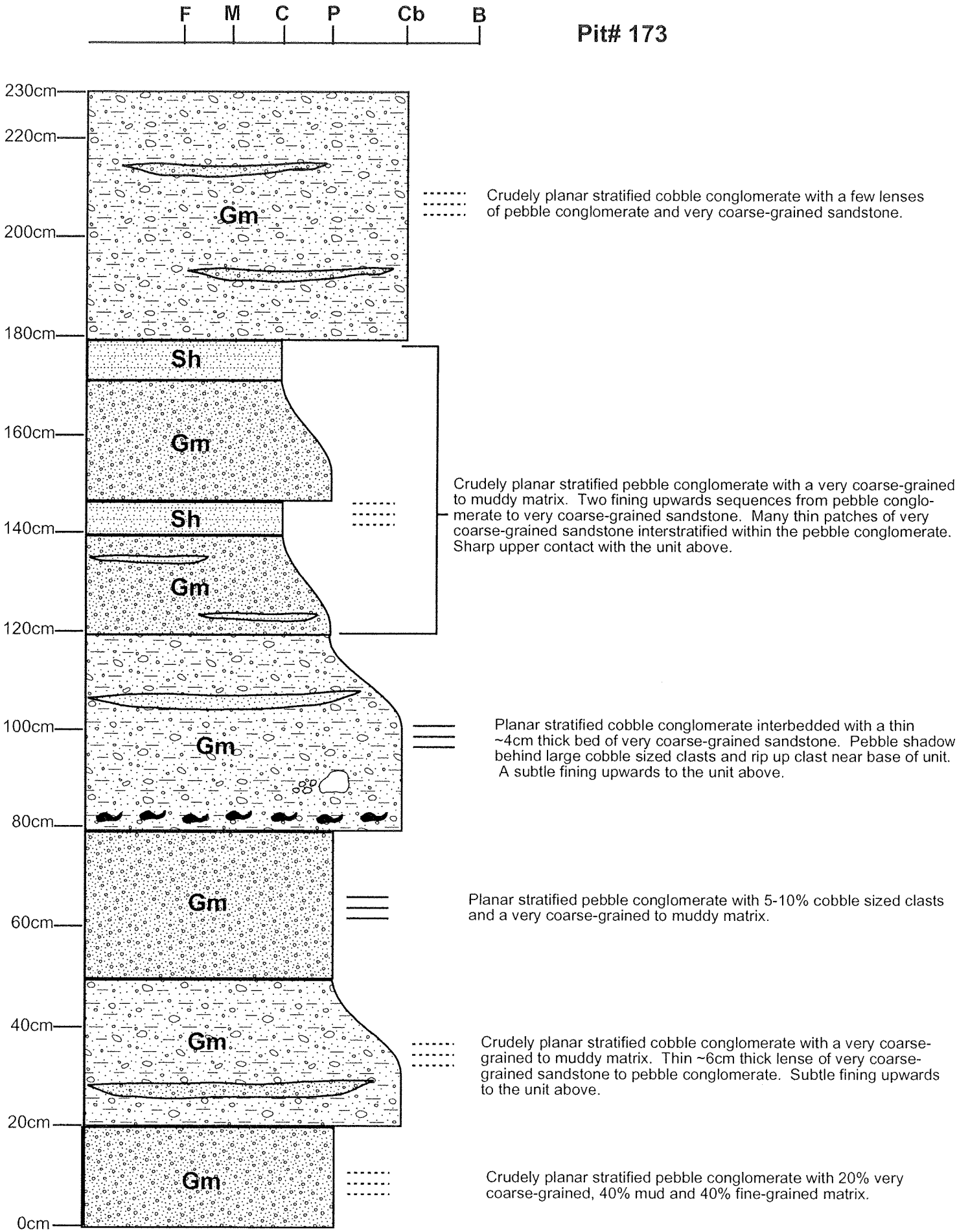
F M C P Cb B
Pit# 173
230cm
220cm
200cm
180cm
160cm
140cm
120cm
100cm
80cm
60cm
40cm
20cm
0cm
Gm
Sh
Gm
Sh
Gm
Gm
Gm
Gm
Gm
Crudely planar stratified cobble conglomerate with a few lenses of pebble conglomerate and very coarse-grained sandstone.
Crudely planar stratified pebble conglomerate with a very coarse-grained to muddy matrix. Two fining upwards sequences from pebble conglomerate to very coarse-grained sandstone. Many thin patches of very coarse-grained sandstone interstratified within the pebble conglomerate. Sharp upper contact with the unit above.
Planar stratified cobble conglomerate interbedded with a thin ~4cm thick bed of very coarse-grained sandstone. Pebble shadow behind large cobble sized clasts and rip up clast near base of unit. A subtle fining upwards to the unit above.
Planar stratified pebble conglomerate with 5-10% cobble sized clasts and a very coarse-grained to muddy matrix.
Crudely planar stratified cobble conglomerate with a very coarse-grained to muddy matrix. Thin ~6cm thick lense of very coarse-grained sandstone to pebble conglomerate. Subtle fining upwards to the unit above.
Crudely planar stratified pebble conglomerate with 20% very coarse-grained, 40% mud and 40% fine-grained matrix.

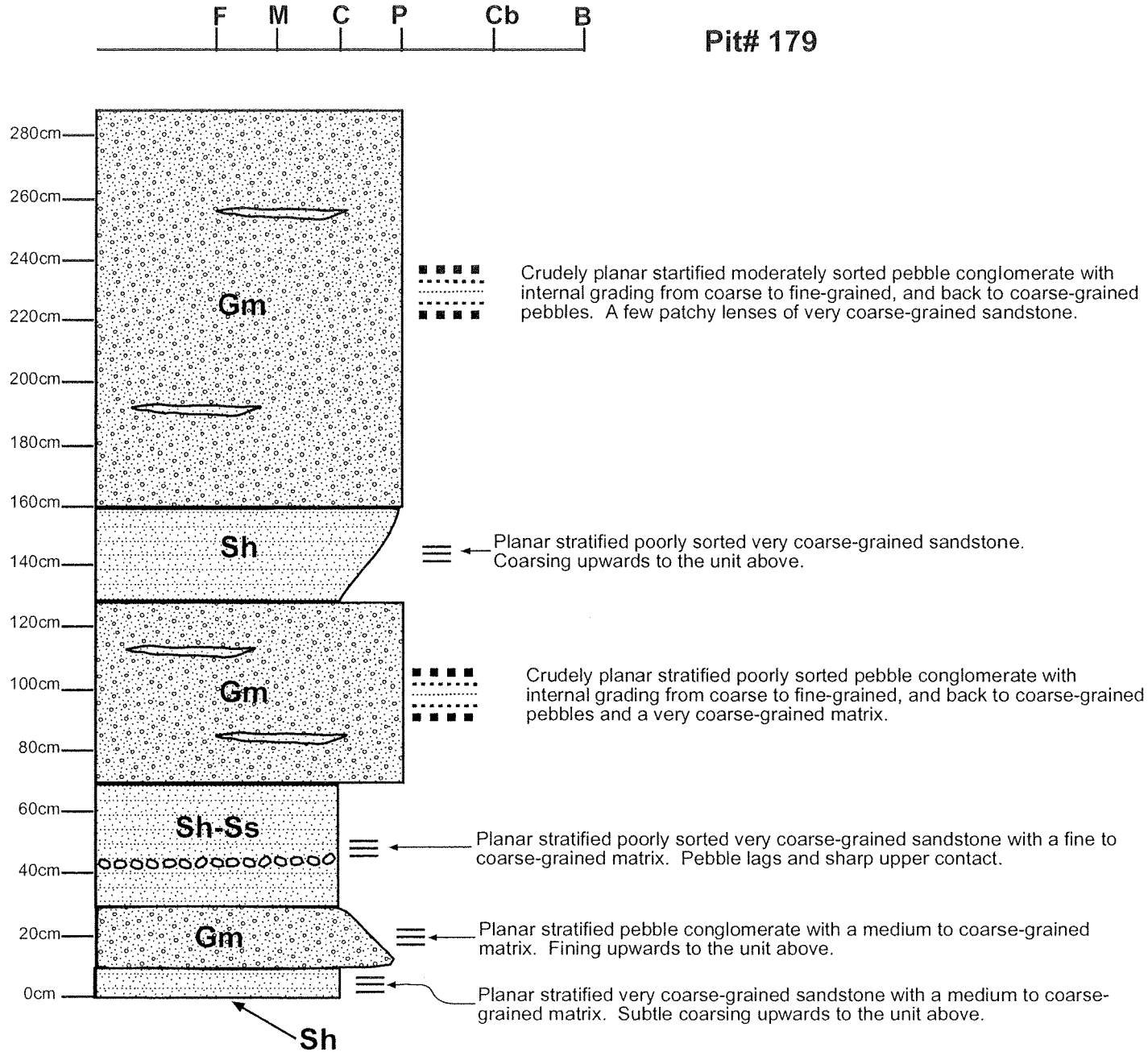
F
M
C
P
Cb
B
Pit# 179
280cm
260cm
240cm
220cm
200cm
180cm
160cm
140cm
120cm
100cm
80cm
60cm
40cm
20cm
0cm
Gm
Sh
Gm
Sh-Ss
Gm
Sh
Crudely planar startified moderately sorted pebble conglomerate with internal grading from coarse to fine-grained, and back to coarse-grained pebbles. A few patchy lenses of very coarse-grained sandstone.
Planar stratified poorly sorted very coarse-grained sandstone. Coarsing upwards to the unit above.
Crudely planar stratified poorly sorted pebble conglomerate with internal grading from coarse to fine-grained, and back to coarse-grained pebbles and a very coarse-grained matrix.
Planar stratified poorly sorted very coarse-grained sandstone with a fine to coarse-grained matrix. Pebble lags and sharp upper contact.
Planar stratified pebble conglomerate with a medium to coarse-grained matrix. Fining upwards to the unit above.
Planar stratified very coarse-grained sandstone with a medium to coarse-grained matrix. Subtle coarsing upwards to the unit above.

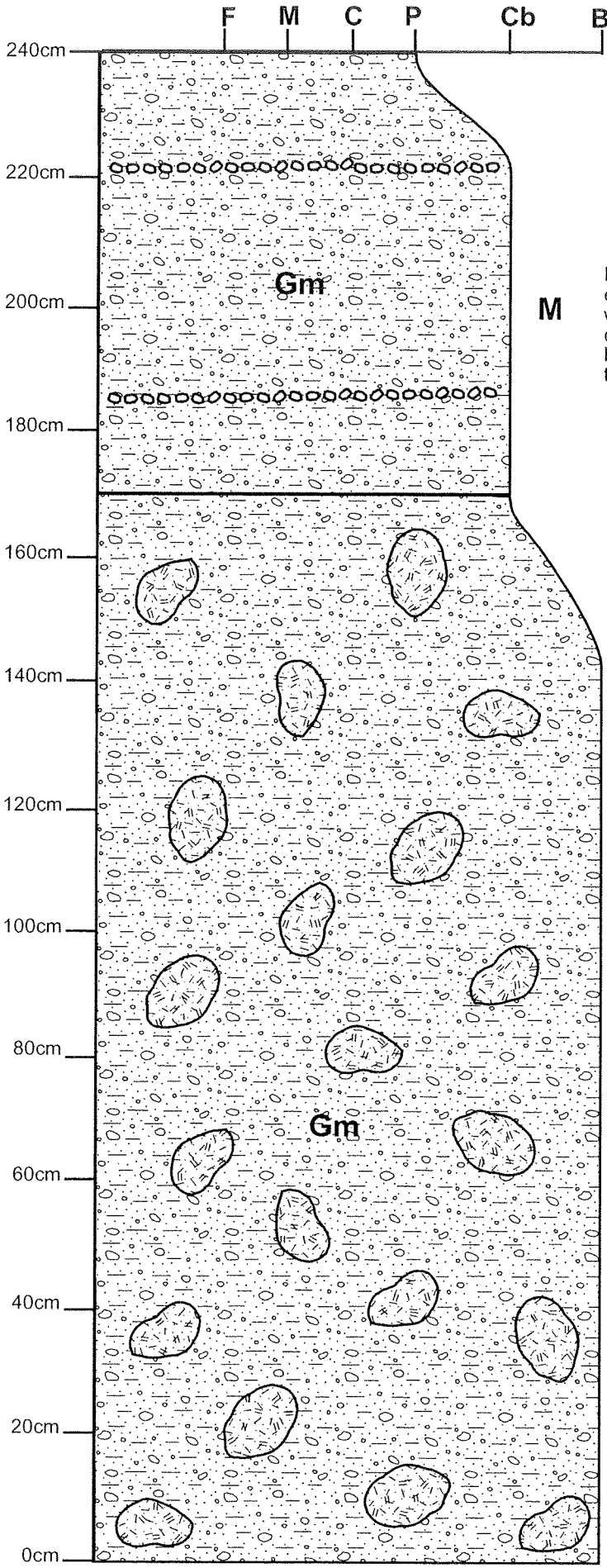

Pit# 187

M

Massive poorly sorted cobble conglomerate with a very coarse-grained to muddy matrix. Crude planar stratification with a couple of laterally persistent pebble lags. Overall the matrix consist of ~30-40% mud and has a swirly texture to it. If unit below is a debris flow, this unit looks very much like a reworked top of unit below.

M

Massive large cobble to boulder conglomerate. Has a very muddy and fine pebble matrix. No sedimentary structures and very chaotic looking with a swirly muddy matrix inbetwee boulder and cobble size clast. Possiable debris flow.

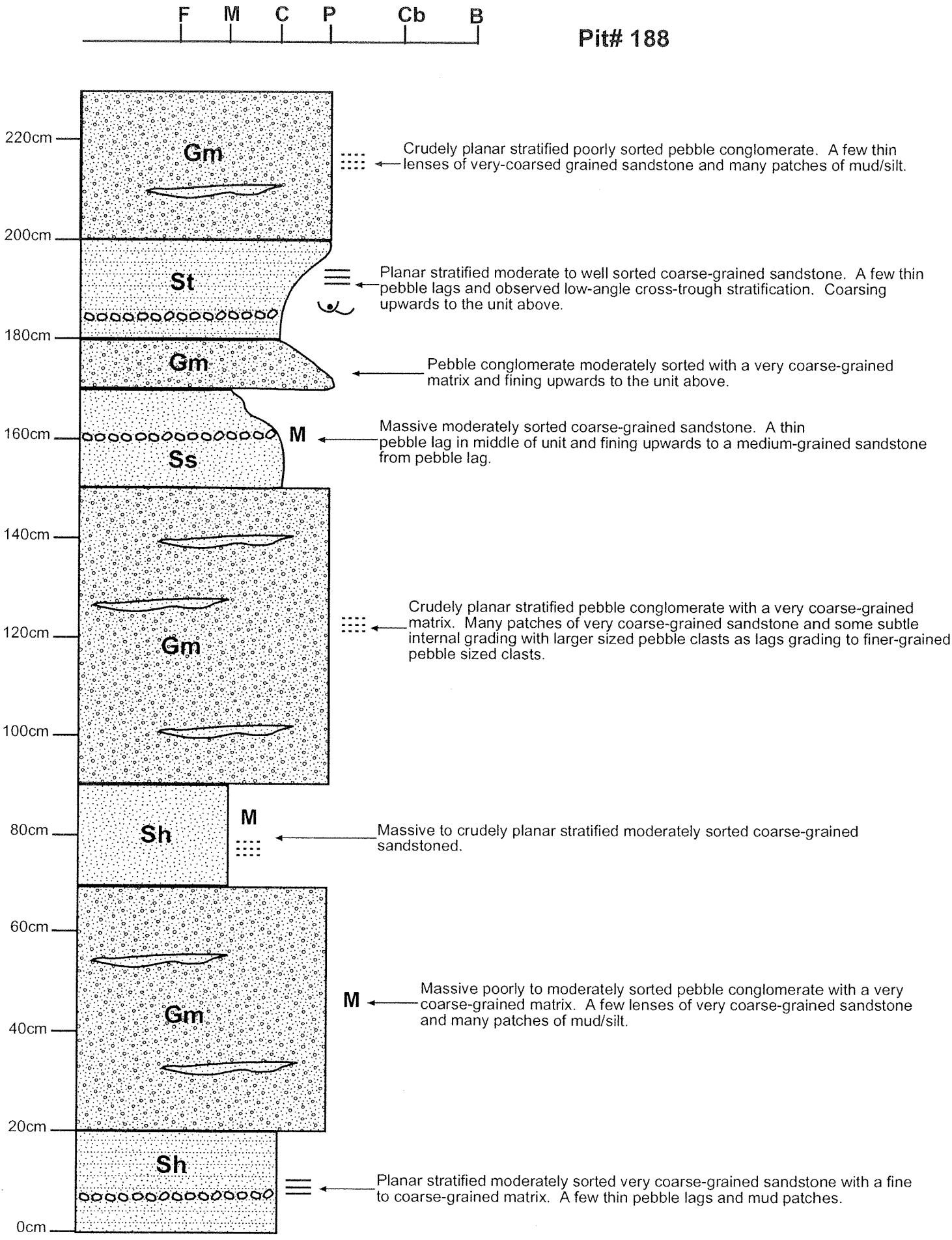
F M C P Cb B
Pit# 188
220cm
200cm
180cm
160cm
140cm
120cm
100cm
80cm
60cm
40cm
20cm
0cm
Gm
St
Gm
Ss
Gm
Sh
Gm
Sh
M
M
M
Crudely planar stratified poorly sorted pebble conglomerate. A few thin lenses of very-coarsed grained sandstone and many patches of mud/silt.
Planar stratified moderate to well sorted coarse-grained sandstone. A few thin pebble lags and observed low-angle cross-trough stratification. Coarsing upwards to the unit above.
Pebble conglomerate moderately sorted with a very coarse-grained matrix and fining upwards to the unit above.
Massive moderately sorted coarse-grained sandstone. A thin pebble lag in middle of unit and fining upwards to a medium-grained sandstone from pebble lag.
Crudely planar stratified pebble conglomerate with a very coarse-grained matrix. Many patches of very coarse-grained sandstone and some subtle internal grading with larger sized pebble clasts as lags grading to finer-grained pebble sized clasts.
Massive to crudely planar stratified moderately sorted coarse-grained sandstoned.
Massive poorly to moderately sorted pebble conglomerate with a very coarse-grained matrix. A few lenses of very coarse-grained sandstone and many patches of mud/silt.
Planar stratified moderately sorted very coarse-grained sandstone with a fine to coarse-grained matrix. A few thin pebble lags and mud patches.

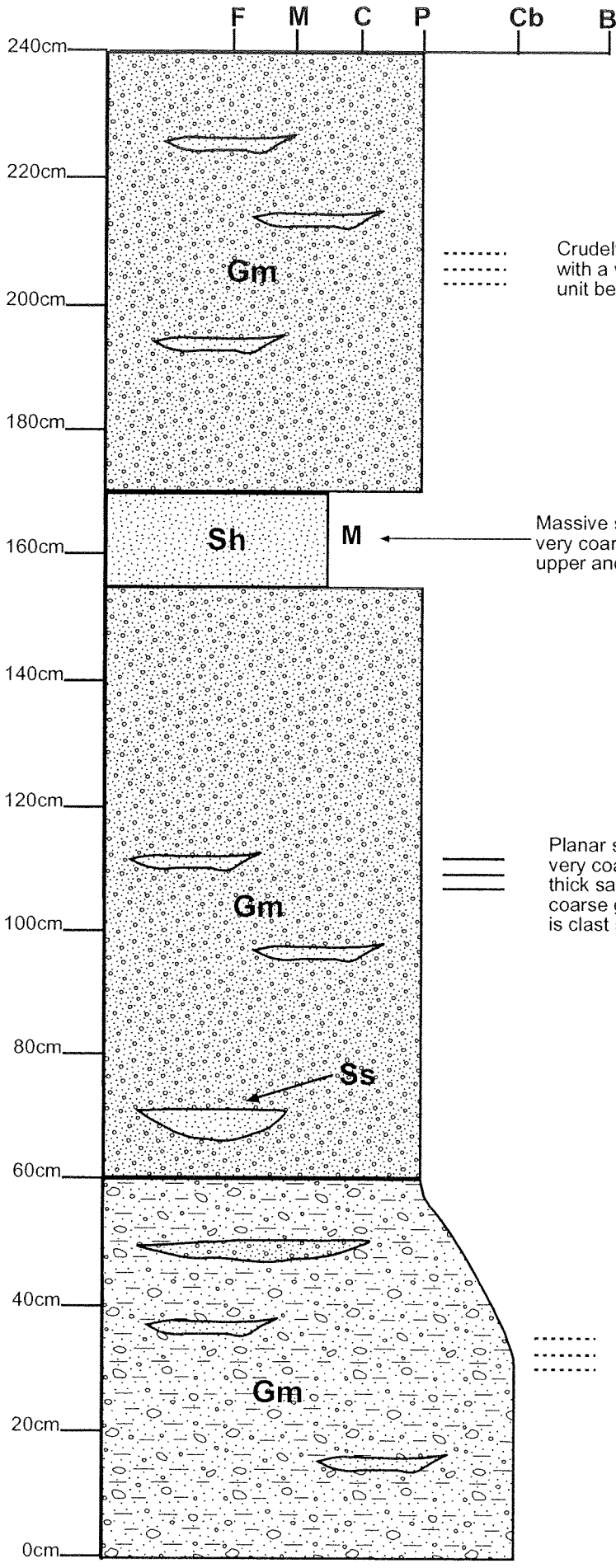

Pit# 189

Crudely planar stratified moderately well sorted pebble conglomerate with a very coarse-grained matrix. Very similar to pebble conglomerate unit below except without the chute channel feature.

Massive sandstone that is ~80% coarse-grained, and 20% very coarse grained. Laterally continuious and has a sharp upper and lower contact.

Planar stratified moderately well sorted pebble conglomerate with a very coarse-grained matrix. 10cm from the base of the unit is a 10-15cm thick sandstone lense with an erosive base. A few patches of very coarse grained sandstone and pebble conglomerate. Overall the unit is clast supported.

Crudely planar stratified moderately sorted cobble conglomerate with a very coarse-grained matrix. A few lenses of pebble conglomerate and patches of very coarse grained sandstone. Subtle fining upwards to unit above.

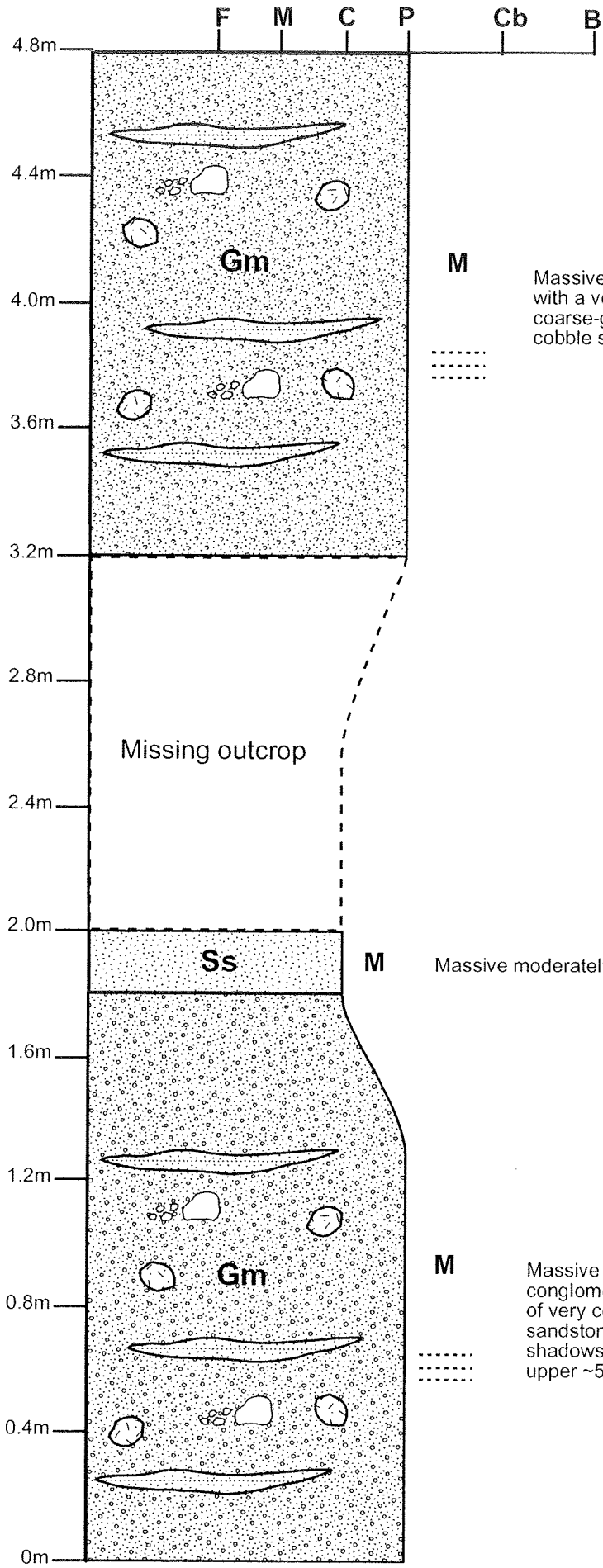

Pit# 191

Massive to crudely planar stratified poorly sorted pebble conglomerate with a very coarse-grained to muddy matrix. Many lenses of very coarse-grained sandstone and a few pebble shadows behind larger cobble sized clasts.

Massive moderately sorted very coarse-grained sandstone.

Massive to crudely planar stratified moderate to poorly sorted pebble conglomerate with a very coarse-grained to muddy matrix. Many lenses of very coarse-grained sandstone. A few of the very coarse-grained sandstone lenses appear to be graded and 7-10cm thick. A few pebble shadows behind larger cobble sized clasts. Fining upwards within the upper ~50cm of the unit.

Pit# 194

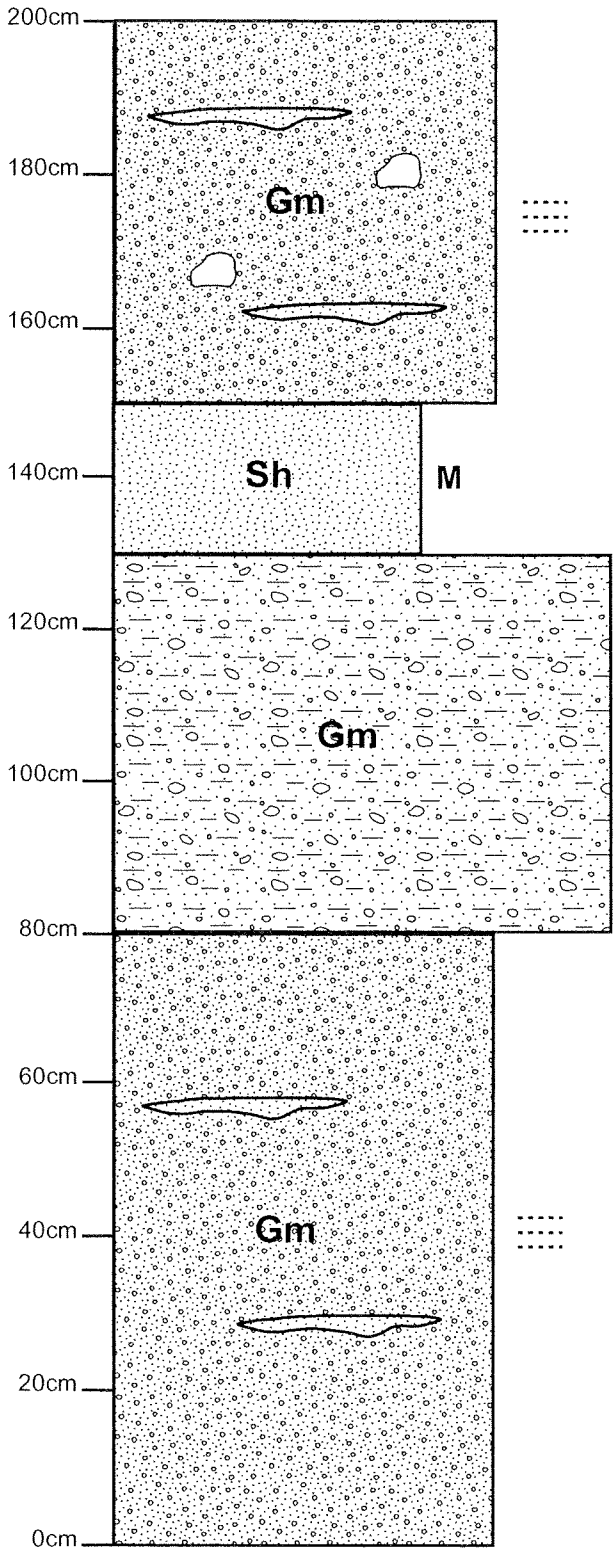

M

M

Crudely planar stratifed, poor to moderately-well sorted pebble conglomerate with a few irregular spaced apart cobble sized clasts. A few patches/lenses of very coarse-grained sandstone. Some internal grading from coarse-grained pebbles to finer-grained pebbles.

Massive moderately sorted very coarse-grained sandstone with ~10% pebbles. Moderately quartz rich with ~30% quartz grains.

Massive poorly sorted cobble conglomerate that has 60-70% very coarse-grained to 30-40% pebble size grained matrix. Note some mud draping around larger cobble sized clasts.

Crudely planar stratified poor to moderately sorted fine-grained pebble conglomerate with a few very thin coarser-grained pebble lags and a very coarse-grained matrix. A few patches of very coarse-grained sandstone Subtle internal grading from coarse-grained pebble lags to a finer-grained pebble conglomerate.

F M C P Cb B

Pit# 195

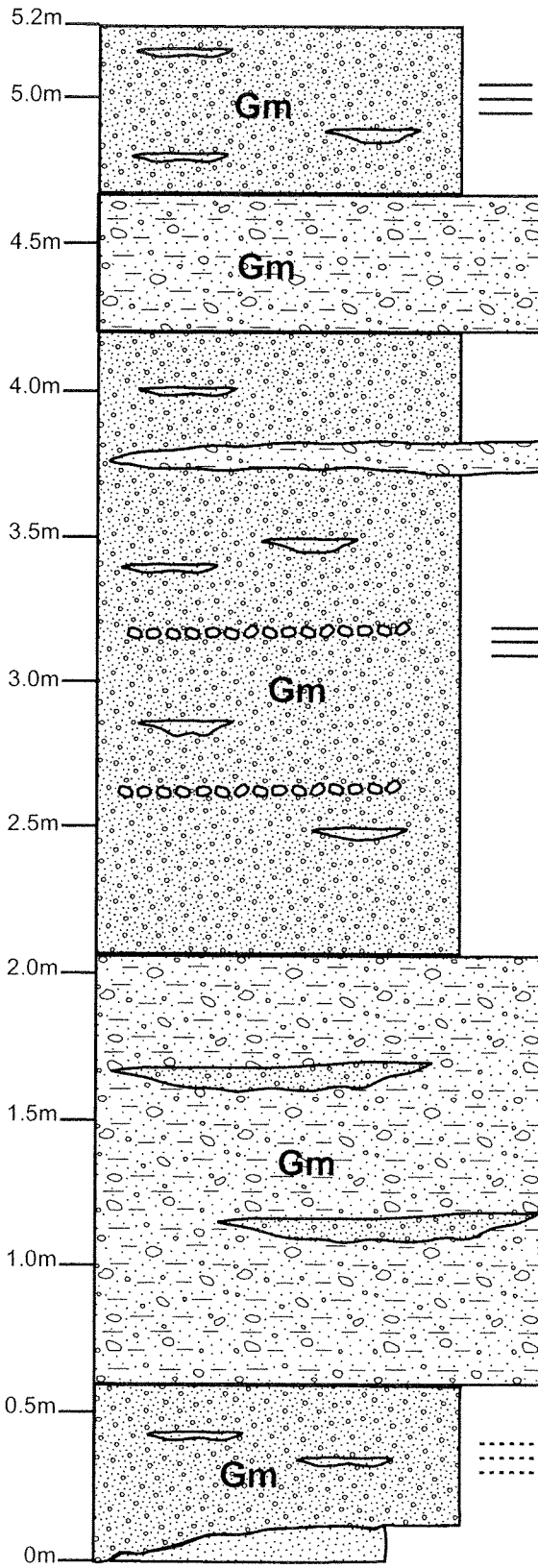

Planar stratified pebble conglomerate with a very coarse-grained matrix. A few patches of very coarse-grained sandstone.

Massive poorly sorted cobble conglomerate with ~40% pebble sized clasts and 60% very coarse-grained matrix.

Planar stratified pebble conglomerate with a very coarse to coarse-grained matrix. A few larger sized pebble lags with a thin cobble conglomerate interstratified within the pebble conglomerate. A few subtle internally graded beds from fine-grained pebbles to coarser-grained pebbles.

Massive poorly sorted cobble conglomerate with a very coarse-grained matrix. Many patches of very coarse-grained sandstone and a few very thin pebble conglomerate beds that give a crude planar stratification appearence.

Crudely planar stratifed moderately well sorted pebble conglomerate with a coarse-grained matrix. A couple patches of very coarse-grained sandstone. Low angle truncation of a very coarse-grained sandstone unit below.

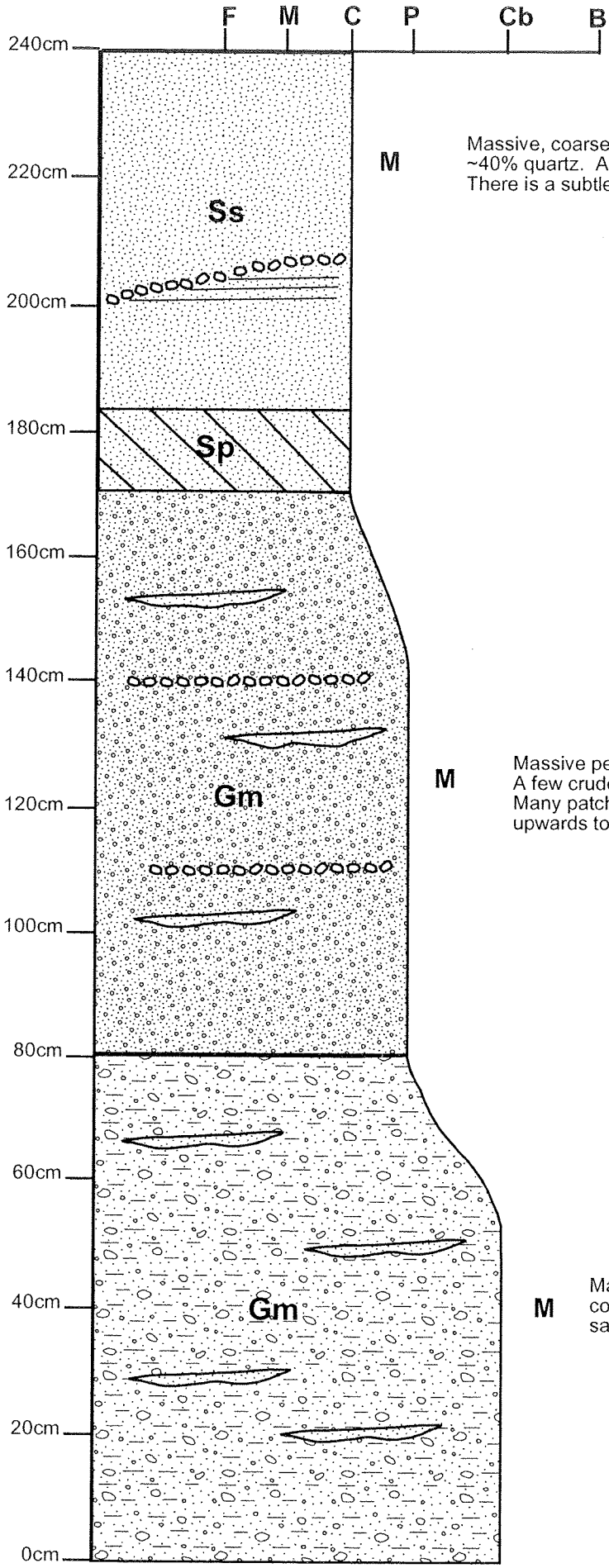

Pit# 196

M

Massive, coarse-grained sandstone that is moderately well-sorted and contains ~40% quartz. A few pebble lags that are slighty truncating and erosive. There is a subtle planar cross-stratification within the lower 10-15cm of the unit.

M

Massive pebble conglomerate with a very coarse-grained matrix. A few crudely planar stratified features with coarser grained pebble lags. Many patches of very coarse-grained sandstone with a very subtle fining upwards to unit above.

M

Massive poorly sorted cobble conglomerate with a very coarse-grained matrix. Many patches of very coarse-grained sandstone and a very subtle fining upwards to the unit above.

Appendix B

Whole Rock Geochemistry

Method	Sample	002-072908	003-072908	006-072908	007-072908	008-072908	009-072908
ICP-AES	SiO2	64.82	72.96	77.70	82.22	72.46	72.36
ICP-AES	TiO2	0.71	0.51	0.65	0.56	0.33	0.60
ICP-AES	Al2O3	11.08	16.16	6.40	6.28	9.08	8.60
ICP-AES	Fe2O3	10.12	3.61	7.66	5.40	5.53	8.89
ICP-AES	MnO	0.19	0.03	0.15	0.10	0.18	0.16
ICP-AES	MgO	6.59	1.41	2.17	0.44	2.78	2.94
ICP-AES	CaO	4.70	0.58	1.40	0.56	6.51	2.92
ICP-AES	Na2O	1.02	2.73	3.64	3.74	2.95	2.31
ICP-AES	K2O	0.65	1.91	0.11	0.63	0.12	1.15
ICP-AES	P2O5	0.13	0.10	0.11	0.07	0.06	0.08
	(ppm)						
ICP-AES	Ba	289	450	31	115	67	155
ICP-AES	Sr	165	256	177	126	296	115
ICP-AES	Be	1	2	1	1	1	1
ICP-AES	Co	50	13	39	24	24	33
ICP-AES	Cr	582	24	228	115	159	287
ICP-AES	Cu	42	34	63	21	26	39
ICP-AES	Ni	303	24	139	56	92	152
ICP-AES	V	171	63	170	128	91	203
ICP-AES	Zn	126	101	96	74	68	107
ICP-AES	Pb	18	<15	<15	<15	15	<15
ICP-AES	Sc	25	8	9	5	15	20
ICP-AES	Y	13	10	7	5	9	11
ICP-AES	S	592	<60	347	256	456	115
ICP-AES	Li	23	22	24	12	13	21
ICP-MS	Rb	21.2	65.2	3.4	19.7	3.8	37.8
ICP-MS	Ba	278.5	433.3	28.2	109.9	65.4	141.7
ICP-MS	Sr	167	259	173	127	292	116
ICP-MS	Cs	1.168	2.896	0.222	1.002	0.247	2.021
ICP-MS	Be	0.52	1.3	0.67	0.73	0.45	0.65
ICP-MS	Mo	0.55	0.85	1.01	0.33	0.45	0.29
ICP-MS	Ta	0.3	0.7	0.4	0.4	0.3	0.2
ICP-MS	Hf	2.44	4.52	2.86	2.61	1.94	1.7
ICP-MS	Ga	15.15	23.08	13.63	13.4	10.27	16.78
ICP-MS	Nb	3.89	7.42	3.84	3.98	2.94	2.71
ICP-MS	Sn	0.82	1.53	0.78	0.85	0.73	0.94
ICP-MS	Zr	93	180	104	94	69	63
ICP-MS	Co	50.4	15.2	40.5	22.8	24.8	33
ICP-MS	Cr	>600	27	224	111	164	285
ICP-MS	Cu	46	37	64	24	29	41
ICP-MS	Ni	321	28	144	59	97	157
ICP-MS	Zn	111	93	82	63	58	91
ICP-MS	V	192	67	168	126	96	207
ICP-MS	Pb	7.3	10.1	4.7	4.3	6.7	5
ICP-MS	Th	2.57	5.3	1.42	0.89	3.54	0.66
ICP-MS	U	3.69	1.53	0.85	0.86	0.73	0.37
ICP-MS	Sc	30.1	11.1	10.3	6.2	17.3	21.2
ICP-MS	Y	15.31	11.66	7.77	5.33	10.1	11.99
ICP-MS	La	10.95	14.87	6.27	3.07	15.42	5.42
ICP-MS	Ce	24.2	37.4	13	6.1	30.8	12.9
ICP-MS	Pr	3.01	3.63	1.53	0.69	3.46	1.73
ICP-MS	Nd	12.55	13.26	6.22	2.61	12.69	7.57
ICP-MS	Sm	3	2.59	1.28	0.58	2.22	1.94
ICP-MS	Eu	0.959	0.683	0.382	0.198	0.522	0.688
ICP-MS	Gd	3.02	2.24	1.23	0.62	2.03	2.11
ICP-MS	Tb	0.471	0.349	0.194	0.115	0.301	0.35
ICP-MS	Dy	2.9	2.1	1.2	0.8	1.9	2.3
ICP-MS	Ho	0.581	0.422	0.272	0.184	0.389	0.466
ICP-MS	Er	1.71	1.21	0.86	0.59	1.15	1.36
ICP-MS	Tm	0.244	0.174	0.138	0.093	0.17	0.201
ICP-MS	Yb	1.632	1.139	0.989	0.671	1.098	1.307
ICP-MS	Lu	0.239	0.174	0.155	0.102	0.179	0.199
ICP-MS	Bi	0.156	0.254	0.099	0.058	0.12	0.077
ICP-MS	Cd	0.19	0.09	0.21	0.1	0.2	0.17
ICP-MS	Li	25.2	26.3	25.1	13	13.2	21.4
ICP-MS	Sb	1.41	0.23	0.5	0.42	0.45	0.44
ICP-MS	Ti	4291	3156	3650	3157	1934	3454
ICP-MS	Tl	0.143	0.326	0.027	0.136	0.027	0.256
ICP-MS	W	5.4	7.9	6.1	13.9	30.3	6.7

Method	Sample	010-072908	011-072908	012-072908	013-072908	DC-002	DC-011
ICP-AES	SiO2	70.25	77.98	88.44	68.40	63.92	69.12
ICP-AES	TiO2	0.86	0.62	0.28	0.94	0.59	0.96
ICP-AES	Al2O3	10.62	8.32	4.13	9.76	9.65	8.74
ICP-AES	Fe2O3	10.20	6.51	4.08	10.23	6.48	11.16
ICP-AES	MnO	0.12	0.12	0.12	0.16	0.10	0.18
ICP-AES	MgO	3.07	1.32	0.50	3.49	8.13	3.85
ICP-AES	CaO	0.77	1.62	0.07	2.96	8.42	2.37
ICP-AES	Na2O	2.65	2.31	1.67	3.55	2.11	2.59
ICP-AES	K2O	1.33	1.06	0.66	0.33	0.21	0.94
ICP-AES	P2O5	0.14	0.12	0.05	0.19	0.40	0.11
	(ppm)						
ICP-AES	Ba	324	232	207	24	89	257
ICP-AES	Sr	70	152	55	245	770	159
ICP-AES	Be	2	1	1	1	1	2
ICP-AES	Co	45	29	18	34	37	48
ICP-AES	Cr	232	152	158	180	495	459
ICP-AES	Cu	60	35	10	<6	66	77
ICP-AES	Ni	132	95	57	93	278	225
ICP-AES	V	208	153	68	193	108	247
ICP-AES	Zn	123	81	51	102	72	136
ICP-AES	Pb	15	<15	<15	<15	<15	18
ICP-AES	Sc	24	14	4	12	14	23
ICP-AES	Y	17	15	3	14	9	11
ICP-AES	S	<60	<60	<60	<60	<60	682
ICP-AES	Li	20	12	8	27	25	25
ICP-MS	Rb	39.1	18.2	21.4	9	6.3	29.4
ICP-MS	Ba	260	186.3	196.2	21.8	86.7	221.2
ICP-MS	Sr	73	146	60	243	760	155
ICP-MS	Cs	2.157	1.28	0.926	0.517	0.364	1.559
ICP-MS	Be	0.91	0.67	0.67	0.52	0.55	0.75
ICP-MS	Mo	0.46	0.35	0.5	0.2	0.14	0.35
ICP-MS	Ta	0.4	0.5	0.3	0.5	0.4	0.2
ICP-MS	Hf	2.91	3.41	1.91	3.44	3.26	2.24
ICP-MS	Ga	18.81	15.19	9.23	17.17	12.37	18.77
ICP-MS	Nb	5.04	5.34	3.13	7.22	7.45	3.74
ICP-MS	Sn	1.04	0.9	0.54	0.89	1.06	2.17
ICP-MS	Zr	113	126	67	145	125	81
ICP-MS	Co	45	28.5	19.6	32.7	35.5	47.2
ICP-MS	Cr	227	144	154	181	499	442
ICP-MS	Cu	62	37	12	8	65	79
ICP-MS	Ni	133	94	63	99	282	232
ICP-MS	Zn	103	68	44	85	61	116
ICP-MS	V	206	153	70	195	115	246
ICP-MS	Pb	3.2	6	6.5	5.3	5.2	3.9
ICP-MS	Th	1.44	2.62	1.38	0.9	10.16	0.62
ICP-MS	U	0.63	1.08	0.83	0.59	2.01	0.38
ICP-MS	Sc	20.7	13.3	4.6	13.6	15.4	22.3
ICP-MS	Y	15.27	15.68	3.39	16.18	10.05	11.21
ICP-MS	La	7.07	8.32	1.44	4.56	69.69	5.43
ICP-MS	Ce	17.5	19.4	4.7	11.2	151.7	11.6
ICP-MS	Pr	2.08	2.43	0.4	1.48	17.95	1.42
ICP-MS	Nd	9.11	9.73	1.51	6.35	64.51	5.85
ICP-MS	Sm	2.33	2.25	0.35	1.67	8.11	1.41
ICP-MS	Eu	0.867	0.718	0.113	0.597	2	0.435
ICP-MS	Gd	2.63	2.42	0.4	1.98	4.47	1.61
ICP-MS	Tb	0.42	0.415	0.084	0.361	0.486	0.282
ICP-MS	Dy	2.7	2.9	0.6	2.5	2.2	1.9
ICP-MS	Ho	0.564	0.613	0.132	0.562	0.384	0.417
ICP-MS	Er	1.63	1.87	0.41	1.73	1	1.26
ICP-MS	Tm	0.235	0.29	0.061	0.26	0.137	0.187
ICP-MS	Yb	1.508	1.937	0.393	1.728	0.831	1.248
ICP-MS	Lu	0.218	0.306	0.056	0.262	0.128	0.176
ICP-MS	Bi	0.104	0.081	0.122	0.047	0.083	0.141
ICP-MS	Cd	0.07	0.12	0.09	0.07	0.06	0.19
ICP-MS	Li	20.6	10.9	8.7	27.7	24.4	24.8
ICP-MS	Sb	0.69	0.6	0.24	0.58	0.13	1.44
ICP-MS	Ti	5027	3517	1578	5614	3422	5612
ICP-MS	Tl	0.279	0.208	0.126	0.061	0.032	0.208
ICP-MS	W	3.3	10.3	9.7	4.5	14.5	7.2

Method	Sample	DC-015	DC-017	DC-019	DC-023	DC-028	DC-029
ICP-AES	SiO2	64.34	66.15	72.27	68.80	62.98	70.30
ICP-AES	TiO2	0.92	0.32	0.77	0.86	0.76	0.86
ICP-AES	Al2O3	10.76	8.57	8.47	15.02	11.04	7.77
ICP-AES	Fe2O3	12.81	6.03	10.16	6.34	9.61	10.94
ICP-AES	MnO	0.19	0.16	0.14	0.08	0.22	0.19
ICP-AES	MgO	3.58	10.23	2.52	1.64	5.72	3.98
ICP-AES	CaO	4.52	7.70	2.79	2.21	8.14	3.32
ICP-AES	Na2O	2.82	0.25	1.61	2.57	1.04	2.08
ICP-AES	K2O	0.01	0.37	1.16	2.29	0.36	0.37
ICP-AES	P2O5	0.06	0.15	0.10	0.19	0.15	0.18
	(ppm)						
ICP-AES	Ba	6	95	276	864	87	55
ICP-AES	Sr	152	142	92	261	177	104
ICP-AES	Be	1	1	1	2	1	1
ICP-AES	Co	66	31	46	18	39	51
ICP-AES	Cr	309	942	283	121	678	415
ICP-AES	Cu	115	20	92	31	83	45
ICP-AES	Ni	159	306	167	46	299	214
ICP-AES	V	305	91	180	142	178	214
ICP-AES	Zn	133	61	122	108	113	121
ICP-AES	Pb	19	<15	15	<15	16	24
ICP-AES	Sc	36	14	20	17	28	13
ICP-AES	Y	18	7	15	18	18	9
ICP-AES	S	113	<60	1226	662	<60	77
ICP-AES	Li	32	34	18	12	27	28
ICP-MS	Rb	0.3	11.4	36.1	67.3	12.7	12.7
ICP-MS	Ba	2.5	88.1	239.4	818.3	81.2	50.2
ICP-MS	Sr	146	146	98	253	183	107
ICP-MS	Cs	0.081	0.488	1.551	3.638	0.549	0.55
ICP-MS	Be	0.26	0.75	0.71	0.93	0.4	0.52
ICP-MS	Mo	0.18	0.15	0.44	0.48	0.45	0.26
ICP-MS	Ta	<0.2	<0.2	0.4	0.6	0.3	0.4
ICP-MS	Hf	1.59	1.15	2.48	4.37	2.23	3
ICP-MS	Ga	16.04	9.11	16.09	19.95	13.97	16.07
ICP-MS	Nb	2.1	1.55	4.4	8.47	4.01	5.29
ICP-MS	Sn	1.48	0.53	2.56	1.33	0.77	0.81
ICP-MS	Zr	53	44	92	183	87	120
ICP-MS	Co	62.8	32.5	46.9	17.7	41.2	51.5
ICP-MS	Cr	284	>600	287	122	>600	422
ICP-MS	Cu	111	24	98	35	90	50
ICP-MS	Ni	158	315	178	52	327	224
ICP-MS	Zn	108	52	108	97	101	105
ICP-MS	V	288	111	191	144	201	225
ICP-MS	Pb	1.4	1.5	4.1	5.8	7.2	6.4
ICP-MS	Th	0.27	1.36	1.71	3.85	1.91	1
ICP-MS	U	0.12	0.37	0.7	1	0.55	0.62
ICP-MS	Sc	36.6	16.2	21	19.7	33.3	15
ICP-MS	Y	19.69	7.5	16.78	19.53	20.66	10.62
ICP-MS	La	2.8	5.97	10.18	23.27	13.69	11.23
ICP-MS	Ce	7.9	12.7	23.2	55.2	29.1	24.3
ICP-MS	Pr	1.25	1.65	2.88	6.55	3.59	3.06
ICP-MS	Nd	6.26	6.85	11.27	25.41	14.38	12.48
ICP-MS	Sm	2.1	1.59	2.55	4.85	3.28	2.8
ICP-MS	Eu	0.732	0.553	0.708	1.43	0.863	0.734
ICP-MS	Gd	2.96	1.53	2.68	4.3	3.44	2.36
ICP-MS	Tb	0.521	0.225	0.44	0.622	0.557	0.323
ICP-MS	Dy	3.7	1.4	2.9	3.7	3.6	1.9
ICP-MS	Ho	0.79	0.28	0.617	0.728	0.73	0.395
ICP-MS	Er	2.34	0.78	1.8	2.07	2.09	1.2
ICP-MS	Tm	0.348	0.113	0.265	0.301	0.297	0.185
ICP-MS	Yb	2.298	0.709	1.73	1.886	2.005	1.268
ICP-MS	Lu	0.353	0.106	0.257	0.287	0.295	0.191
ICP-MS	Bi	0.041	0.022	0.149	0.062	0.117	0.108
ICP-MS	Cd	0.1	0.09	0.13	0.09	0.2	0.23
ICP-MS	Li	29.5	35.6	19.9	12	30.3	29.5
ICP-MS	Sb	0.88	0.21	0.26	1.47	0.26	0.16
ICP-MS	Ti	5195	1845	4731	5202	4846	5230
ICP-MS	Tl	<0.005	0.055	0.209	0.545	0.064	0.074
ICP-MS	W	9.3	11.3	13.3	<0.5	0.6	0.5

Method	Sample	DC-035	DC-039
ICP-AES	SiO2	67.60	69.00
ICP-AES	TiO2	0.80	0.88
ICP-AES	Al2O3	9.95	10.53
ICP-AES	Fe2O3	11.11	8.78
ICP-AES	MnO	0.20	0.14
ICP-AES	MgO	3.04	1.74
ICP-AES	CaO	4.94	6.13
ICP-AES	Na2O	1.79	2.72
ICP-AES	K2O	0.52	0.01
ICP-AES	P2O5	0.06	0.08
	(ppm)		
ICP-AES	Ba	101	17
ICP-AES	Sr	126	233
ICP-AES	Be	1	1
ICP-AES	Co	45	38
ICP-AES	Cr	349	173
ICP-AES	Cu	107	28
ICP-AES	Ni	123	69
ICP-AES	V	257	219
ICP-AES	Zn	95	110
ICP-AES	Pb	<15	<15
ICP-AES	Sc	35	30
ICP-AES	Y	17	19
ICP-AES	S	<60	<60
ICP-AES	Li	24	20
ICP-MS	Rb	17.8	0.5
ICP-MS	Ba	86.9	13.5
ICP-MS	Sr	129	235
ICP-MS	Cs	0.718	0.121
ICP-MS	Be	0.22	0.53
ICP-MS	Mo	0.17	0.3
ICP-MS	Ta	<0.2	0.3
ICP-MS	Hf	1.41	2.78
ICP-MS	Ga	14.6	18.95
ICP-MS	Nb	2.07	4.43
ICP-MS	Sn	0.38	1.43
ICP-MS	Zr	49	107
ICP-MS	Co	46.5	37.8
ICP-MS	Cr	359	179
ICP-MS	Cu	114	34
ICP-MS	Ni	136	76
ICP-MS	Zn	83	97
ICP-MS	V	277	232
ICP-MS	Pb	1.7	4.4
ICP-MS	Th	0.45	1.88
ICP-MS	U	0.15	0.59
ICP-MS	Sc	38.5	33.8
ICP-MS	Y	18.74	20.61
ICP-MS	La	3.24	12.93
ICP-MS	Ce	8.5	29.6
ICP-MS	Pr	1.23	3.64
ICP-MS	Nd	5.93	14.62
ICP-MS	Sm	1.87	3.26
ICP-MS	Eu	0.707	1.152
ICP-MS	Gd	2.54	3.42
ICP-MS	Tb	0.462	0.562
ICP-MS	Dy	3.2	3.6
ICP-MS	Ho	0.696	0.764
ICP-MS	Er	2.12	2.2
ICP-MS	Tm	0.329	0.326
ICP-MS	Yb	2.154	2.065
ICP-MS	Lu	0.329	0.306
ICP-MS	Bi	0.009	0.058
ICP-MS	Cd	0.11	0.15
ICP-MS	Li	25.3	20.9
ICP-MS	Sb	0.68	1.84
ICP-MS	Ti	4972	5537
ICP-MS	Tl	0.1	0.005
ICP-MS	W	<0.5	26.4